

Assessment of macro models of masonry infilled RC frames  
with opening



A Thesis Submitted in Partial Fulfillment of the Requirements  
for the Degree of Master of Engineering in Civil Engineering  
Department of Civil Engineering  
Faculty Of Engineering  
Chulalongkorn University  
Academic Year 2023

การประเมินแบบจำลองที่เหมาะสมสำหรับโครงคอนกรีตเสริมเหล็กที่มีผนังอิฐก่อแบบมีช่องเปิด



วิทยานิพนธ์นี้เป็นส่วนหนึ่งของการศึกษาตามหลักสูตรปริญญาวิศวกรรมศาสตรมหาบัณฑิต  
สาขาวิชาวิศวกรรมโยธา ภาควิชาวิศวกรรมโยธา  
คณะวิศวกรรมศาสตร์ จุฬาลงกรณ์มหาวิทยาลัย  
ปีการศึกษา 2566

Thesis Title                      Assessment of macro models of masonry infilled RC  
frames with opening  
By                                      Miss Sreyneth Lath  
Field of Study                      Civil Engineering  
Thesis Advisor                      Professor ANAT RUANGRASSAMEE, Ph.D.

---

Accepted by the FACULTY OF ENGINEERING, Chulalongkorn University  
in Partial Fulfillment of the Requirement for the Master of Engineering

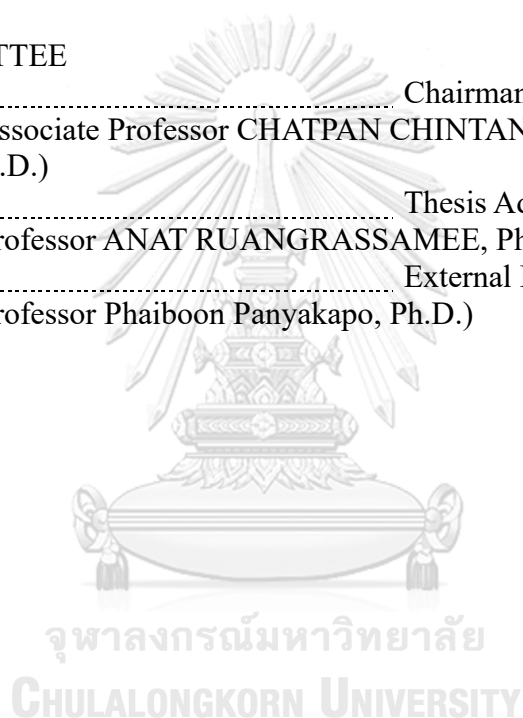
..... Dean of the FACULTY OF  
ENGINEERING  
(Professor SUPOT TEACHAVORASINSKUN, D.Eng.)

THESIS COMMITTEE

..... Chairman  
(Associate Professor CHATPAN CHINTANAPAKDEE,  
Ph.D.)

..... Thesis Advisor  
(Professor ANAT RUANGRASSAMEE, Ph.D.)

..... External Examiner  
(Professor Phaiboon Panyakapo, Ph.D.)



สไลเนค ลาด : การประเมินแบบจำลองที่เหมาะสมสำหรับโครงคอนกรีตเสริมเหล็กที่มีผนังอิฐก่อแบบมีช่องเปิด. ( Assessment of macro models of masonry infilled RC frames with opening) อ.ที่ปรึกษาหลัก : อาณัติ เรืองรัมย์

งานวิจัยนี้มีวัตถุประสงค์เพื่อศึกษาแบบจำลอง 3 รูปแบบสำหรับโครงคอนกรีตเสริมเหล็กที่มีผนังอิฐก่อแบบมีช่องเปิดหน้าต่างและประตูตรงกลางผนัง โดยได้ศึกษาแบบจำลองหลายค่ายัน แบบจำลองชิ้นส่วนผนังย่อย และแบบจำลองที่ใช้ตัวประกอบลดค่า ในการวิเคราะห์ได้ใช้การวิเคราะห์แบบผลัดกันข้างแบบไม่เชิงเส้นด้วยโปรแกรม SAP2000 จากการเปรียบเทียบกับผลการทดสอบพบว่าแบบจำลองที่ใช้ตัวประกอบลดค่าให้ค่าสติเฟนเสริมต้นได้ใกล้เคียงการทดสอบ และแบบจำลองชิ้นส่วนผนังย่อยให้ค่ากำลังรับแรงค้ำข้างได้ใกล้เคียงกับผลการทดสอบ



สาขาวิชา      วิศวกรรมโยธา

ลายมือชื่อนิติ

ปีการศึกษา    2566

.....  
ลายมือชื่อ อ.ที่ปรึกษาหลัก

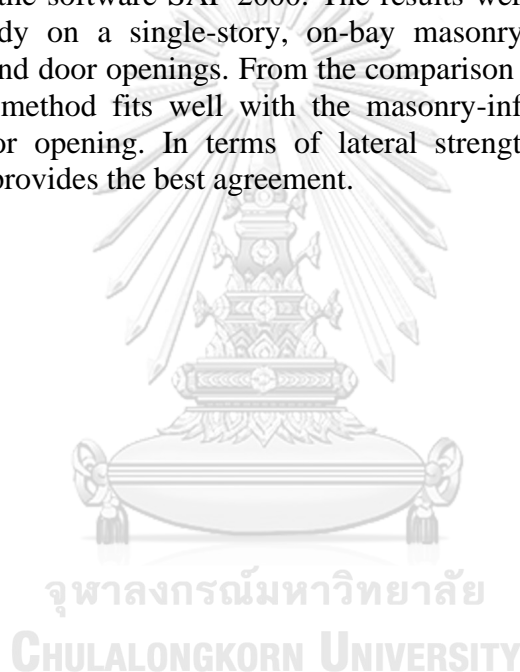
.....

# # 6472082921 : MAJOR CIVIL ENGINEERING

KEYWORD Masonry infilled RC frame, Central window and door opening  
D: openings, Macro model, Multi-strut model

Sreyneth Lath : Assessment of macro models of masonry infilled RC frames with opening. Advisor: Prof. ANAT RUANGRASSAMEE, Ph.D.

This study aims to investigate the behavior of masonry infilled reinforced concrete structures in the presence of central windows and doors under lateral seismic loading through macro-modeling simulations. The primary objective is to assess and evaluate three macro models, including the multiple equivalent strut method, discretized macro element method, and reduction factor method, in the seismic performance evaluation of masonry-infilled RC frames with central window and door openings. To achieve this, a nonlinear push-over analysis will be conducted using the software SAP 2000. The results were compared with a recent experimental study on a single-story, on-bay masonry-infilled RC frame with central window and door openings. From the comparison of the initial stiffness, the reduction factor method fits well with the masonry-infilled RC frame with the window and door opening. In terms of lateral strength, the discretized macro element method provides the best agreement.



Field of Study: Civil Engineering

Student's Signature

Academic Year: 2023

Advisor's Signature

.....

## ACKNOWLEDGEMENTS

I sincerely thank Prof. Dr. Anat Ruangrassamee, my advisor, for their invaluable guidance, unwavering support, and encouragement throughout my master's journey in the Department of Civil Engineering at the Faculty of Engineering, Chulalongkorn University.

I am equally thankful to my esteemed committee members, Assoc. Prof. Dr. Chatpan Chintanapakdee and Prof. Dr. Phaiboon Panyakapo, for their insightful suggestions and constructive comments that significantly contributed to the enhancement of this work. In addition, my deep gratitude goes to the Scholarship Program of Chulalongkorn University for ASEAN or Non-ASEAN Countries, which provided crucial financial support during my master's program.

Lastly, I want to express my heartfelt thanks to my friends, whose companionship and support enriched my academic journey, making it both enjoyable and memorable. I extend my gratitude to my family and all those who offered their support and encouragement throughout this transformative experience.

Sreyneth Lath

## TABLE OF CONTENTS

	<b>Page</b>
.....	iii
ABSTRACT (THAI) .....	iii
.....	iv
ABSTRACT (ENGLISH).....	iv
ACKNOWLEDGEMENTS.....	v
TABLE OF CONTENTS.....	vi
LIST OF TABLES .....	ix
LIST OF FIGURES .....	xi
CHAPTER 1 INTRODUCTION.....	1
1.1 RESEARCH SIGNIFICANCE .....	1
1.2 RESEARCH OBJECTIVES.....	3
1.3 SCOPES OF RESEARCH .....	4
CHAPTER 2 LITERATURE REVIEW.....	5
2.1 BEHAVIOR OF INFILLED RC FRAME WITHOUT OPENING.....	5
2.1.1 UNSTRENGTHENING INFILLED TYPE.....	6
2.1.2 STRENGTHENING INFILLED TYPE.....	10
2.1.3 INFILLED FRAME STRENGTH RATIO AND ASPECT RATIO.....	14
2.2 BEHAVIOR OF INFILLED RC FRAME WITH OPENING.....	17
2.3 NUMERICAL MODELS OF MASONRY-INFILLED FRAME.....	31
2.3.1 INFILLED FRAME WITHOUT OPENINGS.....	32
2.3.2 INFILLED FRAME WITH OPENING .....	42
2.4 OVERVIEW OF EXISTING EXPERIMENTAL STUDY.....	51
2.4.1 BARE FRAME (BF).....	54
2.4.2 INFILLED FRAME WITH CENTRAL DOOR (DF) .....	55
2.4.3 INFILLED FRAME WITH CENTRAL WINDOW OPENING (WF)....	56

CHAPTER 3 METHODOLOGY .....	58
3.1 MULTIPLE EQUIVALENT STRUT METHOD .....	60
3.1.1 NONLINEAR PROPERTIES OF RC FRAME .....	60
3.1.2 MASONRY INFILLED FRAME WITH OPENING.....	63
3.2 DISCRETIZED MACRO ELEMENT METHOD .....	67
3.2.1 NONLINEAR PROPERTIES OF RC FRAME .....	67
3.2.2 MASONRY INFILLED FRAME.....	69
3.3 REDUCTION FACTOR METHOD .....	73
3.3.1 NONLINEAR PROPERTIES OF RC FRAME .....	73
3.3.2 MODELING INFILLED FRAME .....	73
3.4 SELECTED SOFTWARE AND EXPECTED RESULT .....	79
CHAPTER 4 ANALYTICAL MODELS.....	81
4.1 MULTIPLE EQUIVALENT STRUT PROCEDURE (METHOD 1).....	81
4.1.1 CALIBRATION OF THE ANALYTICAL MODEL METHOD 1 .....	81
4.1.2 ANALYTICAL STUDY OF RC BARE FRAME.....	84
4.1.3 ANALYTICAL STUDY OF MASONRY INFILLED RC FRAME WITH WINDOW OPENING (WF) .....	85
4.1.4 ANALYTICAL STUDY OF MASONRY INFILLED RC FRAME WITH DOOR OPENING (DF) .....	86
4.1.5 PARAMETER STUDY .....	87
4.2 DISCRETIZED MACRO ELEMENT PROCEDURE (METHOD 2).....	89
4.2.1 CALIBRATION OF THE ANALYTICAL MODEL METHOD 2 .....	89
4.2.2 NONLINEAR PROPERTIES OF RC FRAME .....	92
4.2.3 MODELING INFILLED FRAME WITH WINDOW OPENING (WF).93	
4.2.4 MODELING INFILLED FRAME WITH DOOR OPENING (DF).....	97
4.3 REDUCTION FACTOR PROCEDURE (METHOD 3).....	100
4.3.1 NONLINEAR PROPERTIES OF RC FRAME .....	100
4.3.2 MODELING OF EQUIVALENT STRUT .....	100
4.3.3 MECHANICAL PROPERTIES OF STRUTS .....	101
CHAPTER 5 CONCLUSIONS .....	108



REFERENCES ..... 109  
VITA ..... 118



## LIST OF TABLES

	<b>Page</b>
Table 2.1 Reinforcement detail of frame member .....	52
Table 2.2. Geometrical characteristics of the openings of models.....	52
Table 2.3. Material properties of concrete, reinforcement, and masonry .....	52
Table 2.4 Material properties of masonry .....	52
Table 3.1 The studied specimens .....	58
Table 3.2 Parameters to model infilled frame with opening.....	65
Table 3.3 Calibration of the orthogonal link interface Kareem & Pantò (2019) .....	72
Table 3.4 Selection formula width of the equivalent strut .....	74
Table 3.5 Selected reduction factor formula for central opening.....	75
Table 4.1 Reinforcement detail of frame member of verification study .....	81
Table 4.2. Material properties of concrete, reinforcement.....	82
Table 4.3 Modeling parameter of the shear plastic hinge of the verification study.....	82
Table 4.4 Material properties of masonry .....	83
Table 4.5 Geometrical properties of the strut with door opening (IF-19).....	83
Table 4.6 Modeling parameter of the shear plastic hinge of column.....	84
Table 4.7 Geometrical properties of the strut with door opening (WF).....	85
Table 4.8 Geometrical properties of the strut with door opening (DF) .....	86
Table 4.9 Displacement, force, and stiffness at yield of the WF and DF .....	87
Table 4.10 Modeling parameter of the flexure plastic hinge of the verification study	89
Table 4.11 Geometrical and mechanical parameters to model link .....	91
Table 4.12 Modeling parameters of the flexural plastic hinge of the frame member ..	92
Table 4.13 Geometrical and mechanical parameters of the links of WF .....	94
Table 4.14 Geometrical and mechanical parameters of the links of DF .....	97
Table 4.15 The effective strut width for window opening (WF) .....	100
Table 4.16 The effective strut width for door opening (DF).....	101
Table 4.17 Modeling parameters for force-displacement of masonry infill Leeanansaksiri et al. (2018) .....	105



จุฬาลงกรณ์มหาวิทยาลัย  
**CHULALONGKORN UNIVERSITY**

## LIST OF FIGURES

	<b>Page</b>
Figure 1.1 Soft first story with torsional irregularity and severe damage to the corner column Lukkunaprasit et al. (2015).....	1
Figure 1.2 Shear failure on ground floor column Lukkunaprasit et al. (2015).....	2
Figure 2.1 Modes of failure of masonry in-filled frames P. G. Asteris et al. (2011) .....	5
Figure 2.2 Damage Patterns Mehrabi Armin et al. (1996), (a) Sliding of Bed Joints, (b) Shear Failure Columns, (c) Corner Crushing.....	6
Figure 2.3. Standard brick units and locked brick units .....	8
Figure 2.4 Details of a test specimen Kim & Yu (2021).....	10
Figure 2.5 Configuration of CFRP strips for strengthening Erdem et al. (2006) .....	11
Figure 2.6 Alternative CFRP retrofitting scheme Yuksel et al. (2010) .....	12
Figure 2.7 Hinge locations formed in RC frame Alwashali et al. (2017): (a) Specimen WF, (b) Specimen SF .....	15
Figure 2.8 Failure mechanisms of columns Wararuksajja et al. (2020).....	16
Figure 2.9 Summary of the specimen types in the database Huang & Burton (2020)	17
Figure 2.10 Final Crack Patterns Buonopane & White (1999 ).....	19
Figure 2.11 Wall dimensions Yáñez et al. (2004) .....	20
Figure 2.12 Collapse mechanisms Kakaletsis & Karayannis (2007).....	21
Figure 2.13 Failure modes of the specimen and the activated stress field, (a) Specimen PW1, (b) Specimen PW2, (c) Specimen PW3 and (d) Specimen PW4.....	23
Figure 2.14 Damage pattern and resistance mechanisms Mansouri et al. (2014).....	25
Figure 2.15 Test specimens Zhai et al. (2016) .....	26
Figure 2.16 Major load resistance of specimens presence of central and eccentric openings Mansouri et al. (2018) .....	28
Figure 2.17 Test specimens Humayun Basha et al. (2020).....	30
Figure 2.18 Geometry and dimension of specimens Khan et al. (2023).....	31
Figure 2.19 Strength envelope for masonry infill walls and the analytical model Mostafaei & Kabeyasawa (2004).....	33
Figure 2.20 Proposed multi-strut model Crisafulli & Carr (2007) .....	33

Figure 2.21 Multi-strut model proposed Burton & Deierlein (2014) .....	34
Figure 2.22 Proposed strut-model configuration Roosta & Liu (2022).....	35
Figure 2.23 Force distribution on the infilled frame.....	35
Figure 2.24 Proposed macro model for infilled frame Chrysostomou et al. (2002)....	36
Figure 2.25 Proposed model of masonry infilled steel frame Wael W. El-Dakhakhni (2003).....	36
Figure 2.26 Proposed macro model and force-displacement curve. ....	37
Figure 2.27 Scheme of two non-parallel equivalent struts Fiore et al. (2012).....	38
Figure 2.28 Hysteretic pivot law Cavaleri & Di Trapani (2014a) .....	38
Figure 2.29 FEM model employed for the structural analyses Cavaleri & Di Trapani (2014a) .....	38
Figure 2.30 M1 model from Cavaleri & Di Trapani (2014b) .....	39
Figure 2.31 M2 model from Cavaleri & Di Trapani (2014b) .....	39
Figure 2.32 Proposed model Furtado et al. (2015) .....	40
Figure 2.33 Proposed macro model Fiore et al. (2016) .....	41
Figure 2.34 Considered strut models Yekrangnia & Mohammadi (2017).....	41
Figure 2.35 Macro model proposed by Yekrangnia & Mohammadi (2017).....	41
Figure 2.36 An infilled frame with a window opening model as an equivalent spring. ....	43
Figure 2.37 Proposed multiple struts with monolithic infills and with separating infills respectively Thiruvengadam (1985) .....	45
Figure 2.38 Concept compressive strut infilled with an opening Kakaletsis & Karayannis (2008).....	45
Figure 2.39 Compression Strut Analogy ASCE (2013).....	46
Figure 2.40 Macro model of the infill panel with a window opening Jia et al. (2023)	47
Figure 2.41 Macro model of the infill panel with a door opening Jia et al. (2023).....	47
Figure 2.42 Bare frame (BF) NRCT (2023) .....	53
Figure 2.43 Infilled frame with door opening (DW) NRCT (2023) .....	53
Figure 2.44 Infilled frame with window opening (WF) NRCT (2023) .....	54
Figure 2.45 Hysteresis behavior of specimen BF NRCT (2023).....	54
Figure 2.46 Force displacement of specimen BF NRCT (2023) .....	55

Figure 2.47 Hysteresis behavior of specimen DF NRCT (2023).....	55
Figure 2.48 Force displacement of specimen DF NRCT (2023).....	56
Figure 2.49 Hysteresis behavior of specimen WF NRCT (2023).....	56
Figure 2.50 Force displacement of specimen BF NRCT (2023).....	57
Figure 3.1 Scope of research study .....	58
Figure 3.2 Framework of research Methodology .....	59
Figure 3.3 Analytical model of RC bare frame.....	61
Figure 3.4 Solution procedure of Method 1.....	61
Figure 3.5 Shear plastic hinge Sezen & Patwardhan (2012) force-displacement.....	63
Figure 3.6 Proposed strut model for IF with an opening Yekrangnia & Asteris (2020) .....	64
Figure 3.7 Stress-strain model for confined and unconfined concrete Kent & Park (1971).....	66
Figure 3.8 Solution procedure of Method 2.....	67
Figure 3.9 Constitutive law for diagonal shear springs .....	70
Figure 3.10 Constitutive law for orthogonal Links.....	72
Figure 3.11 model for simulation infilled frame model by Calio & Pantò (2014).....	72
Figure 3.12 Model of the infilled frame with central door opening Calio & Pantò (2014).....	72
Figure 3.13 Solution procedure of Method 3.....	73
Figure 3.14 Force-displacement relation for infilled adopted by Mucedero et al. (2020).....	76
Figure 3.15 Stress-strain relationship of masonry prism Leeanansaksiri et al. (2018)	78
Figure 3.16 Force displacement of the equivalent strut of masonry infills Leeanansaksiri et al. (2018).....	79
Figure 4.1 Comparison of experimental and analytical results of bare frames by using Method 1 .....	82
Figure 4.2 Comparison of experimental and analytical results of WF using multiple equivalent struts. ....	83
Figure 4.3 Compare the result of BF between analytical and experimental results ....	84

Figure 4.4 Compare result of WF between analytical and experimental results using Method 1 .....	85
Figure 4.5 Compare result of DF between analytical and experimental results .....	86
Figure 4.6 Parameter study of modulus elasticity of infill for WF .....	87
Figure 4.7 Parameter study of modulus elasticity of infill for DF .....	88
Figure 4.8 Modeling nonlinear bare frame in SAP 2000 using Method 2 .....	90
Figure 4.9 Comparison of experimental and analytical result of bare frame by using Method 2 .....	90
Figure 4.10 Compare fully infilled frame between analytical and experimental results using Method 2 .....	91
Figure 4.11 Comparison of analytical analysis with experimental result of BF .....	92
Figure 4.12 Modeling of masonry infilled frame with window opening Method 2 ....	93
Figure 4.13 Horizontal interface link 1 of WF .....	94
Figure 4.14 Vertical interface link 1 of WF .....	95
Figure 4.15 Diagonal link panel 1 of WF .....	95
Figure 4.16 Comparison results of the analytical model using the discretized macro element with the experimental result. ....	95
Figure 4.17 Modeling of masonry infilled frame with door opening Method 2 .....	97
Figure 4.18 Horizontal interface link 1 of DF .....	98
Figure 4.19 Vertical interface link 1 of DF .....	98
Figure 4.20 Diagonal link for panel 1 of DF .....	98
Figure 4.21 Force-displacement of masonry strut for WF Holmes (1961) for WF ...	102
Figure 4.22 Force-displacement of masonry strut for WF Holmes (1961) for DF ....	102
Figure 4.23 Force-displacement of masonry strut for WF Mainstone (1972) for DF	102
Figure 4.24 Force-displacement of masonry strut Mainstone (1972) for DF .....	103
Figure 4.25 Force-displacement of masonry strut Liauw & Kwan (1984) for WF ...	103
Figure 4.26 Force-displacement of masonry strut for WF Liauw & Kwan (1984) for DF .....	103
Figure 4.27 Comparison result of WF Panagiotakos & Fardis (1996) varying strut widths .....	104

Figure 4.28 Comparison result of DF Panagiotakos & Fardis (1996) varying strut widths.....	104
Figure 4.29 Force-displacement of masonry Leeanansaksiri et al. (2018).....	105
Figure 4.30 Comparison analytical and experimental result of WF Leeanansaksiri et al. (2018).....	106
Figure 4.31 Comparison analytical and experimental result of DF Leeanansaksiri et al. (2018).....	106
Figure 4.32 Compare analytical model with experimental results of WF .....	107
Figure 4.33 Compare the analytical model with the experimental results of DF .....	107





## CHAPTER 1

### INTRODUCTION

#### 1.1 RESEARCH SIGNIFICANCE

Masonry walls are frequently used as interior or exterior partition walls in a wide range of buildings. During the design phase, it is common to consider only the gravity load on masonry walls, often neglecting the stiffness of the masonry panel and its interaction with the infill and frame. As a result, hazardous or unexpected outcomes can occur, especially in regions prone to seismic activity. However, observations from past earthquakes have revealed that masonry-infilled frames significantly affect a structure's behavior, exhibiting both favorable and unfavorable effects. Lukkunaprasit et al. (2015) report on field evidence gathered from a past 6-magnitude Richter earthquake in northern Thailand, highlighting how masonry walls improved the structural resilience of buildings, thus serving as a safeguard for assessment. Conversely, engineers must meticulously assess the risk of shear failure in columns and beam-column joints when undertaking the design phase. It effectively conveys that the masonry-infilled frame around the staircases is stiffer than the RC frame, resulting in more seismic force being applied to the corner column of the RC frame causing severe damage in Figure 1.1.



Figure 1.1 Soft first story with torsional irregularity and severe damage to the corner column Lukkunaprasit et al. (2015)



Figure 1.2 Shear failure on ground floor column Lukkunaprasit et al. (2015)

The presence of openings in the masonry-infilled frame could lead to the short column effect due to the partial height (1m) of the masonry panel. The original 3m column of the building was reduced to 1m, resulting in severe shear failure in the column Figure 1.2. During seismic events, masonry-infilled (RC) frames with openings experience substantial forces, making their response to seismic loads a vital aspect to be carefully addressed in the structural design process. Understanding how these structures respond to earthquakes is essential for ensuring their safety and performance.

Many experimental studies have been conducted to investigate the response of frame-infilled masonry presence of opening various shapes and locations. Openings, such as windows or doors, in the infill panel, can alter the stress distribution and failure mechanism. Openings create stress concentrations around their edges, which can lead to localized failure modes, such as corner cracking or separation of the infill from the frame.

Considering the cost and time inefficiencies associated with experimental studies, we employed an analytical model to simulate the behavior of infilled frames, both with and without openings. Based on existing experimental data, three analytical approaches are introduced: macro, meso, and micro. The macro model is typically the most used approach due to its simplicity and practicality when compared to the other two Methods. Since the 1960s, researchers have commonly employed the macro approach to study the behavior of solid masonry-infilled frames. In this approach, the infilled panel is typically replaced by an equivalent strut with properties simulating those of masonry. Although macro modeling has shown to be useful in replicating the

behavior of solid masonry-infilled frames, the addition of openings introduces a level of complexity that has not been fully addressed. These openings disrupt the continuity of the masonry infill and can lead to localized stress concentrations and irregular stress distributions. Predicting how openings will affect the overall structural performance and precisely simulating the relationship between the infill, openings, and surrounding frame are also challenging tasks.

The research gap can be addressed by acquiring experimental data and establishing dependable design guidelines. Multiple macro-level simulation Methods are available for modeling masonry infilled frames, and the primary objective is to assess and compare these diverse approaches. Through this evaluation, we aim to pinpoint the most reliable Methods for simulating the complex interactions within these frames, ultimately enhancing our comprehension and design capabilities in real-world construction scenarios.

## 1.2 RESEARCH OBJECTIVES

To comprehend the structural behavior of masonry-infilled RC frames, numerous experimental studies incorporating various parameters were conducted to study their behavior. The response of infilled RC frames under cyclic loads is complex and depends on multiple factors. To mitigate research costs, and times and facilitate verification, numerical models were employed and manifested as analytical models, namely micro models, meso-models, and macro models.

For practical and computational efficiency purposes, the macro approach is chosen to predominate in assessing the performance of masonry-infilled RC frames. The aim of the study:

1. To study various macro models to simulate the performance of masonry infill RC frame with and without opening
2. To compare and evaluate the level of accuracy of macro models using existing experimental studies from NRCT (2023) as a reference.

### 1.3 SCOPES OF RESEARCH

The structural behavior of RC frames with a central opening including windows and doors that have masonry infill, are evaluated. Several well-known analytical models using macro modeling Methods are assessed and validated by comparing them with existing experimental data NRCT (2023) in the literature review. The limitations of this study are mentioned below:

- Only the lateral in-plane loading subjected to masonry-infilled RC frames.
- Consider only unreinforced masonry infilled panels.
- Only central windows and door openings are discussed in this study.
- The RC structural member (beam and column) considers only the unstrengthening ones.



## CHAPTER 2

### LITERATURE REVIEW

#### 2.1 BEHAVIOR OF INFILLED RC FRAME WITHOUT OPENING

Masonry-infilled RC frames are commonly used in construction due to their structural efficiency and aesthetic appeal. According to research, the absence of infills significantly affects how RC frames behave, and influence their stiffness, strength, energy dissipation, and overall structural response Ghassan Al-Chaar et al. (2002; Holmes (1961; Huang et al. (2016; Mehrabi Armin et al. (1996; Misir et al. (2012; Zovkic et al. (2013).

It's crucial to acknowledge that the failure mechanisms mentioned above are influenced by various factors, including the properties of the masonry material, the quality of construction, the design detailing, and the intensity of applied loads. The failure mechanism of such frames can depend on various factors, including the type of infill, aspect ratio, relative strength of the frame and infill, and the presence of openings. Dias-Oliveira et al. (2022), review the exhaustive list of experimental work and analytical modeling to understand the factors and its consequences determining infill masonry behavior, have drawn slightly different conclusions on some parameters to be considered such as wall aspect-ratio (height/length), openings on the walls, wall, and frame stiffness and so on. Through the experimental and analytical results, different failure modes of masonry infilled frames were categorized into five separate and identifiable modes P. G. Asteris et al. (2011; El-Dakhkhni Wael et al. (2003) including corner crushing, diagonal compression, sliding shear, diagonal cracking, and frame failure, as shown in Figure 2.1.

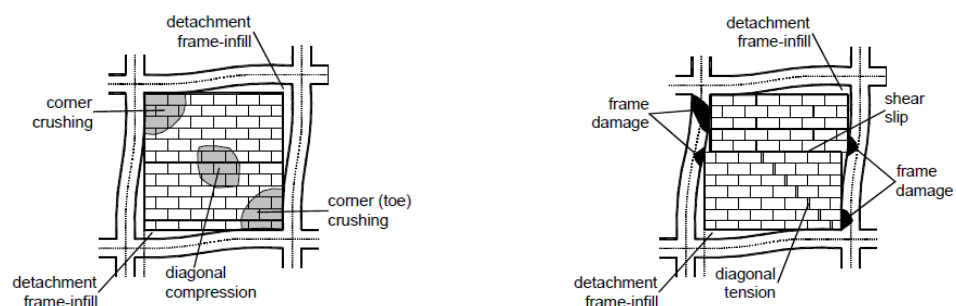


Figure 2.1 Modes of failure of masonry in-filled frames P. G. Asteris et al. (2011)

### 2.1.1 UNSTRENGTHENING INFILLED TYPE

Mehrabi Armin et al. (1996) describe an experimental investigation in which twelve-haft scale, single-story frame specimens were evaluated with both solid and hollow concrete masonry panels representing strong and weak infills. Two types of frames were designed: one designed to withstand wind loads, the other for severe earthquake forces. Brittle shear failure was observed in the columns of specimens characterized by weak frames and strong panels. The findings of this study indicate that infilled panels can enhance the performance of RC frames, but the load resistance and energy-dissipation capability are better in specimens with strong frames and strong panels. The stiffness and load resistance of the weak frame-weak panel specimen were 15 and 1.5 times larger than a bare frame, respectively, while the weak frame-strong panel specimen exhibited 50 times larger stiffness and 2.3 times greater load resistance. In comparison to specimens with weak frames and weak panels, specimens with strong frames and strong panels were more capable of withstanding loads and dissipating energy.

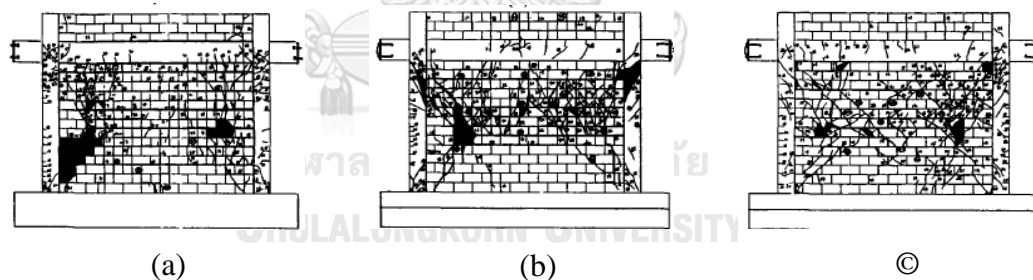


Figure 2.2 Damage Patterns Mehrabi Armin et al. (1996), (a) Sliding of Bed Joints, (b) Shear Failure Columns, (c) Corner Crushing

To assess seismic vulnerability, Ghassan Al-Chaar et al. (2002) conducted an experiment involving five half-scale, single-story models of brick and concrete masonry infilled RC frames with varying bay numbers, exposed to in-plane monotonic loading. When compared to bare frames, RC frames with infill have higher initial stiffness, residual strength, and ultimate strength. Additionally, this improvement is made while preserving the load-deflection behavior's ductility. The bare frame experiences over 5 times greater lateral displacement at peak load compared to the CMU (Concrete masonry unit) infilled RC frame. Single-bay brick

and concrete masonry infilled frames demonstrate similar load-deflection characteristics. Both frames achieve a peak load approximately 2.5 times higher than the bare frame, consistent with a Mehrabi Armin et al. (1996) study which reported a 1.5 times increase in load for infilled frames. The number of bays seems to impact maximum and residual resistance, failure mechanisms, and the distribution of shear stress. The double-bay CMU frame exhibited a peak load that was 3.9 times greater than the peak load of the single-bay frame, while in the case of the triple-bay brick, the increase was only 1.2 times, indicating a non-linear growth in capacity.

A variety of tests are included in the study Centeno et al. (2008), including a monotonic test and several shake table tests. For these experiments, two identical 1/2 scale gravity-load designed reinforced concrete frames (GLDRC) were employed. These frames featured unreinforced masonry infill walls constructed from hollow concrete blocks. Finding out how the infill-frame relationship, the reduction of stiffness, and the failure mechanisms interact was the objective. For static monotonic lateral loading, the unreinforced masonry (URM) specimen showed a diagonal crack pattern at 0.30% drift, hairline flexural cracks in the tension column at 0.60% drift, shear sliding at 1.00% drift, yielding at 1.25% drift, rebar slip at 1.65% drift, and rebar slip failure at lap splice region at 3.80% drift with no loss in strength. For the dynamic shake table test, the URM wall suffered various damages during tests, including mortar cracking, shear sliding, and masonry block collapse.

Zovkic et al. (2013) performed a series of experiments on ten RC frames which were built at a size of 1:2.5 and designed in compliance with EC8. The study included nine specimens with three different infill types (weak with AAC blocks, medium with MO5 brick blocks, and strong with MO10 brick blocks), as well as an unfilled frame. The experiment was focused on assessing the general performance of these specimens under cyclic lateral loads as well as constant vertical loads. The findings revealed that, compared to a frame without infill, a structure with an infilled frame exhibited noticeably higher initial strength, damping, and stiffness. Until the frame itself became dominant at 0.75% drift, the masonry infill efficiently covered the load capacity range from extremely low values (0.05%) up to certain levels of drift. Up to a drift of 0.1%, the structures showed linear monolithic features; at 0.3% drift,

they reached their maximal lateral capabilities; and at 0.75% drift, they maintained these capacities. Beyond this, their actions were governed by the frame's response.

Misir et al. (2012) conducted three 1/2-scale infilled RC frame specimens using various masonry infills, including standard and locked bricks, shown in Figure 2.3, were tested under cyclic quasi-static loading, each featuring different infill conditions. The result shows that the locked brick infill frame locked brick frame (LBF) experiences significantly less damage at high drift levels. At a 3.5% drift ratio, the locked brick frame specimen showed minimal brick breakage, with only plaster cracks observed, while the Standard brick frame (SBF) specimen lost numerous bricks due to diagonal forces. Remarkably, the absence of mortar in the standard brick frame specimen results in higher lateral resistance and stiffness in comparison to bare frame (BaF) and Lock brick frame specimens. The standard brick frame specimen also exhibits the highest energy dissipation, surpassing BaF and LBF specimens by 2.78 and 1.71 times, respectively, at a 1.5% drift level near the peak load levels.



Figure 2.3. Standard brick units and locked brick units

In their study, Tawfik Essa et al. (2014) performed a scheme of experimentation to study the behavior and ductility of high-strength RC frames (H.S.R.C) with infill walls under cyclic load. The parameters under investigation involve altering the frame panel from non-infill to infill, varying the thickness of the infill wall, and changing the type of bricks. The study involved testing four 1/2-scale specimens, including a bare frame (F1), infilled frames with 12cm red brick thickness (F2), 6cm red brick thickness (F3), and 12cm cement brick thickness (F4), examining variations in panel infill, infill wall thickness, and brick type. The result showed that the lateral load resistance for F2, F3, and F4 was greater than (F1) by about 184%, 61%, and 99%, respectively. The ductility factor for F2, F3, and F4 was less than the (F1) by about 57%, 51%, and 46%, respectively. The infill wall thickness influences



the rate of stiffness degradation in the frame, with a 158% greater initial stiffness observed in the 12 cm thick wall compared to the 6 cm thick wall.

Basha & Kaushik (2016) report an experiment of eleven half-scale, single-story RC frames in low-rise buildings with full-scale and half-scale masonry infills when subjected to slow cyclic lateral loading within the plane. The study was divided into two stages. Results from the first phase, eight frames were used in the study, and the results showed that, compared to the corresponding bare frames, brick infills at half and full scales displayed significantly higher stiffness between 7 and 10 times, strength between 1.6 and 2.5 times, and energy dissipation between 1 and 2.3 times.

Huang et al. (2016) investigated the seismic resistance of RC structures filled by weak panels and their interaction through experimental testing. The study investigated how the hysteresis behavior of infilled frames affects infill material properties and the aspect ratio panel. Five 1/2-scale RC frame specimens that were built based on the Chinese seismic code were used for this experiment. The test specimens consist of a bare frame (BF), a solid clay brick infilled frame (SCB), two hollow concrete block infilled frames (HCB) with panel aspect ratios of 1.5 and 2.0, and an aerated concrete block infilled frame (ACB). The study's findings demonstrated that the infilled frames surpassed bare frames during earthquakes, particularly regarding strength and energy dissipation capacity. Specimens IF-1, IF-2, and IF-4, which had the same aspect ratios but different infill materials SCB, HCB, and ACB, showed peak load increases of 60.8%, 36.9%, and 20.4%, respectively, compared to the control specimen BF. In terms of ductility factor, BF, SCB (IF-1), HCB(IF-2), and ACB (IF-4) infilled frame specimens with identical aspect ratios exhibited values of 6.02, 6.98, 3.86 and 7.42 respectively, indicating superior deformation performance. The cumulative energy dissipation of the infilled frames was approximately 1.07 to 1.34 times higher than the bare frame, indicating the positive impact of infills on the energy dissipation capacity.

Cai & Su (2017) investigated how full-scale RC (RC) frames filled with various lightweight materials responded to earthquakes. This study involves applying cyclic loads to the frames and focuses on a few different characteristics, including lateral strength, stiffness, damage pattern, ductility, and energy dissipation capacity.

The study was conducted using experimental testing of RC frames filled with panels made of autoclaved lightweight concrete (ALC), gypsum blocks, and hollow bricks (MHB). The paper concludes that the use of MHBs as infill material had a notable impact on the seismic response of infilled RC frames before the emergence of primary diagonal cracks. As a result of the relative motion between ALC panels, the frame incorporating ALC panels exhibited hysteretic behavior like the bare frame. Conversely, the specimen utilizing PBs showcased an intermediate level of hysteretic behavior, positioned between the frame with MHB blocks and ALC panels.

Kim & Yu (2021) conducted experiments on five specimens, which consisted of four masonry-infilled frames and a bare frame with different construction precision and masonry thickness to examine the impact of construction precision and the interaction between infill and the frame, illustrated in Figure 2.4. Specimens with thin walls exhibited diagonal tensile cracks alongside horizontal bed joint sliding cracks, while specimens with thick walls primarily experienced cracks in the diagonal direction, and specimens without a gap displayed numerous small cracks, whereas specimens with a gap demonstrated a limited number of large cracks.

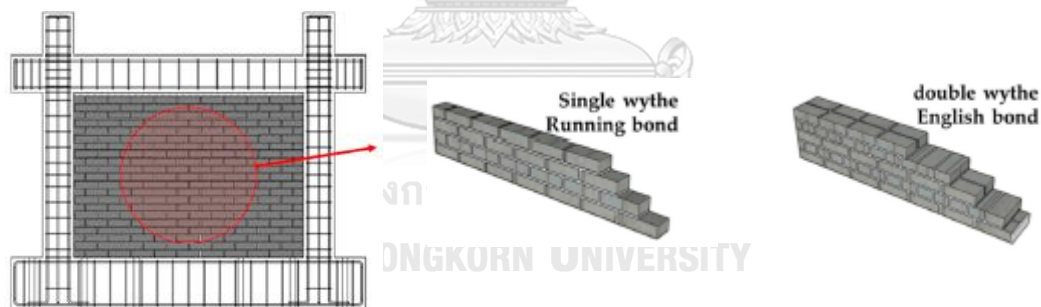


Figure 2.4 Details of a test specimen Kim & Yu (2021)

### 2.1.2 STRENGTHENING INFILLED TYPE

It is acknowledged that the strength of the masonry infill contributes significantly to the RC frame. The failure modes of infilled frames under in-plane loading include infilled crushing at the corner, diagonal infilled failure due to compression or cracking, shear sliding on the bed-joint of the panel, flexural failure of the frame, or combinations of the failure modes. Numerous research endeavors have been carried out to safeguard against these failure modes by investigating various Methods to reinforce masonry infill panels.

Erdem et al. (2006) conducted experiments using two 1/3-scale test specimens of two-story, three-bay non-ductile RC (RC) frames subjected to reversed cyclic quasi-static loading. One of the frames had a middle bay that contained masonry-infilled panels strengthened by diagonally placed CFRP strips, illustrated in Figure 2.5. In comparison to the RC bare frame, the results showed a considerable improvement in both lateral strength and stiffness, which were roughly four and ten times greater, respectively. Nonetheless, the story's drift capacity was quite limited, measuring just 0.4%.

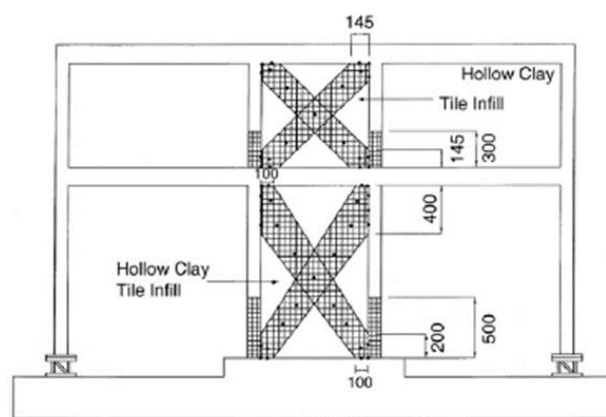


Figure 2.5 Configuration of CFRP strips for strengthening Erdem et al. (2006)

Altin et al. (2008) examined the performance of ten 1/3-scale, single-bay, single-story, clay brick-infilled, non-ductile RC frames with a panel length-height ratio of 1.73 under cyclic load. The researchers reinforced the masonry panels with diagonal carbon fiber reinforced polymer (CFRP) strips using various widths and three distinct configurations, including symmetric placement on both sides and placement either inside or outside the masonry walls. Their findings indicated that CFRP could enhance the test samples' stiffness and strength by approximately 0.54 to 1.61 times and 2.81 to 5.40 times, respectively, in comparison to the unstrengthening specimens. However, the lateral load capacity suddenly dropped after the ultimate load was reached. Symmetrically reinforced specimens demonstrated increased lateral strength and stiffness. specimens with CFRP strips of equal width applied to either the interior or exterior surface of the infill wall exhibited comparable levels of lateral strength and stiffness. Increasing the width of the CFRP strip resulted in enhanced strength and stiffness. Increasing the width of the CFRP strip from 13% to 20%, the

initial stiffness of the frame increases by 50% for both sides strengthening, and 31% to 36% for strengthening one side.

Yuksel et al. (2010) presented the results of their experiments on six 1/3 scale single-bay, single-story specimens of non-ductile RC frames with hollow clay brick infills. The researchers retrofitted these frames with different configurations of carbon fiber reinforced polymer (CFRP), such as cross-braced and cross-diamond-braced strips, as shown in Figure 2.6. The results showed that retrofitting the frames led to a significant boost in strength ranging from 14% to 69%, compared to the infilled frames without retrofitting. Moreover, the initial stiffness of the strengthened frames increased by 2.86 to 4.03 times more than the stiffness of the infilled frames without strengthening. Furthermore, when subjected to a 1% story drift, the strengthened specimens exhibited 1.6 to 2.7 times greater cumulative energy dissipation than the infilled frames without strengthening. When comparing specimens at the same story drift levels, the cross-braced and cross-diamond-braced frame specimens demonstrated significantly lower damage than the other specimens in the tests. The results from the experiment revealed significant potential in utilizing cross-diamond bracing to strengthen current-infilled RC frames against in-plane seismic loads.

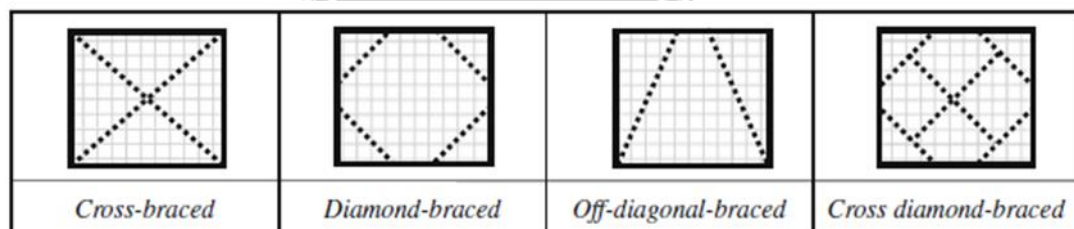


Figure 2.6 Alternative CFRP retrofitting scheme Yuksel et al. (2010)

Gokce Kurt et al. (2012) utilized to examine the seismic response of two-story, three-bay frame structures with hollow clay tile infill when subjected to three different levels of Duzce ground motion scaling (50%, 100%, and 140%). This investigation aimed to assess the effectiveness of two retrofit Methods, namely fiber-reinforced polymers and precast concrete panels, on the seismic performance of these buildings. The control sample underwent extensive damage at the full-scale level, progressing to a state of collapse. This was attributed to the loss of stability of the infill wall and substantial deterioration to the columns at the perimeter. The retrofitted test structures successfully endured the most intense level of ground motion, which was 140% of the

Duzce standard. Both retrofitted schemes, aimed at achieving similar strength and stiffness properties, exhibited satisfactory performance, with the CP application reducing overall displacement demands while the FRP retrofitted specimen effectively preserved the integrity of the wall and dissipated energy through rocking.

Erol & Karadogan (2016) experimented on non-ductile masonry-infilled RC frames reinforced with diagonal CFRP strips. The experimental study involved two parts: conducting diagonal tension tests on 28 masonry wall panels and subjecting six one-story, one-bay RC frames to cyclic in-plane lateral loads. The results showed that the lateral strength of the reinforced specimens increased by approximately 0.23 to 0.79 times, compared to the specimens without reinforcement. Energy dissipation values are reduced in bare frame specimens, whereas there is no notable distinction in energy dissipation values between the infilled reference specimen and the reinforced specimens.

Leeanansaksiri et al. (2018) investigated how three full-scale RC frames using various forms of reinforcement responded to earthquakes. These featured a frame made of plain concrete (BF), a frame filled with brick masonry (W), and a frame with masonry fill that was reinforced with an extended metal sheet (W-SR). Under cyclic loading conditions, the examination was carried out. Expanded metal sheet (W-SR) reinforcement for infilled frames produced lateral strengths, stiffness, and energy dissipation capacities that were 1.25, 1.26, and 1.27 times more than the infilled brick frame (W), respectively. The infill panel's strength is significantly increased by its use of ferrocement with expanded metal, avoiding the sliding failure mode from switching to the corner crushing mode.

Longthong et al. (2020) conducted a study on enhancing the strength of RC frames and brick infill panels by utilizing the ferrocement technique reinforced with expanded metal, aiming to prevent shear failure in the frame's beams and columns as well as corner compression failure in the infill panel, while subjecting the frames to both constant vertical load and lateral cyclic load. The strengthened frames exhibited a remarkable strength improvement of 64% and 87%, while the ductility capacity increased by 77% and 66% for the bare frame and the infilled frame respectively.

### 2.1.3 INFILLED FRAME STRENGTH RATIO AND ASPECT RATIO

Smith & Carter (1969) introduces an analytical approach to assess the stiffness and strength of horizontally loaded infilled frames. Additionally, it explores how the length-height ratios of the infill and the stiffness relationship between the column and the infill impact the strength associated with diagonal cracking. The results show that the diagonal cracking strength of the infill is affected by the length-height proportions of the infill.

Mehrabi Armin et al. (1996) conducted experiments on twelve 1/2-scale models of single-story, single-bay, infilled concrete masonry panels with RC frames. The frames were categorized into two types: weak frame was designed to resist wind load and strong frame was designed to resist strong earthquake. Three main failure mechanisms were observed Mehrabi Armin et al. (1996), which depended on the surrounding frame and infill panel strength ratios.

- Weak frames-weak infilled: frame flexural failure and shear sliding along the bed joint of the infill panel.
- Weak frame-strong infill: column shear failure was predominant.
- Strong frame-strong infilled: the corner crushing of the unreinforced masonry (URM) panel, a diagonal strut mechanism was found to develop.

After the first stage of the Basha & Kaushik (2016) experiment, which indicated the use of relatively weak masonry, shear failure predominantly occurred in columns. This resulted in an enhancement of column shear design in compliance with current seismic standards, followed by the retesting of three improved frames in the second stage. Three ways were used to improve the shear strength of columns, including improved shear capacity throughout the length of the column, in critical regions and using high strength bars in critical regions. The resulting experiment showed that the lateral load carrying capacity and energy dissipation capacity were approximately 1.2 to 2.4 times and 1.42 to 1.78 times higher, respectively than the bare frames. The result of the experiment showed the occurrence of shear failure at higher drift levels in the improved frames. The inadequacy of the current design regulations was highlighted by the realization that shear collapse in columns could not be prevented.

Five half-scale, single-story RC frame specimens were tested by Huang et al. (2016) using infill-panel aspect ratios of 1.5 and 2.0 and various weak masonry-infill materials. The specimens were evaluated under seismic loading and constant axial compression. The utilization of the same hollow concrete block (HCB) infill in a panel with an aspect ratio of 2.0 leads to a 23% increase in peak load compared to an infilled frame with an aspect ratio of 1.5, while exhibiting displacement ductility factors of only 3.86 and 2.76, respectively.

Alwashali et al. (2017) explored the effect of varying frame strength on the seismic performance of masonry infill walls using two half scale specimens featuring various RC frames and the same masonry infill walls. WF (weak frame) and SF (strong frame) specimens have boundary frame-to-masonry infill lateral strength ratios of 0.4 and 1.5, respectively. The results showed that increasing the shear strength ratio of frame to masonry improved the strength and avoided sudden brittle behavior. However, the early stiffness and story drift at peak strength were not significantly affected by changing the strength of the frames. In comparison to a weaker frame, the shear strength of the masonry-infilled strong frame improved by up to 1.5 times excluding frame shear strength. The capacity of the masonry infill in the horizontal plane is primarily determined by the specific failure mode, which includes diagonal compression and sliding shear failures. Experimental results reveal a combination of compression and sliding failures. According to the study, the masonry compressive prism strength as well as the ratio of shear strength of frame-infill were both directly connected with the deformation limits of the infill.

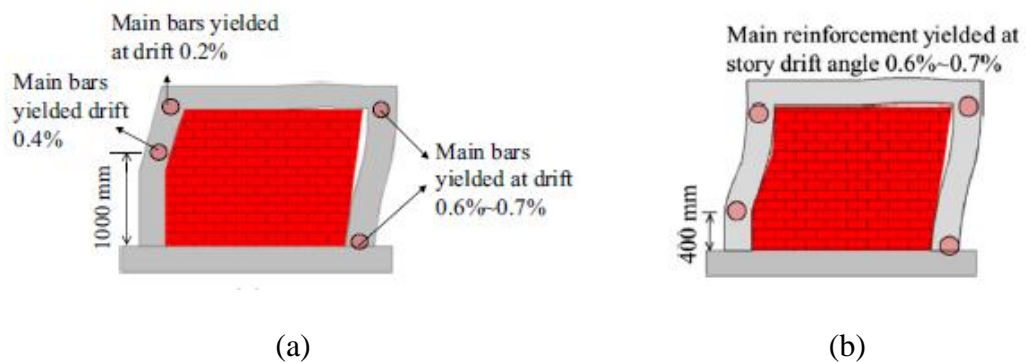


Figure 2.7 Hinge locations formed in RC frame Alwashali et al. (2017): (a) Specimen WF, (b) Specimen SF

In the study of Wararuksajja et al. (2020), two full-scale intermediate reinforced concrete (RC) moment-resisting frame specimens were subjected to experimentation. The purpose was to investigate the interplay between infill concrete block walls and frames. The specimens were primarily differentiated by the compressive strength of the block wall and the shear strength of the columns. These variations aimed to represent significant disparities in both the strength of the frames and the infill walls. From the experiment, due to corner crushing, an initial gap arises in the infill wall of frames with strong infill as shown in Figure 2.8.b. The column mechanism is then followed by rapid column failure due to shear caused by a short captive column. However, in cases where the infill within frames is not strong, the infill wall being crushed moves downwards, leading to a gap that slowly widens until the columns undergo either shear or flexural failure. This phenomenon is referred to as the column-infilled mechanism.

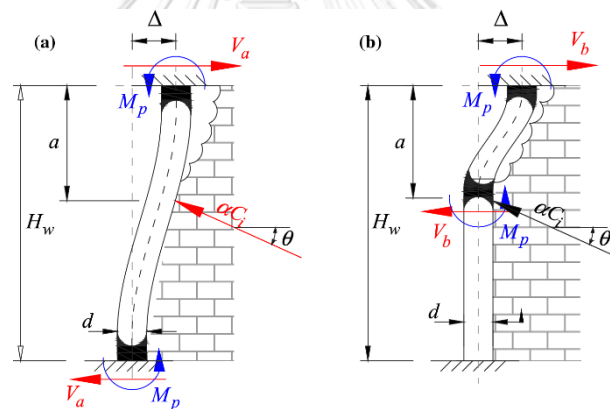


Figure 2.8 Failure mechanisms of columns Wararuksajja et al. (2020)

Based on the analysis of existing literature, it is evident that studying infilled frames is crucial due to their significant impact on a building's overall structural behavior. Infilled frames offer advantages like increased stiffness, strength, ductility, and energy dissipation capacity, playing a vital role in redistributing lateral loads, such as wind and seismic forces, throughout the structure. However, their presence can introduce complexities and vulnerabilities that engineers must consider during the design process. Several studies have highlighted that damage often starts with the infilled walls, leading to alterations in the structure's behavior, eventually resulting in building collapse due to the emergence of soft-story and short-column mechanisms.



Furthermore, the behavior of infilled frames under in-plane loading is influenced by multiple parameters that affect their structural response and performance. These parameters encompass infill material properties, aspect ratio (height to width) of infill panels, frame-infill interaction, frame member properties, construction quality, and others. A comprehensive understanding and proper consideration of these parameters are essential for precisely analyzing and designing infilled frames, ensuring that structures are resilient and capable of withstanding lateral cyclic loads effectively.

## 2.2 BEHAVIOR OF INFILLED RC FRAME WITH OPENING

The use of infilled frames with openings is widespread in diverse architectural styles and building Methods, where the openings can be in the form of windows and doors. The comprehensive collection of test results from experiments using infilled frames made of steel and RC Huang & Burton (2020) showed that the number of studies on the behavior of masonry infilled frames with openings is still limited. Remarkably 66.7% of the specimens feature centrally located openings, while 33.3% have openings positioned off-center on the panel.

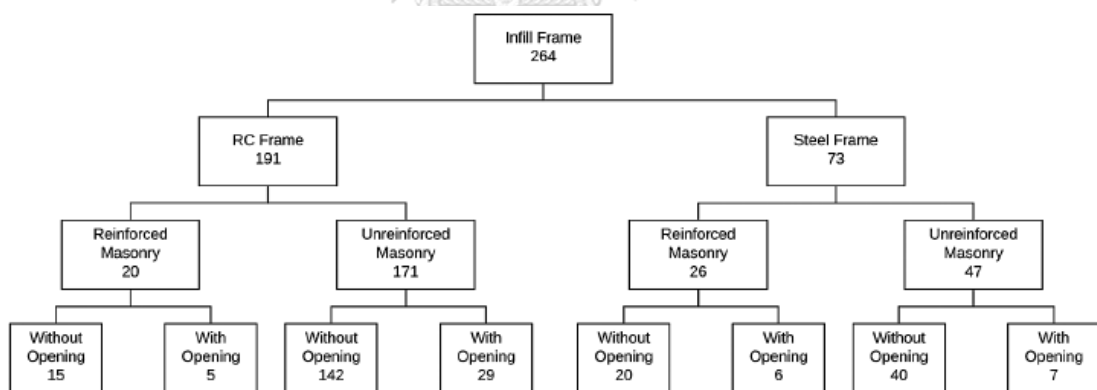


Figure 2.9 Summary of the specimen types in the database Huang & Burton (2020) Here are some papers that investigate the presence of an opening with different aspects such as opening size, opening location, and the boundary surrounding the opening.

Holmes (1961) conducted experiments on steel frames with brickwork and concrete infilling with openings within the infill. These openings led to reductions of 30% and 40%, respectively, in the ultimate load. However, if these openings had been

appropriately reinforced with framing, there would likely have been a minimal reduction in the ultimate load.

D.V. Mallick & R.P. Garg (1971) experimented to investigate how opening positions influenced the lateral stiffness of the infilled frame with and without shear connectors. A self-equilibrating frame was fabricated and tested then compare the results with theoretical prediction using the FEM approach. It is concluded that when an opening is positioned at either end of the loaded diagonal in an infilled frame with shear connectors, its strength diminishes by approximately 75%, and its stiffness experiences a reduction of around 85-90% in comparison to a solid infilled frame. For optimal placement, it is recommended to position door openings at the midpoint of the panel's lower half. As for window openings, it is recommended to position them within either the left or right half of the panel's middle part, situated near the vertical edge. T.C. Liauw & S.W. Lee (1977) reported an experimental study of four-story steel frames with RC infills with and without openings, and infilled frames with and without connectors. The opening was the central door with varying widths was examined in the experiment. It was found that the infilled frame's lateral stiffness and strength were significantly improved both with and without opening, by the infilled frame. The infilled frame with an opening change the behavior of the structure when the opening is across the compression diagonal as a result of producing additional bending and shear in the wall and frame and also reducing the strength and stiffness of the structure.

Schneider (1998 ) present an experimental study of unreinforced masonry-infilled steel frames to evaluate the in-plane seismic behavior. Masonry pier width and number of wythes are the parameters of the study. The steel column was surrounded by infilled walls on each side to represent the interior column. It is observed that the deterioration of infill strength and stiffness is independent of the pier width and number of wythes. With a drift of 0.20%, the infilled stiffness decreases by over 70% compared to its initial effective stiffness, and the remaining stiffness deteriorates with a drift of 2.0%. On the contrary, the ductility of the infilled frame depends on the pier width and number of wythes. Narrow piers exhibited higher ductility compared to wider piers, leading to reduced visible brick damage during large drifts. The infills

made of double wythes generally exhibited greater ductility compared to the infills consisting of single wythes.

Buonopane & White (1999 ) conducted a pseudo-dynamic test on a half-scale, two-story, two-bay reinforced concrete frame with masonry infill. The study focused on frames containing openings positioned centrally within the infilled wall on the second floor, aiming to investigate their seismic performance. Observations reveal that the infill on the first story experienced degradation with lengthy bed joint cracks, leading to a soft story response. Conversely, in the second story, a stepped crack pattern developed, which stabilized the structure and prevented substantial drifts. In the lower story, a strut mechanism forms, which is influenced in terms of its configuration and capacity by multiple shear failure planes. In the second story, the formation of the strut is compelled to occur at a steep incline due to the presence of an opening. This arrangement provides sufficient normal force to prevent bed joint cracking. Both above and below the window openings, the bed joint cracks almost entirely as shown in Figure 2.10. Therefore, window opening causes a possible off-diagonal strut mechanism in the undamaged panel.

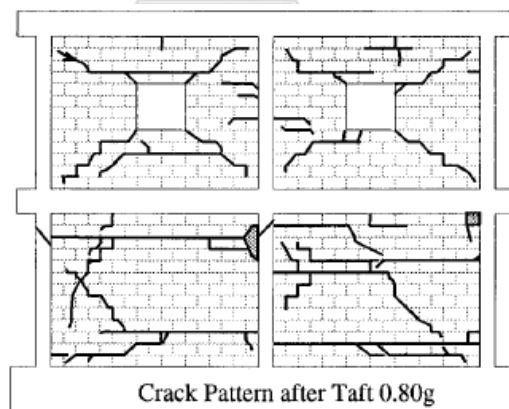


Figure 2.10 Final Crack Patterns Buonopane & White (1999 )

Yáñez et al. (2004) conducted experiments on 16 full-scale specimens infilled RC frame with four pattern openings, as shown in Figure 2.11, and two different types of infills, including 8 specimens with concrete masonry and other 8 specimens with hollow clay brick masonry, underwent testing under lateral cyclic load to evaluate the deformation capacity, stiffness, strength degradation, maximum shear strength, and energy dissipation. It is noticed that each pattern was built with two specimens. The

result of the experiment indicated that two failure mechanisms appeared in all specimens including diagonal cracking and mixed cracking. The infilled frame with an opening ratio of about 30% (pattern 2) carried the lowest maximum strength capacity and initial stiffness compared to the other opening patterns. It can be noticed that the concrete masonry infilled type presents smaller strength degradation than the hollow clay masonry type. Concrete masonry walls have a 25% to 40% lower energy dissipation capability than brick masonry walls when the inter-story drift is 10.5. It is evident that as the net transverse area shrinks, so does the shear capacity.

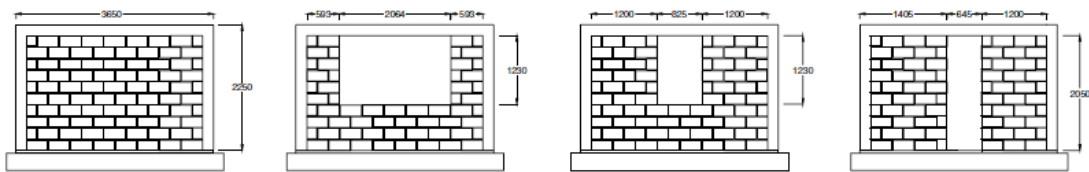


Figure 2.11 Wall dimensions Yáñez et al. (2004)

Kakaletsis & Karayannis (2007) they have carried out a study using eight reduced-scale models of single-story, single-bay frames characterized by a height-to-length ratio of 1/1.5. These models were subjected to simulated cyclic loading, reaching a drift level of 40%. The purpose was to examine how the presence of masonry infills featuring off-center window and door openings affects the earthquake behavior of RC frames. The investigation involved altering the shape and position of the openings as variables. It was observed from the experiment that both solid and opening infilled frames have lateral load carrying capacity, initial stiffness, and energy dissipation capacity varying from 1.38 up to 1.84 times, 1.52 up to 2.48 times, and 1.02 up to 1.57 times higher, respectively, than the bare frames. The ductility factor of the infilled frame corresponds to 85% of the maximum range from 2.54 up to 5.39 while the bare frame and solid infilled frame have ductility of 3.97 and 4.24 respectively. The central opening has the lowest ductility. RC column shear failure was not observed, and the presence of infills prevented beam bending, consequently resulting in the development of plastic hinges as the experiments nearly ended. Positioning the opening close to the infill edge improves the infilled frame's performance by increasing the energy dissipation through friction along the bounding frame, especially for larger piers that enable uniform crack distribution, while placing the opening at the center of the infill weakens the tensile strength within the infill,

causing increased pier deterioration at lower drift levels, with smaller piers being less effectively protected by this energy dissipation mechanism.

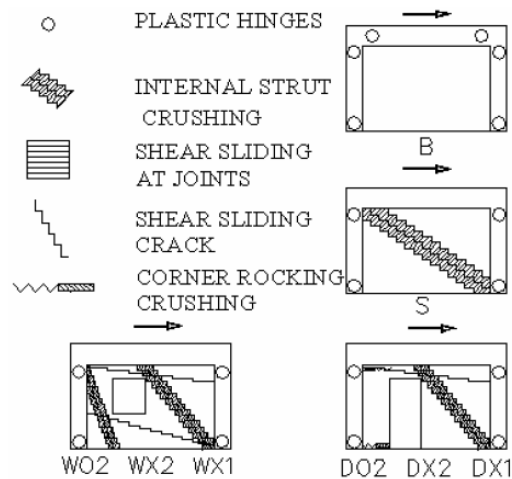


Figure 2.12 Collapse mechanisms Kakaletsis & Karayannis (2007)

Kakaletsis & Karayannis (2008) conducted a study to examine the seismic response of masonry-infilled frames containing openings. The investigation specifically concentrated on the impact of central openings including windows and doors on the hysteresis properties of infilled frames. Furthermore, the study explored the behavior of masonry infills with varying compressive strength (both weak and strong) but similar shear strength. Experiments were performed on seven models of single-story, single-bay frames at a scale of one-third. These models were subjected to repeated horizontal loading until they reached a displacement of 40%. The experimental findings highlight that the presence, behavior, and failure of infills, even in scenarios with openings, can substantially enhance the performance of RC (R/C) frames. Moreover, specimens featuring strong infills demonstrate superior performance compared to those with weak infills, as evidenced by their observed load resistance, ductility, stiffness, and capacity to dissipate energy. As evidence from the result of the experiment indicated comparing infilled frames with apertures to bare frames, the lateral strength of the infilled frames exhibited a noticeably larger magnitude from 1.33 to 1.54 times, while the presence of fully infill panel with weak and strong infills increased the resistance by 1.84 and 1.65 times respectively; the infills with openings also substantially increased the initial stiffness (1.57-2.50 times) and ductility factor (3.20-6.77 times) of the frames, with solid weak and strong infills

exhibiting even higher stiffness (2.48 and 2.62 times) and ductility (4.24 and 6.31 times) values. Furthermore, the overall energy dissipation capacity of infilled frames containing openings ranged from 1.02 to 1.43 times that of frames without infill, while solid weak, and strong infills had capacities 1.57 and 1.42 times greater respectively.

Kakaletsis & Karayannis (2009) conducted an experiment on eight of the one-third scale of

frame specimens with different shapes and the size of the opening tested under reversed cyclic to observe the seismic performances. The results of the experiment demonstrated that different types of openings have an impact on diminishing the strength, stiffness, and ability to dissipate energy in all the testes of infilled frames. For window openings spanning 25% to 50% of the length of the masonry infill, the mean decrease in lateral resistance, initial stiffness, and cumulative energy dissipation capacity was 18.7%, 26.3%, and 4.3% respectively. Conversely, door openings within the same width range resulted in an average reduction of 28.7% in lateral resistance, 30.3% in initial stiffness, and 27% in capacity to dissipate energy cumulatively. Increased openings appear to a greater ductility and a higher ultimate limit state.

Tasnimi & Mohebkhah (2011) investigate the impact of various void distributions and shapes on the seismic response of steel frames in the center region of clay brick masonry infill. Six single-story steel frame specimens were constructed and subjected to experimental testing. These specimens included the following configurations: a bare frame, fully infilled walls, a frame with a central opening, a frame with strong piers and weak spandrels, a frame with weak piers and strong spandrels, and a frame with a central door. The researchers found that subjecting infill panels, whether with or without openings, to cyclic in-plane loads at the roof level leads to an enhancement in the earthquake resistance of the steel frames. The strength and stiffness of the specimen fully infilled frame (SW) were 6.15 and 3.06 times greater respectively than those of the specimen bare frame (BF). The ductility of frames featuring infill and openings is influenced by the failure mode, as shown in Figure 2.13, exhibited by the infill piers, and they generally exhibit lower ductility factors due to pier diagonal tension or toe crushing failure compared to frames with

solid infill. Frames containing deep spandrels allowing the formation of cracks along the robust spandrel beam exhibit greater energy dissipation compared to frames with shallow one including the position of the lintel beam above the opening effectively transmit the inclined forces from the spandrel to the adjacent infill piers.

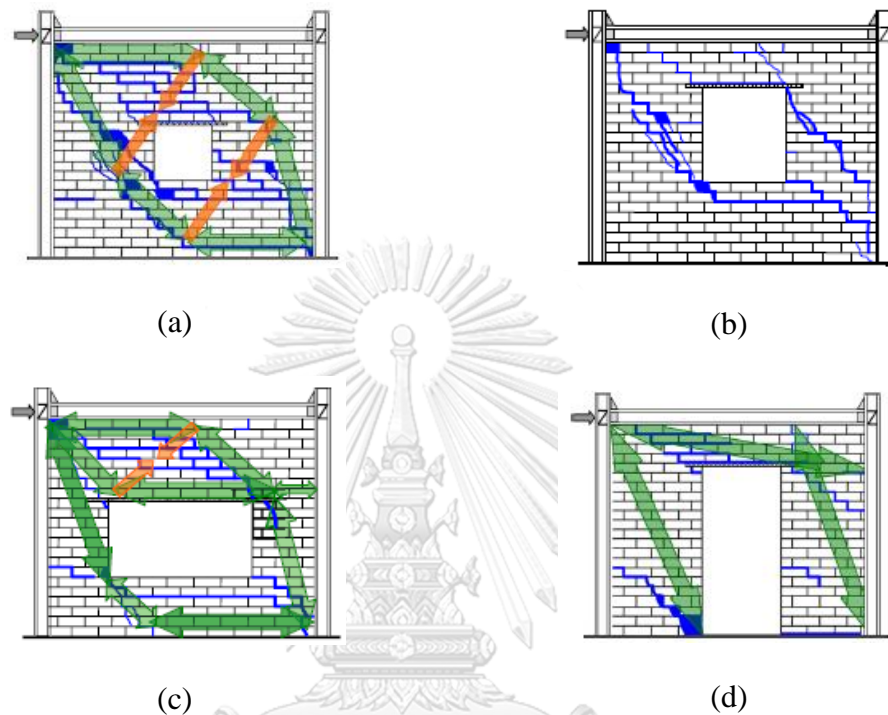


Figure 2.13 Failure modes of the specimen and the activated stress field, (a) Specimen PW1, (b) Specimen PW2, (c) Specimen PW3 and (d) Specimen PW4

P.G. Asteris et al. (2011) study experimental results involved three parameters, including clay brick infill, opening size as a percentage of the infill area, and the location of the opening within the frame Kakaletsis & Karayannis (2007; Kakaletsis & Karayannis (2008), to classify the potential ways in which RC frames with openings can fail, the study employed ten reduced-scale models of single-bay, single-story structures. These models were subjected to gradually applied cyclic horizontal forces. A comparison of crack patterns in specimens with door and window openings in weak infill panels revealed that failure mechanisms were governed by plastic hinges, internal crushing of masonry segments, and shear sliding of masonry zones. The well-known failure modes of diagonal compression mode and diagonal cracking were eliminated by the infill panel's diagonal opening.

Sigmund & Penava (2013) conduct the experimental study of ten scale 1/2.5 of one-story, one-bay, masonry infilled RC frames designed according to Eurocode with openings specimens were tested. Medium-sized openings for windows and doors were positioned both centrally and off-center and were constructed with and without adjoining vertical columns. Masonry infill contributes to stiffness, strength, and damping within a low drift range, with damage levels increasing at higher drifts. Framed-wall structures possess a stiffness three times greater than bare frames and tie columns play a role in enhancing strength and stiffness, particularly at larger drift. One large pier is better than two smaller ones for lateral strength and stiffness, and window openings are more favorable than door openings due to premature loss of stability in masonry absence of ties. Infill with an opening affects the failure mechanism, with diagonal cracks and corner crushing in specimens without ties, while ties prolong strength and stiffness in specimens with ties. The infilled panel plays a beneficial role in enhancing the stiffness, strength, and damping of the infilled frame, resulting in higher ductility values and behavior factors compared to confined masonry walls. However, it's important to consider potential soft story mechanisms.

Mansouri et al. (2014) conducted an empirical investigation involving six reduced-scale, single-story, single-bay frame models. These models featured varying arrangements of openings such as shape (windows and doors), size (regular or massive), and placement (either eccentric or central). The specimens were subjected to lateral loading within the plane of the structure. The experiment's findings showed that the existence of openings influences the mechanism of failure as illustrated in Figure 2.14, enhances the level of damage, and decreases the stiffness, strength, and ductility of the frame-infilled wall. Strength, effective stiffness, and energy dissipation capacity were decreased by 29%, 34%, and 23%, respectively, because of the reduced door opening. Average reductions in strength, effective stiffness, and energy dissipation capacity were 23%, 8%, and 11%, respectively, due to the window openings. The plastic hinges were found in all frames without brittle shear failure on the column because of the relatively low infilled of specimens. Meanwhile, the fully infilled frame failed due to shear sliding at the bed joint, while the infilled frame with openings experienced a mix of shear sliding at the bed joint and diagonal cracking of the pier panel wall, resulting in a more ductile behavior in the fully infilled frame.



When assessing door and window of equivalent size and positioning, it was observed that the door opening incurred more pronounced decreases in ultimate strength, stiffness, and dissipating energy than the presence of a window. The load resistance mechanism and degree of damage to the specimen were unaffected by widening the opening, while stiffness and energy dissipation capacity were decreased.

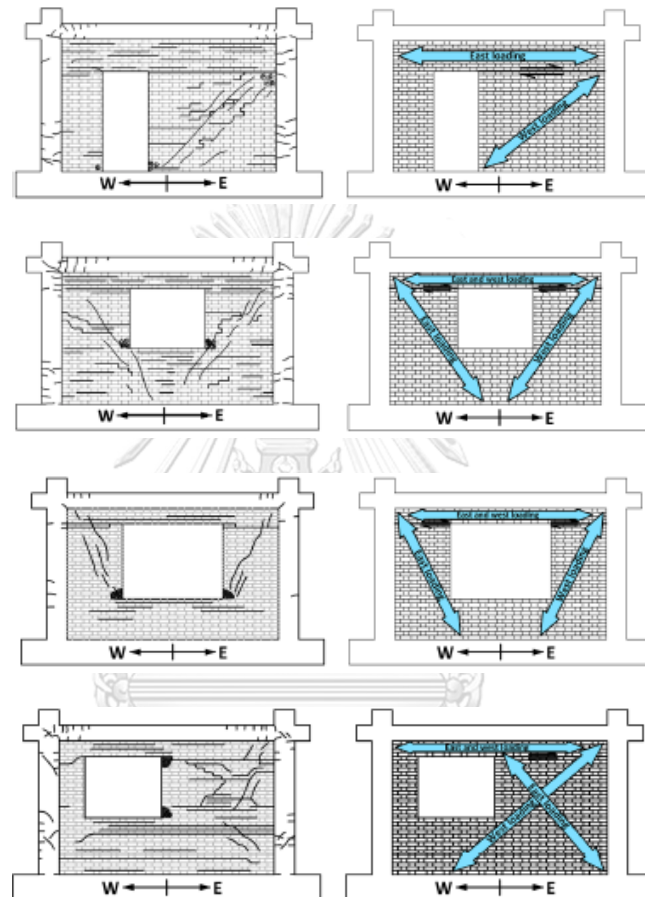


Figure 2.14 Damage pattern and resistance mechanisms Mansouri et al. (2014)

Zhai et al. (2016) presented findings from testing four full-scale reinforced concrete (RC) frame specimens. These frames were infilled with weak masonry and were subjected to both vertical and quasi-static lateral cyclic loading. The objective was to examine the seismic behavior of these frames in the presence and absence of openings. The initial three samples share a panel aspect ratio of 0.93. They vary in infill configuration, encompassing an unadorned frame, a solid infilled frame, and an infilled frame with a centrally positioned opening accounting for 20% of the total area, as shown in Figure 2.15. The last specimen has a 0.72 aspect ratio of panel with a central window opening of 20%. Due to the relatively lower strength of the masonry

infill in the frames, observations showed that at the base of columns, the formation of plastic hinges and the absence of brittle shear failure. For a fully infilled panel, diagonal cracks initially emerged at the center of the infilled panel, subsequently propagating towards the corners before leading to crushing. In the case of the infill consisting of an opening, the central opening's corners were where cracks first appeared, and they spread to the masonry infill's edge, while alterations to the aspect ratio of the panel influenced the extent of damage experienced by the lateral piers and the lower spandrel. Specimen 2, 3, and 4 reached their maximum loads at the drift of 0.53%, 1.34% and 1.59% respectively. After reaching the peak load, specimen 2 dropped the resistance dramatically and specimens 3 and 4 were constant and slightly decreased respectively. The solid infill wall dramatically increased the lateral stiffness and strength at a small drift ratio, greatly improving the overall seismic performance of the structure, while the central window opening reduced the stiffness and strength, and it found that the infill wall had a greater impact on stiffness than load-resisting capacity. The infilled RC frame absorbed more energy dissipation than the bare frame. The energy dissipation of specimens 2, 3, and 4 was greater than that of the bare frame by 32%, 45%, and 33%, correspondingly.

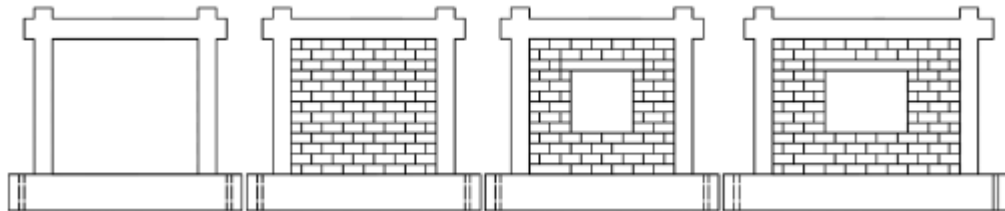


Figure 2.15 Test specimens Zhai et al. (2016)

Su et al. (2016) examine the seismic performance of three full-scale RC frames including strength, stiffness, ductility, and energy dissipation capacity under cyclic loads, and with a focus on the effects of infills and openings, tests were conducted on the structures. The test specimens include a bare frame, an infilled frame with door and window opening (25.7% opening ratio), and a fully infilled frame. The experiment shows that at the initial state, infilled masonry walls, particularly those without openings, have a substantial impact on the stiffness and capacity to withstand deformations of reinforced concrete frames. The findings indicate that incorporating MHB infills can alter the failure pattern of the reinforced concrete (RC) frame,

shifting it from a mode where the beams are stronger than the columns to a mode where the columns are stronger than the beams. Despite the diminished effectiveness of the diagonal strut action within the partially infilled wall, the force-displacement characteristics and damage progression of the infilled frame remained remarkably consistent and stable. In terms of maximum lateral strength, the fully infilled frame and partially infilled frame carried 2.79 times and 1.64 times better than the bare frame respectively. The completely infilled reinforced concrete (RC) frame displays its maximum initial stiffness, which is 5.85 times greater than the stiffness demonstrated by the frame without any infill, followed by the partially infilled frame by about two times. The frame fully infilled exhibited a ductility ratio of 1.37 followed by a bare frame and opening with 2.13 and 2.65 respectively. The result also indicated that the fully infilled and partially infilled have higher total energy dissipation about 1.4 times and 1.24 times respectively compared to the bare frame.

Niyompanitpattana & Warnitchai (2017) describes an experimental study of the global and local effects on a gravity load-designed RC frame with the infilled panel consisting of a length-to-height aspect ratio of 2.7. Five RC frames, designed for gravity loads at half scale and possessing an aspect ratio of 2.7, underwent testing. These frames incorporated different types and sizes of openings within masonry infill walls and were subjected to cyclic quasi-static loads. There were four distinct infill wall arrangements tested: a fully infilled wall, a partial height wall, and two partial width walls. The result concludes that the seismic response of gravity load-design RC frames with long spans is significantly impacted by the exiting of the opening in the infill panel. It is significantly distinct from conventional diagonal struts in those two formations of compressive struts on the fully infilled wall, instead of the corner itself, the upper strut extremities are directed to the base with a substantial offset from the opposite corner. The side opening exhibited behavior akin to a single strut. The side opening functioned similarly to a single strut, becoming active only when the wall was subjected to force from the frame. This led to an asymmetrical cyclic force-deformation behavior in the infilled frame.

Mansouri et al. (2018) reported on an experiment result of six, 1/2 scale RC frames with weak masonry infill with various shapes, sizes, and locations were

subjected to horizontal in-plane loading. A fully infilled frame, a bare frame, two specimens with windows at center of various sizes, a specimen with an eccentric window, and a specimen with an eccentric door are all test specimens. The suggested analytical approach for analyzing the horizontal strength of infilled frames depends on considering the observed failure mechanism of the test.

The lateral strength of the frame-infilled weak panel can be approximated as the combined flexural bare frame strength and the panel shear strength. At the ultimate limit state, when the corner crushing is exhibited on the panel, lateral strength could be estimated through the corner crushing failure mode. The primary mechanism for resisting loads in infilled frames with central openings was the development of compression struts and diagonal cracking within the masonry pier on the windward side. This ultimately determined the lateral strength of the infill panel, with calculations based on the lowest values of corner crushing resistance and diagonal tension on the pier on the windward side. The lateral resistance of the infill containing eccentric openings could be determined by analyzing diagonal tension, corner crushing behaviors, and the sliding of bed joints.

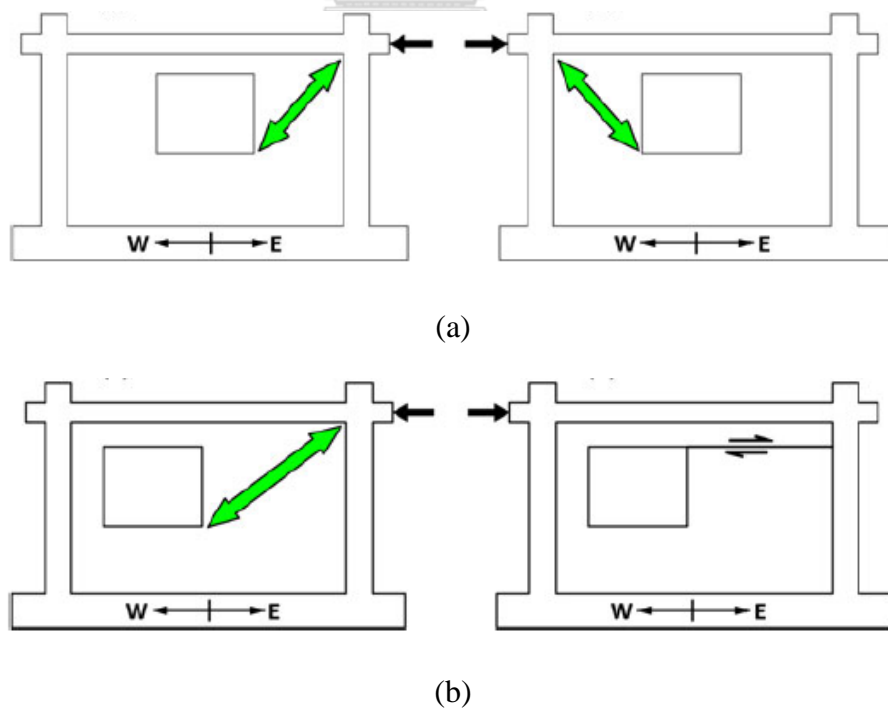


Figure 2.16 Major load resistance of specimens presence of central and eccentric openings Mansouri et al. (2018)

Maidiawati (2019) studied the experimental results of six 1/4-scale, single-bay, single-story brick masonry RC frames with central openings. The test specimens incorporated a bare frame, a solid infilled frame, a frame infilled by 20% opening with and without rebar reinforcement, and an infilled frame with 40% with and without rebar reinforcement. The embedded steel was placed below and above the opening. It is concluded that the presence of an opening diminishes the stiffness, lateral strength, and energy dissipation of the RC-infilled frame system. Nevertheless, infilled frames with opening ratios of 25% and 40% demonstrate superior performance when compared to the bare frame specimen. The additional embedded rebars did not yield a substantial improvement in the performance of the RC frame system, but it effectively resisted significant out-of-plane deformation.

Ahani et al. (2019) enhanced the accuracy of accounting for the presence of openings, on a half-scale, infilled aspect ratio 1.5, clay brick infilled RC frame with a central opening percentage of 19%, was tested and studied under lateral cyclic loading. The result of the experiment was utilized to reproduce the behavior infilled frame through a simplified micro-modeling Method. The initial crack in the masonry infill appeared along the upper portion of the opening and on both sides with deeper diagonal cracks than the upper and lower cracks of the opening. The infilled structure demonstrated collapse as horizontal cracks developed in the top and lower sections, together with inclined cracks on both sides of the opening, during the final stage of loading.

Eight half-scale, single-story RC frames with aspect ratios of 1.0 were used in an experiment by Humayun Basha et al. (2020) to investigate the horizontal load response of RC frames with a range of central apertures and fly-ash brick masonry infill with area ratios of 3%, 10%, 20%, 30%, 40%, and 50%, as shown in Figure 2.17. The experiment shows that masonry-infilled RC frames with central apertures perform superior to frames without openings, with less lateral stiffness, better lateral deformation, and greater dissipation energy. As the size of the openings increased, the lateral strength and stiffness of the frames with openings decreased. However, these values remained higher than those of the frame without any infill. The lateral load response of masonry-infilled RC frames with wall openings differs from that of

frames without openings, with cracks caused by shear in columns initiating at a greater drift ratio than flexural cracking. Openings in the frame-filled wall showed it to have lateral strength ranging from 2.1 to 1.25 times more than the bare frame, whereas the completely infilled frame showcased a capacity approximately 2.5 times greater than that of the bare frame. The capacity for withstanding lateral loads varied between 2.0 and 1.3 times for opening sizes of 10%, 20%, and 40%, respectively, while it was discovered that infilled frames with apertures had an initial stiffness that was 10 to 4 times greater than that of the bare frame. The energy dissipation of the infilled frame with an area openings ratio of 3% to 30% dissipated higher than the bare frame from 1.08 to 2.44 times while the specimen with an area opening ratio of 10% was found to be the highest one. Specimens with area opening ratios of 40% and 50% were found to be less than the bare frame.

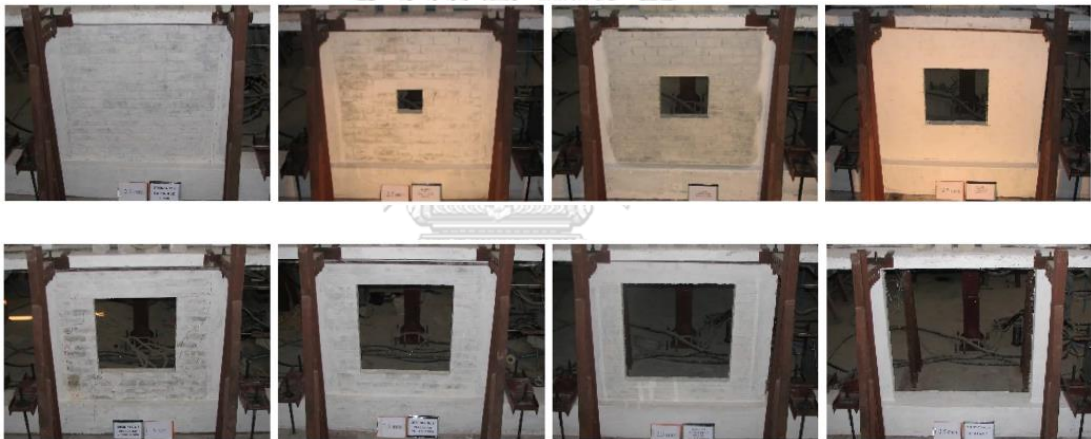


Figure 2.17 Test specimens Humayun Basha et al. (2020)

Khan et al. (2023) investigate a lateral cyclic loading setup on eight 2/3-scale, square panel, hollow brick RC frames. The study included testing of an infilled frame with different sizes and locations of openings, notably (central window, side window, and central door), and with and without infill. Two replicas were made for the infilled frame with the opening. Openings within masonry infills significantly change the total seismic responses. When compared to the bare frame, the fully infilled frame's initial rigidity was around 21 times greater; however, the presence of openings caused this initial stiffness to be lowered by nearly 70%. With a specified opening ratio, the peak load did not show a significant decrease in comparison to the fully infilled frame.

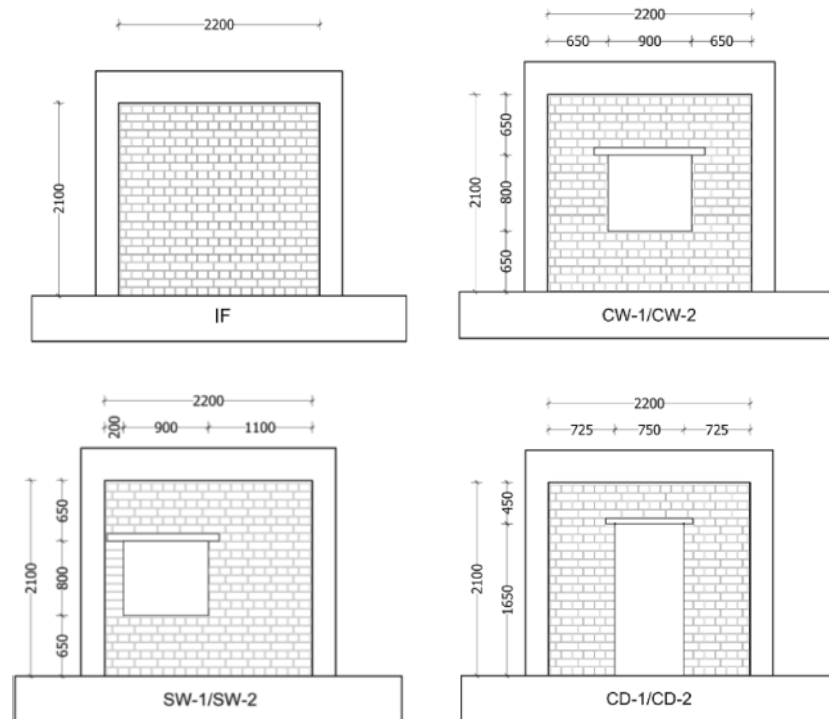


Figure 2.18 Geometry and dimension of specimens Khan et al. (2023)

The behavior of infilled frames with openings becomes more complex during cyclic loading. An infilled frame with openings commonly has improved lateral stiffness, lateral strength, and energy dissipation as compared to a bare frame. However, the presence of openings can potentially weaken the diagonal strut action of the partially infilled walls, impacting lateral load redistribution and leading to a stress concentration around the openings. To mitigate these weaknesses, engineers need to systematically evaluate the failure mode of an infilled frame featuring window or door openings. Several factors come into play, including the dimensions and placement of the openings, the properties of the infill material, the frame's structural arrangement, and the nature of the applied loads. Thorough consideration of these factors is essential to ensure the structure's safety and resilience under various loading scenarios.

### 2.3 NUMERICAL MODELS OF MASONRY-INFILLED FRAME

The various modeling approaches can be employed at various levels of detail, these include micro, meso, and macro modeling techniques.

- Micro modeling considers the individual masonry units, mortar joints, reinforcement, and concrete, accounting for their material properties, geometry, and interactions. Micro modeling allows for a detailed analysis of local phenomena, such as cracking, bond behavior, and failure mechanisms at the microscale.
- Meso modeling tries to depict the interaction of the surrounding concrete frame and the masonry infills. The masonry infill and concrete frame are modeled separately, with explicit consideration of their individual properties and interaction interfaces. Meso modeling allows for a more detailed analysis of stress distribution, interface behavior, and damage mechanisms within the masonry infill and at the infill-frame interface.
- Macro modeling focuses on representing the overall behavior of the MIRCF system without explicitly considering the individual components within it. In this approach, the masonry infill and concrete frame are treated as homogenized entities with simplified material properties. This approach is suitable for preliminary analysis, quick assessments, and evaluation of the overall behavior of MIRCF systems.

This study will utilize and focus only on the macro modeling approach to evaluate the behavior of RC frame-infilled masonry panels with and without opening under horizontal cyclic load.

### 2.3.1 INFILLED FRAME WITHOUT OPENINGS

#### Spring Models

Mostafaei & Kabeyasawa (2004) developed an approach to model masonry infill wall as the horizontal spring model as illustrated in Figure 2.19, which was obtained from a force-displacement curve. Two critical failure modes such as sliding shear and compression failure are considered to estimate maximum lateral strength to develop the strength-displacement curve. The paper also indicated that the horizontal spring almost has the same responses as the diagonal spring model.



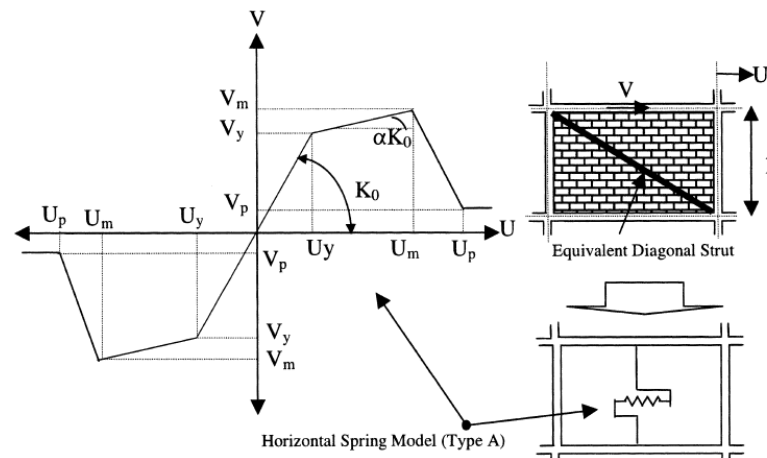


Figure 2.19 Strength envelope for masonry infill walls and the analytical model Mostafaei & Kabeyasawa (2004)

Crisafulli & Carr (2007) proposes a novel macro-model for the assessment of the overall performance of masonry panel-filled RC frames. The proposed model is implemented as a 4-node panel element and is based on the formulation involving multiple struts, as shown in Figure 2.20. The model considers the compressive and shear characteristics of masonry distinctly by employing a double truss mechanism and incorporating a shear spring in both horizontal and vertical directions. The model is capable of simulating various shear-related failure modes that are observed in masonry infills, and it effectively captures the in-plane behavior of frames with infill.

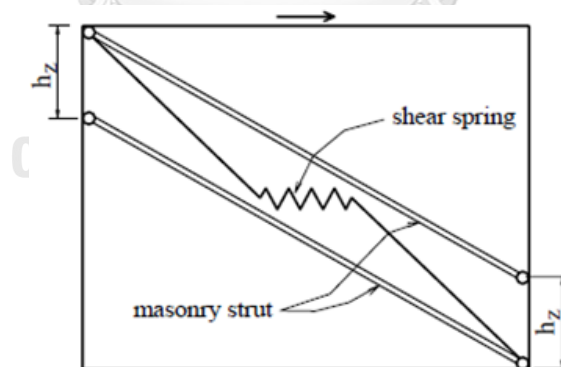


Figure 2.20 Proposed multi-strut model Crisafulli & Carr (2007)

Burton & Deierlein (2014) proposed a dual-strut model with two compression struts (off-diagonal strut and central strut) and zero-length spring elements implemented at the end of elastically defined frame members, as illustrated in Figure 2.21. Although the spring elements were intended to represent the flexural plasticity, shear deterioration, and decline in the axial bearing capacity of the frame member, the

inelastic dual strut accurately depicts how the masonry infill responds after reaching its maximum strength and how it interacts with the surrounding frame.

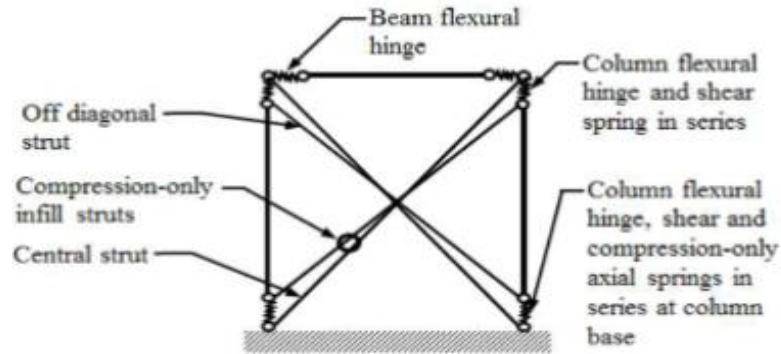


Figure 2.21 Multi-strut model proposed Burton & Deierlein (2014)

Caliò & Pantò (2014) proposed an innovative approach for the simulation of the infilled frame behavior under seismic. The suggested model consists of a basic macro-element representing the masonry infill, which is an articulated quadrilateral with rigid edges connected to four hinges and two diagonal nonlinear springs. Each side of the quadrilateral can interact with other parts and is denoted as an interface, which is made up of a distributed nonlinear orthogonal spring and an additional longitudinal spring. And the means of lumped plasticity beam–column is used to represent the frame member.

Roosta & Liu (2022) create and utilize a novel macro model for simulating the performance of reinforced concrete frames with masonry infill under in-plane loading. This model incorporates failure due to shear sliding, diagonal compressive, and interaction between frame and infill by using a multi-strut-spring configuration as shown in Figure 2.22. The suggested model has two types of equivalent strut components that transmit loads to the frame and to the beam-column connections, as well as a shear spring in the center of the infill. The column shear demand can be captured by the shear spring's representation of shear behavior and shear failure along the mortar joint, but it is unable to reproduce the base shear failure on the column.

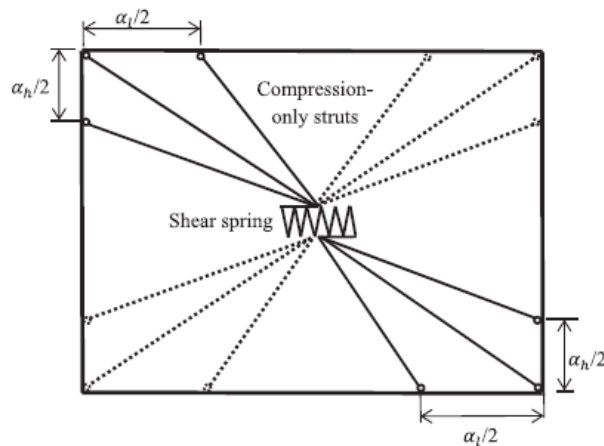


Figure 2.22 Proposed strut-model configuration Roosta & Liu (2022)

### Equivalent compressive strut

introduced an inelastic analysis and design approach utilizing the concept of equivalent diagonal struts for steel frames containing infill panels subjected to in-plane forces, as illustrated in Figure 2.23. This Method maintains a correlation between the length of the contact zones, influenced by the plastic moments of the reinforced concrete (RC) components, and the width of the corresponding strut.

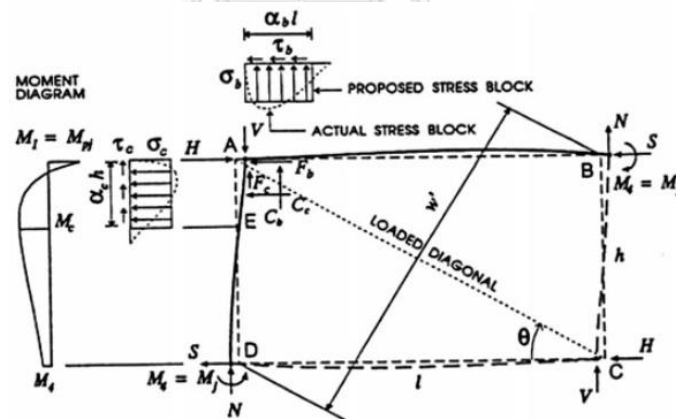


Figure 2.23 Force distribution on the infilled frame

Chrysostomou et al. (2002) introduces a computational model in two dimensions for infill walls that considers both strength and stiffness degradation. The model employs six inclined struts for compression-only purposes to depict infill behavior, along with off-diagonal struts for capturing infill and bounding frame interaction, as shown in Figure 2.24. Due to the model's inexpensive computational cost and ability to simulate most of the significant variables that influence how infilled frames behave and the major of their failure modes, it can be used to analyze

large, realistic structures. By assigning suitable values to the model parameters, the effects of apertures, a lack of fit, and interface characteristics can all be simulated.

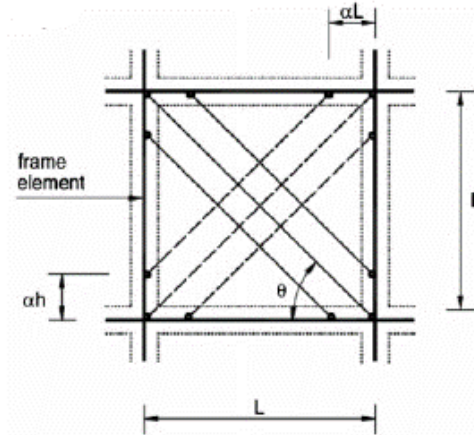


Figure 2.24 Proposed macro model for infilled frame Chrysostomou et al. (2002)

Wael W. El-Dakhakhni (2003) outlines a simple Method to assess the lateral stiffness and strength of steel frames with concrete masonry filling that failed due to corner crushing to calculate the internal forces within the steel frame. Within the proposed technique, every infilled panel is substituted by triple struts employing force-deformation derived from the orthotropic properties of the masonry infill as shown in Figure 2.25. This is carried out employing the ANSYS 5.3.b software package. The suggested analytical Method effectively forecasts the lateral stiffness until failure and the ultimate load-carrying capacity of Concrete Masonry Infilled Steel Frames (CMISF) with a satisfactory level of precision. The approach accommodates the non-linear behaviors present in both the steel frame and the masonry panel. It treats the diagonal tension cracking within the masonry joints as a serviceability limit state rather than a critical failure mode.

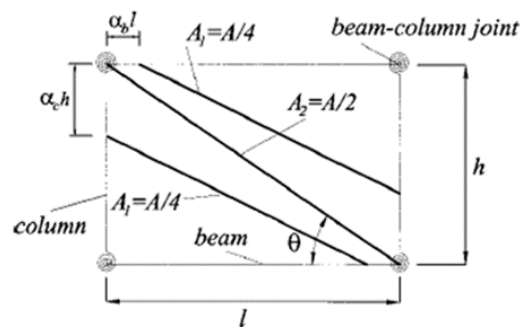


Figure 2.25 Proposed model of masonry infilled steel frame Wael W. El-Dakhakhni (2003)

Rodrigues et al. (2010) enhanced numerical model is put out to more accurately simulate the behavior of masonry infill walls tested with seismic loads. The novel model is introduced through the enhancement of the model with an equivalent double-diagonal compression strut configuration, as illustrated in Figure 2.26, which is frequently employed to demonstrate how infill masonry panels respond to cyclic loads when they exhibit nonlinear behavior. The suggested macro-model can be utilized to assess infilled frame constructions subjected to lateral loads. It effectively illustrates pinching, the progression of damage, degradation in strength and stiffness, hysteretic behavior, and how the structure responds to deformation criteria.

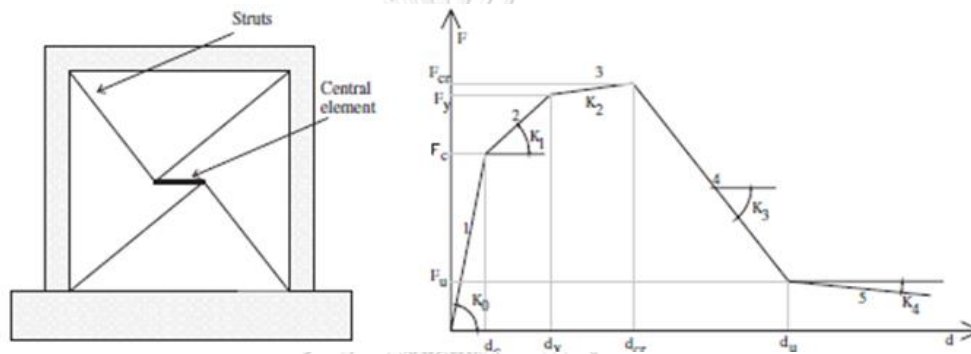


Figure 2.26 Proposed macro model and force-displacement curve.

Fiore et al. (2012) introduced the macro-model incorporating two non-parallel struts per frame to simulate the infill which is capable of simulating the impact of infills on both the overall stiffness of a building and the localized effects on its frame when subjected to earthquake loads. The macro model that is suggested relies on the Finite Element Analysis software Midas/GEN for its foundation by comparing six different schemes which include plate element for frame, single and double strut, and centric and eccentric strut positions. The proposed model, featuring two non-parallel struts, as shown in Figure 2.27, has been demonstrated to accurately capture both the global and local effects of infilled frames concerning displacements and, respectively, stress or internal force in linear behavior.

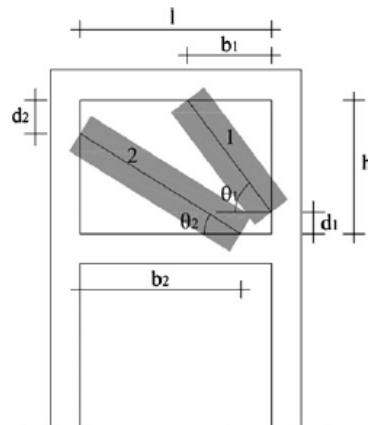


Figure 2.27 Scheme of two non-parallel equivalent struts Fiore et al. (2012)

Cavaleri & Di Trapani (2014a) explores a criterion for simulating the structural response of infill panels through a macro-modeling strategy as in Figure 2.29. This approach employs multilinear plastic link elements governed by a hysteretic Pivot model, as shown in Figure 2.28, to facilitate both linear and nonlinear analyses.

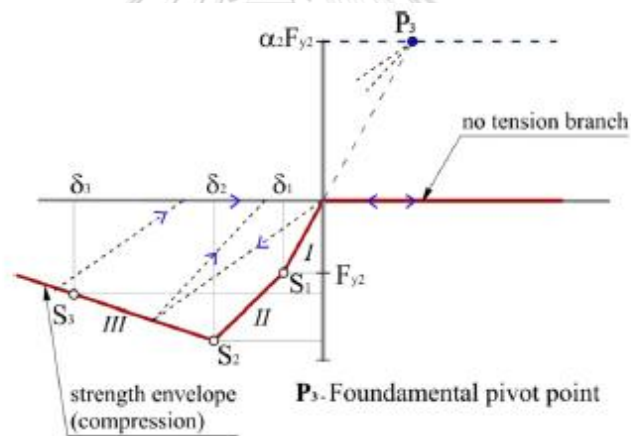


Figure 2.28 Hysteretic pivot law Cavaleri & Di Trapani (2014a)

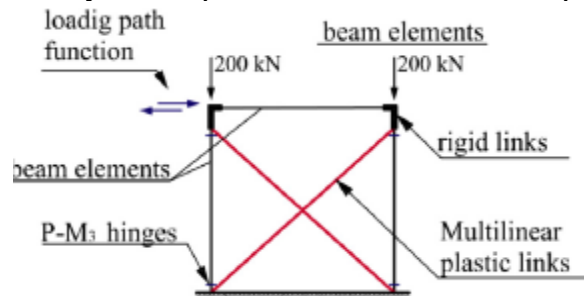


Figure 2.29 FEM model employed for the structural analyses Cavaleri & Di Trapani (2014a)

To consider the impacts of local shear caused by lateral loads at the extremities of brittle RC infilled frames' beams and columns Cavaleri & Di Trapani (2014b)



proposes analytical principles for addressing the shear demand outcomes obtained when a concentric equivalent strut using pinned joint is employed in place of an infill. The comparison of the results from the two modeling Methodologies provides the correction coefficients for local shear forces:

- (M1 model) utilizing the single equivalent strut approach as shown in Figure 2.30
- (M2 model) using plane-shell elements to simulate infills, multi-linear elastic connections (ME link), which only resist compression at the frame-infill interface, and nonlinear beam elements at the contour of the frame as shown in Figure 2.31

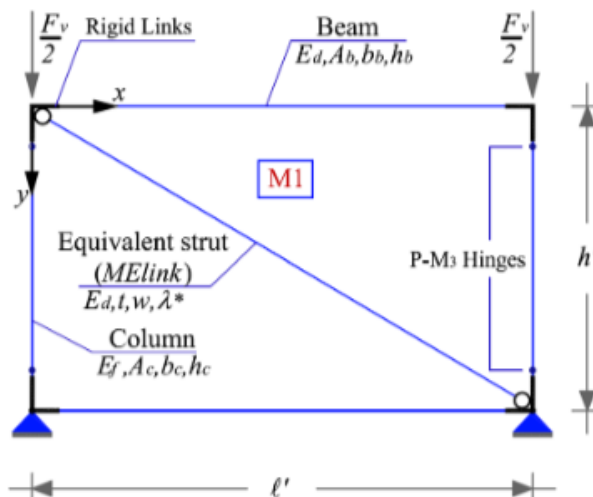


Figure 2.30 M1 model from Cavaleri & Di Trapani (2014b)

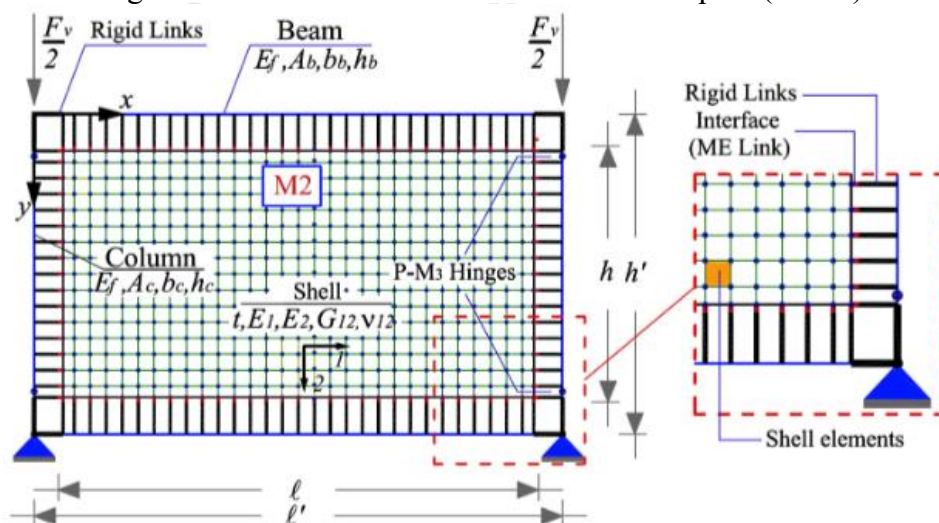


Figure 2.31 M2 model from Cavaleri & Di Trapani (2014b)

Furtado et al. (2015) improved numerical model for simulating masonry infill wall behavior based on Rodrigues et al. (2010) work. The suggested model for masonry infill panels consists of a center element and four support strut elements as illustrated in Figure 2.32. An eight-parameter multi-linear curve that describes this key element's behavior describes its in-plane nonlinear hysteretic behavior. These parameters include characteristics like yielding, maximal strength, residual strength, and cracking. Three more variables, including stiffness degradation, pinching effect, and strength degradation, are used to further regulate the behavior. Regarding base shear and energy dissipation, the numerical model and experimental result match well, with a 5% discrepancy that is regarded tolerable given the utilization of a simplified model.

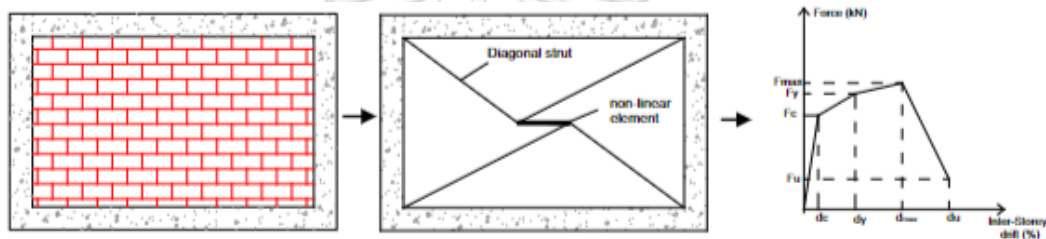


Figure 2.32 Proposed model Furtado et al. (2015)

Fiore et al. (2016) introduced a practical tool of the 'dual-strut model' to capture infill behavior, which captures dangerous local shear failures in pushover analysis. A 4-storey RC frame building was modeled using SAP2000 and five models were considered, including the bare structure and structures with single or double strut infills, as illustrated in Figure 2.33, in all or some stories. Incorporating shear plastic hinges alongside bending hinges in the analysis reveals how extra shear forces that appear at the extremities of beams and columns can significantly alter the structural collapse mechanism when subjected to seismic forces. The outcomes demonstrate that implementing the dual-strut model is capable of accurately representing critical local shear effects. The primary characteristics of the dual-strut model encompass its cost-effectiveness and precision, rendering it especially appropriate for practical engineering applications.



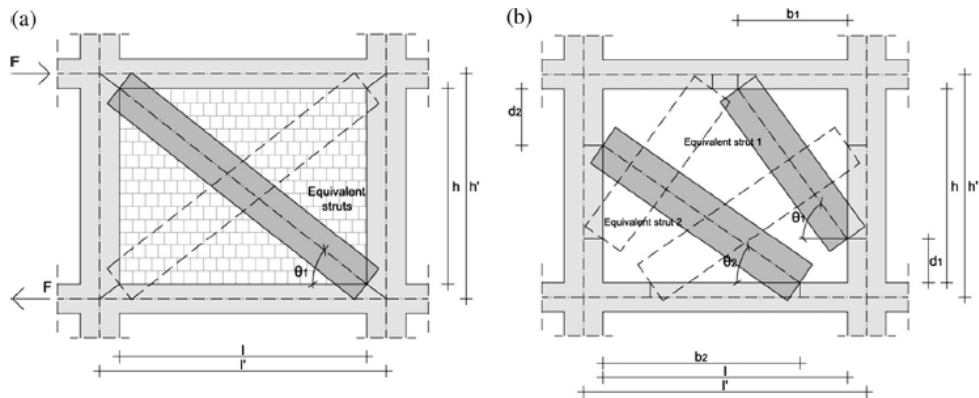


Figure 2.33 Proposed macro model Fiore et al. (2016)

Yekrangnia & Mohammadi (2017) proposes a new strut model for masonry infilled steel frames based on calibrated finite element analyses which are built upon comparisons with established strut models such as ASCE beam-to-beam, ASCE column-to-column and Wael W. El-Dakhakhni (2003) see in Figure 2.34. The benchmark experimental results are utilized to calibrate the analytical models and assumptions. A collection of 75 experimental specimens has been taken into consideration to evaluate the recommended model's shown capacity for the behavior of various infilled frames. The suggested model appropriately depicts both the strength and force-displacement diagram of infilled frames as well as the internal forces of the frames.

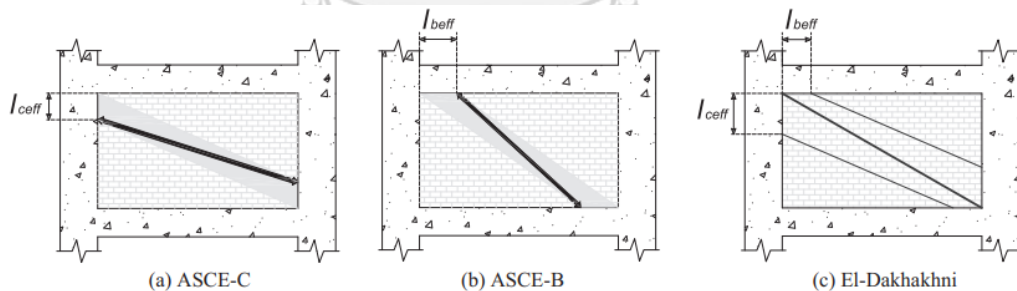


Figure 2.34 Considered strut models Yekrangnia & Mohammadi (2017)

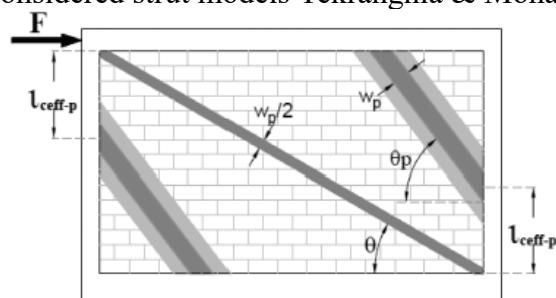


Figure 2.35 Macro model proposed by Yekrangnia & Mohammadi (2017)

Based on observation of the experimental result and FEM study, Wararuksajja et al. (2020) recommended a design Method to prevent local failure in the surroundings frame. This practical design approach is based on the plastic mechanism by taking into account the difference in column shear demand and capacity at various response states. Wararuksajja et al. (2021) extend the above study by extensive investigation of the key parameters and verifying with additional experimental data of infilled RC frame for the suitability of the design Method. The proposed Method's concrete block-infilled RC frame was tested and evaluated using FEA analysis, and the findings demonstrated that local frame failure could be avoided, and ductile behavior resulted.

### 2.3.2 INFILLED FRAME WITH OPENING

Macro modeling is an effective and minimized computational approach utilized to replicate the behavior of frames that have infills containing openings. In this modeling technique, the complexity of infill frame interaction is simplified and represented using lumped parameters, such as equivalent springs or struts. By utilizing macro models, engineers can efficiently analyze the structural response of infilled frames with openings under various loading conditions. Despite some limitations, macro models remain valuable tools for conducting preliminary analyses, optimizing designs, and guiding engineering decisions. It is essential for engineers to use macro models judiciously and be aware of their limitations to interpret the results accurately. Some well-known macro models are presented below by divided into three distinct categories:

- The first Method involves a macro model based on springs, where both the infill walls and frame members are simplified into equivalent springs to represent the overall behavior of the structure. These springs are utilized to mimic the stiffness and deformation characteristics of the infill walls and frame elements.
- The second technique is the multiple strut approach, which aims to replicate the behavior of infilled frames with openings. In this approach, the infill walls surrounding the openings are modeled using several diagonal struts that enclose the openings. The arrangement of these

multiple struts approximates the mechanisms of load transfer and redistribution within the infilled frame system.

- Based on the size of the opening, the third approach indirectly reduces the stiffness and strength of the infill walls. This is accomplished by employing the reduction factors to reduce the width of a diagonal strut. Several researchers Decanini et al. (2014; Tasnimi & Mohebkah (2011); Asteris et al. 2016; Su et al. 2017) have employed this Method for accounting for the impact of openings on the overall structural response.

### Spring Models

To consider the effect of opening in the infilled wall Mostafaei & Kabeyasawa (2004) also developed an approach to model an infilled frame with an opening, which involved dividing the infill panel into smaller elements and modeling them as the multi-spring infilled frame as shown in Figure 2.36. For simplicity, an equivalent model can be applied in the analysis process instead of several spring models for an infill wall with openings or multipart of infill walls. To obtain an equivalent model, pushover analyses were conducted on individual frames both with and without an infill wall. Subsequently, the force-displacement curve of the bare frame will be subtracted from the multi-spring infilled frame to obtain the equivalent envelope for the single-spring model.

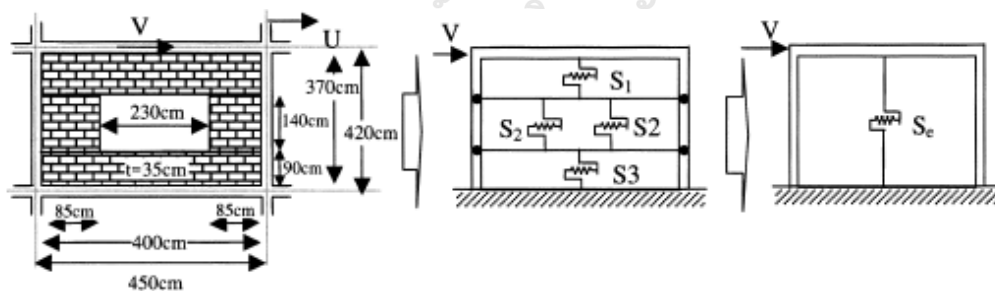


Figure 2.36 An infilled frame with a window opening model as an equivalent spring.

Caliò et al. (2012) introduce an approach that utilizes a discrete macro-element to simulate the in-plane nonlinear characteristics of unreinforced masonry walls, which was later expanded by Caliò & Pantò (2014) to incorporate infill masonry structures. The proposed model is a simple mechanical scheme that articulated quadrilateral rigid edges with two nonlinear diagonal springs and was used to capture the shear response of the masonry wall. The edge of the quadrilateral macro element

consists of the discretized distribution of an orthogonal spring and a longitudinal spring, known as an interface which governs the flexural and sliding failure mechanism modes of the infilled frame. Meanwhile, the nonlinear column beam elements with concentrated plasticity are modeled to capture the frame member behavior.

On the journey to explore better macro modeling for simulating the responses of masonry infilled frames under seismic load, Kareem & Pantò (2019) evaluate two simplified macro-models to investigate the influence of openings and infilled on tall buildings of the non-ductile RC frame. Both the diagonal strut model and the 2D macro-model were performed analysis in SAP 2000 software. Two different formulations of mechanical behavior were adapted to the diagonal strut model. The first one used the constitutive law from Panagiotakos & Fardis (1996) and strut width by Holmes (1961) which equals  $1/3$  of the diagonal length. Another model was adapted to the formulation proposed by Di Trapani et al. (2017). For 2D macro, a model followed the Caliò & Pantò (2014)'s Method. Two different experiments were used to calibrate the result: a single-story masonry RC frame with and without opening, and a 7-story frame for representing tall buildings. The paper concluded that the strut's geometrical and mechanical characteristics, particularly greatly impact the lateral behavior of the systems before and after reaching their peak capacity. Particularly in the context of multi-story frame buildings with openings, the geometrical consistency of the 2D macro model significantly affects to simulation of the nonlinear interactions between infill and frame, resulting in the difference of bending moment and the failure mechanism between the two macro models.

Kareem et al. (2022) evaluate three different Methods of simulating infilled RC frame with an opening including an equivalent diagonal strut model (EDSM) which is based on the Yekrangnia & Asteris (2020), 2D-discretized macro-element model (DMEM) proposed by Caliò & Pantò (2014), and the finite element Method (FEM). The research findings indicate that enlarging the size of openings within infilled RC frames substantially decreases their lateral strength. Additionally, it can be inferred that the lateral stiffness of masonry-infilled RC frames becomes negligible when the opening size exceeds 30% of the infill area. Due to the premature collapse

of the strut, EDSM underestimates the global displacement capacity. The DMEM and FEM model can capture the response more accurately.

#### Multiple equivalent compressive struts

Thiruvengadam (1985) introduced the multiple strut model, which involved substituting infill panels to assess the first few mode shapes of infilled frames with openings as shown in Figure 2.37. This approach considered both solid infills and separate infills for the evaluation. The model consists of a moment-resisting frame and several diagonal struts with pin-jointed and vertical struts.

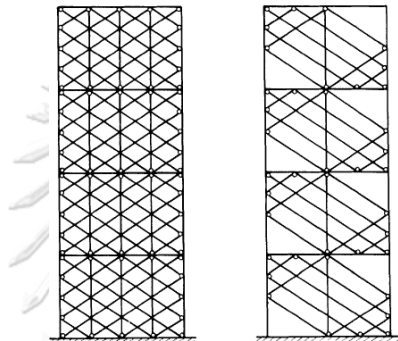


Figure 2.37 Proposed multiple struts with monolithic infills and with separating infills respectively Thiruvengadam (1985)

Observation of the experimental result of seven one-third scale, single-story, one-bay designs of weak and strong infilled RC frame specimens with varying locations and sizes of openings, Kakaletsis & Karayannis (2008) indicates the behavior of infilled with openings is dominated by many compressive zones and the system of compressive struts developed surrounding the opening, illustrated in Figure 2.38.

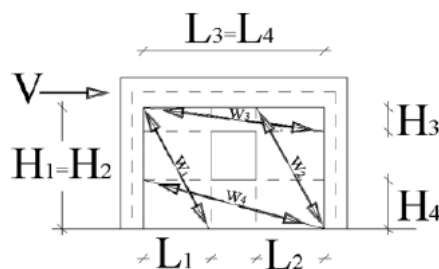


Figure 2.38 Concept compressive strut infilled with an opening Kakaletsis & Karayannis (2008)

ASCE (2013) mentioned two sets of cracks seismic develop at small lateral deformation and initiate the nonlinear behavior under load. The first type of cracks appears along the infill frame boundary, while the second type initializes at the corners of openings and extends 45 degrees across the infill as shown in Figure 2.39.

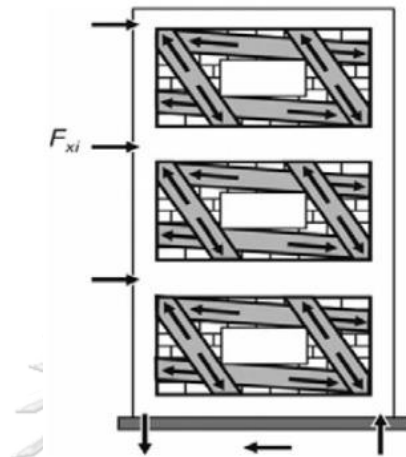


Figure 2.39 Compression Strut Analogy ASCE (2013)

Yekrangnia & Asteris (2020) introduces the concept of employing multiple struts as a technique for capturing the comprehensive force-displacement relationship of infilled frames featuring diverse opening configurations. The approach relies on calibrated finite element modeling (FEM) to observe the attributes of a multiple-strut model for masonry-infilled frames containing openings. They further investigate the parametric assessment of the proposed model against FEM outcomes, considering diverse factors such as opening dimensions and placement, the ratio of opening height to length, infilled frame's height-to-length ratio, and the infill wall's and the frame's relative stiffness. Comparing the obtained outcomes with analytical and experimental observations validates the model's capability to simulate the lateral behavior of infilled frames containing openings effectively and consistently.

To analyze the masonry infilled RC frame with different opening sizes and positions, Jia et al. (2023) proposed a macro model that divides infilled panel into multiple subpanels around the opening and replaced by the double diagonal struts, as illustrated in Figure 2.40 and Figure 2.41, using the OpenSee program. Utilizing a finite element investigation conducted with the ABAQUS software to examine the quasi-static test results of RC infilled frames, both with and without openings Zhai et al. (2016), and considering aspects such as load distribution, stiffness, strength, and

infilled-frame interaction, the concept of strut formation was introduced. From the 52 analyses using the proposed macro model varying opening rate and opening position, it is concluded that the masonry infill wall's presence greatly influenced the initial stiffness and ultimate load-bearing capacity. As the opening rate increased, there was a decrease in both the initial stiffness and load-bearing capacity, following a similar trend when the opening was positioned farther from the center towards the side.

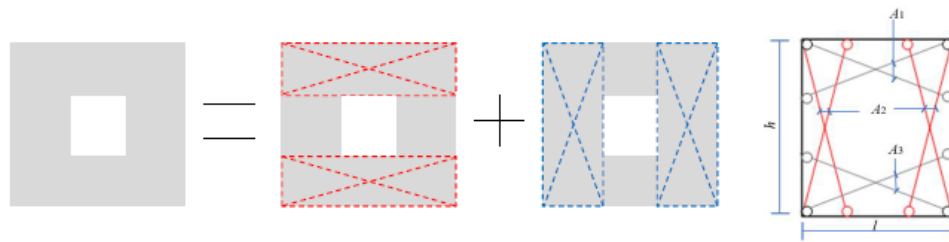


Figure 2.40 Macro model of the infill panel with a window opening Jia et al. (2023)

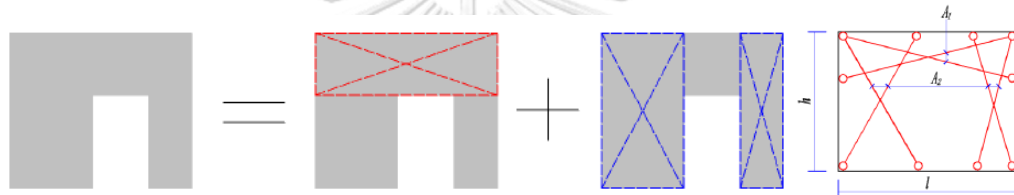


Figure 2.41 Macro model of the infill panel with a door opening Jia et al. (2023)

#### The reduction factor accounted for the opening

G. Al-Chaar et al. (2003) introduced the reduction factor to modify the width of the diagonal strut to take into account the effect of the presence of a central opening infilled frame. To predict the reduction factor that justifies the presence of infill openings, analytical investigations are supplemented by experimental data.

$$R_k, R_s = 0.6 \left( \frac{A_o}{A_p} \right)^2 - 1.6 \left( \frac{A_o}{A_p} \right) + 1 \quad (2.1)$$

Where,  $A_o$  and  $A_p$  represent the area of the opening and infill panel area respectively.

Mondal & Jain (2008) introduced a reduction factor for the diagonal strut's effective width relative to a solid infilled RC frame. This factor is utilized to compute the initial lateral stiffness of the frame when incorporating a center window opening. The analysis relies on the initial stiffness, which is determined by considering 10% of the lateral strength of the frames with infill. The parametric study employs a calibrated Finite Element (FE) model to determine the strut width reduction factors for various opening-area ratios for all the frames, utilizing data from existing

experimental specimens in the literature. The proposed equation of strut-width reduction factor

$$R_k, R_s = 1 - 1.6 \left( \frac{A_o}{A_p} \right) \quad (2.2)$$

The role of infill in providing stiffness becomes negligible when the area of the opening exceeds 40% of the total infill area. The presence of an opening may be ignored if it is less than 5% of the area of the infill panel.

P. Asteris et al. (2011) introduced a reduction factor for modeling infilled frames with openings, drawing from existing finite element outcomes. A reduction factor, denoted as  $\lambda$ , is suggested to serve as a multiplier for established equations, enabling the computation of the reduced equivalent width of compression struts. The same reduction factor can also be applied in models featuring multiple struts to effectively demonstrate how infill walls behave nonlinearly with openings. As the opening percentage exceeds 50%, the stiffness reduction factor approaches zero. The accuracy level of the proposed equations is showcased through a comparison of their results with findings from diverse researchers. The proposed procedure can be used for the practical design of infilled frames with openings.

$$R_k, R_s = 1 - 2 \left( \frac{A_o}{A_p} \right)^{0.54} + \left( \frac{A_o}{A_p} \right)^{1.14} \quad (2.3)$$

Tasnimi & Mohebkah (2011) proposed a straightforward technique for calculating the decrease of stiffness and strength of masonry-infilled frames with central openings. This involves reducing the width ( $w$ ) of the diagonal strut based on the ratio of the opening area to the total infill area, as described by the equation below:

$$w_m = (R_k \text{ or } R_s) \times w \quad (2.4)$$

The reduction factor is based on the resulting experiment of six full-scale, brick masonry infill steel frames having central window and door openings subjected to horizontal cyclic load at roof level. The study demonstrated that the presence of openings in infill panels leads to a reduction in the lateral strength and effective stiffness of infilled frames. To  $R_k$  or  $R_s$  is the reduction factor



$$R_k, R_s = 1.49 \left( \frac{A_o}{A_p} \right)^2 - 2.238 \left( \frac{A_o}{A_p} \right) + 1 \quad \text{for} \quad \left( \frac{A_o}{A_p} \right) < 0.4 \quad (2.5)$$

Mohammadi & Nikfar (2013) revised equations were presented to determine the mechanical characteristics of perforated infill frames, revealing that the decline in ultimate strength brought on by openings depends significantly on the type of confining either steel or concrete frame. The reduction factor is suggested using experimental data and statistical analysis, assessing both the dependability of current empirical formulas for ascertaining mechanical properties of frames with perforated infill. The confining frame material significantly influences the ultimate strength-reduction factor in perforated infilled frames, whereas the initial stiffness-reduction factor remains unaffected by frame material, resulting in the introduction of two distinct formulas for such infills.

Reduction factor for stiffness

$$R_k = 1.1859 \left( \frac{A_o}{A_p} \right)^2 - 1.6781 \left( \frac{A_o}{A_p} \right) + 1 \quad \text{for} \quad \left( \frac{A_o}{A_p} \right) < 0.4 \quad (2.6)$$

Reduction factor for ultimate strength

$$R_s = \begin{cases} -1.085 \left( \frac{A_o}{A_p} \right) + 1 & \text{for} \quad \left( \frac{A_o}{A_p} \right) < 0.4 & \text{RC frame} \\ -2.122 \left( \frac{A_o}{A_p} \right) + 1 & \text{for} \quad \left( \frac{A_o}{A_p} \right) < 0.25 & \text{Steel frame} \end{cases} \quad (2.7)$$

The proposed formula demonstrated superior precision compared to earlier Methods.

ASCE (2013) advises using the following reduction factor to calculate the initial in-plane stiffness of a frame that has unreinforced masonry infill and is infilled with an uncracked panel:

$$R_k = 1 - 2 \left( \frac{A_o}{A_p} \right) \quad (2.8)$$

Mansouri et al. (2014) provided an empirical equation that accounts for the impacts of opening size, shape, and placement, both central and eccentric, to assess the total decreases in both stiffness and strength of infilled frames caused by the

presence of openings. The reduction factor proposed is based on the experimental results.

For stiffness reduction factor

$$R_k = \left(1 - 0.31 \frac{A_o}{A_p}\right) \times \left(2.78 - 1.78 \frac{d_o}{\sqrt{2h_o l_o}}\right) \quad (2.9)$$

For strength reduction factor

$$R_s = \left(1 - 1.1 \frac{A_o}{A_p}\right) \times \left(1.6 - 0.6 \frac{d_o}{\sqrt{2h_o l_o}}\right) \times \left(1 - 0.3 \frac{x}{l}\right) \quad (2.10)$$

Decanini et al. (2014) presented a simplified approach to include the influence of central openings on the strength and stiffness of infilled frames, the study factors in variables such as opening size and the presence of reinforcement within the diagonal no-tension strut. The approach is based on the reduction factor for strength and stiffness which were proposed based on the analysis of the test results and the comparison with other models.

For partially reinforced and unreinforced openings:

$$R_k, R_s = 0.55e^{-0.035 \frac{A_o}{A_p} + 0.44e^{-0.025 \frac{l_o}{l_p}}} \quad (2.11)$$

For reinforced opening

$$R_k, R_s = 0.63e^{-0.020 \frac{A_o}{A_p} + 0.40e^{-0.010 \frac{l_o}{l_p}}} \quad (2.12)$$

Asteris et al. (2015) proposed the reduction factor to account for the presence of the opening, the effect of vertical load, infill panel aspect ratio, and opening. Those proposed analytical expressions were based on a series of FE models calibrating experimental results. It is concluded that the larger openings result in increased contact lengths between the beam-column and the infill. The vertical loads have a substantial impact on the stiffness of the dimensionless strut width in fully infilled panels only when it is small openings. Surprisingly, the recommended reduction factor for the dimensionless strut width is unaffected by the infill panel's length-to-height aspect ratio.

$$R_k = 1 + 0.24\xi - 4.23\xi^2 - 2.6\xi^3 + 12.73\xi^4 - 7.15\xi^5 \quad (2.13)$$

where,  $\xi = l_o/h_o$  opening ratio

Chen & Liu (2015) carried out a study to investigate the behavior of in-plane loading and the structural strength of concrete masonry infill panels that incorporate openings. The study directed its attention to assessing how the dimensions and placement of openings influence the stiffness and strength of infilled frames. A straightforward analytical approach was suggested, employing regression analysis, to establish a connection between the reduction factor in stiffness and strength and the size and position of the opening.

$$R_k, R_s = 1 + f\left(\frac{A_o}{A_p}\right) \cdot g\left(\frac{x}{l}\right) \quad (2.14)$$

where,

$$f\left(\frac{A_o}{A_p}\right) = 2.751\left(\frac{A_o}{A_p}\right)^2 - 3.17\left(\frac{A_o}{A_p}\right)$$

$$g\left(\frac{x}{l}\right) = 1 - 1.121\left(\frac{x}{l}\right)$$

Yekrangnia & Asteris (2020) observed that the presence of substantial central openings has a notable impact on the efficiency of the compressive strut, leading to a direct decrease in the ultimate strength and initial stiffness of structures like IF.

The reduction factor is proposed.

$$R_k, R_s = 1.0 - (0.45\lambda_l h + 0.60) \frac{L_o A_o}{LA} \quad (2.15)$$

To validate the suggested reduction factor, a comparison is conducted between the proposed reduction factor and the values derived from experimental results. The findings indicate that the normalized area of openings and the relative stiffness of the surrounding frame concerning the infill wall are the foremost and pivotal factors influencing the susceptibility of perforated infilled frames.

## 2.4 OVERVIEW OF EXISTING EXPERIMENTAL STUDY

NRCT (2023) conducted an experimental investigation of single-story RC frames with 0.754 aspect ratio height-length that was infilled with central window and door openings. The research encompassed the investigation of six full-scale

specimens of frames with masonry infill, which were subjected to lateral cyclic loading. The experimental setups included various configurations involving both central window and door openings, as well as strengthened frame members and infill panels. The scope of this study focuses solely on unreinforced RC frames infilled with unreinforced masonry panels featuring central openings. The controlled specimens encompass bare frames (BF), frames with a centrally located window (WF), and door opening (DF), as illustrated in Figure 2.42 to Figure 2.44 respectively.

Table 2.1 Reinforcement detail of frame member

RC Members	Size (b x h) mm	Longitudinal rebar		Transverse rebar		Cover (mm)
		Size	Area (mm <sup>2</sup> )	Size	Area (mm <sup>2</sup> )	
Column	(250x250)	4DB16	804.25	RB6@150	188.50	40
Beam	(250x400)	4DB16	804.25	RB6@180	157.08	30
Footing	(1500x400)	20DB16	4021.23	RB9@175	1148.92	30

Table 2.2. Geometrical characteristics of the openings of models

Model name	Opening type	Opening width (mm)	Opening height (mm)	Opening ratio	Opening (%)
BF	Bare frame	3750	2600	1.44	100
DF	Door opening	1000	2000	0.50	20.51
WF	Window opening	1100	1150	0.96	12.97

Table 2.3. Material properties of concrete, reinforcement, and masonry

Concrete			Longitudinal rebar			Transversal rebar	
$E_c$ (MPa)	$f'_c$ (MPa)	$\epsilon_{cu}$ (%)	$E_s$ (MPa)	$f_s$ (MPa)	$f_u$ (MPa)	$f_s$ (MPa)	$f_u$ (MPa)
21538	21	0.35	200000	390	560	235	385

Table 2.4 Material properties of masonry

$w_m$ (kN/m <sup>3</sup> )	$E_m$ (MPa)	$f_m$ (MPa)
18	4081	7.42

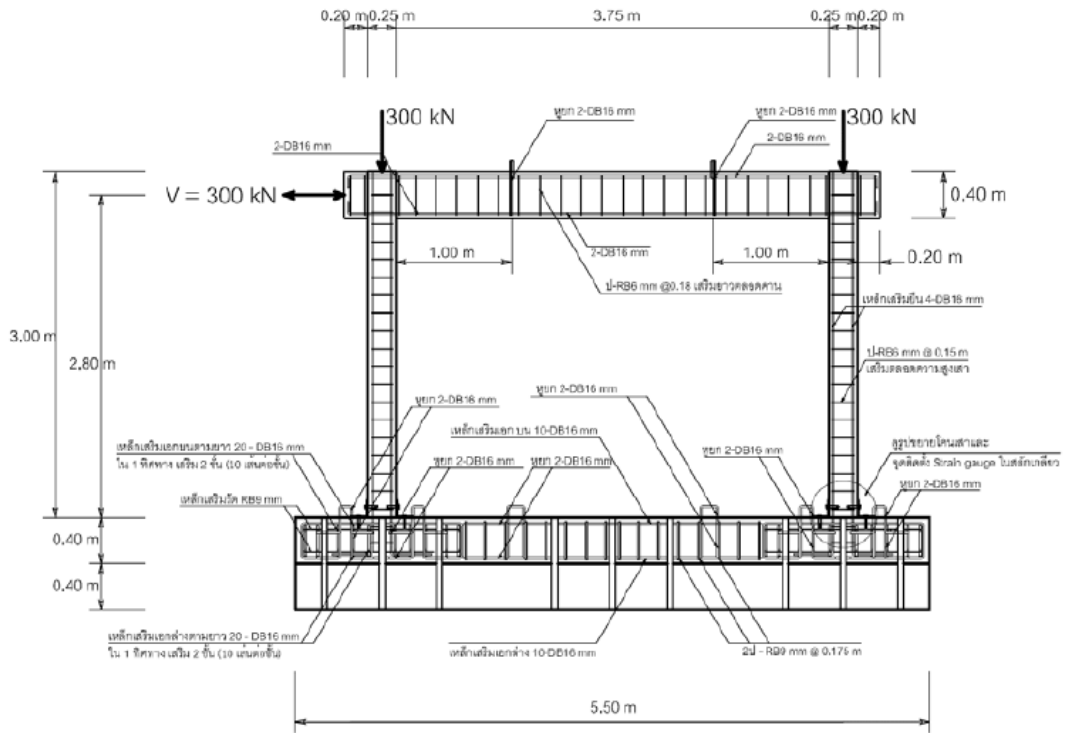


Figure 2.42 Bare frame (BF) NRCT (2023)

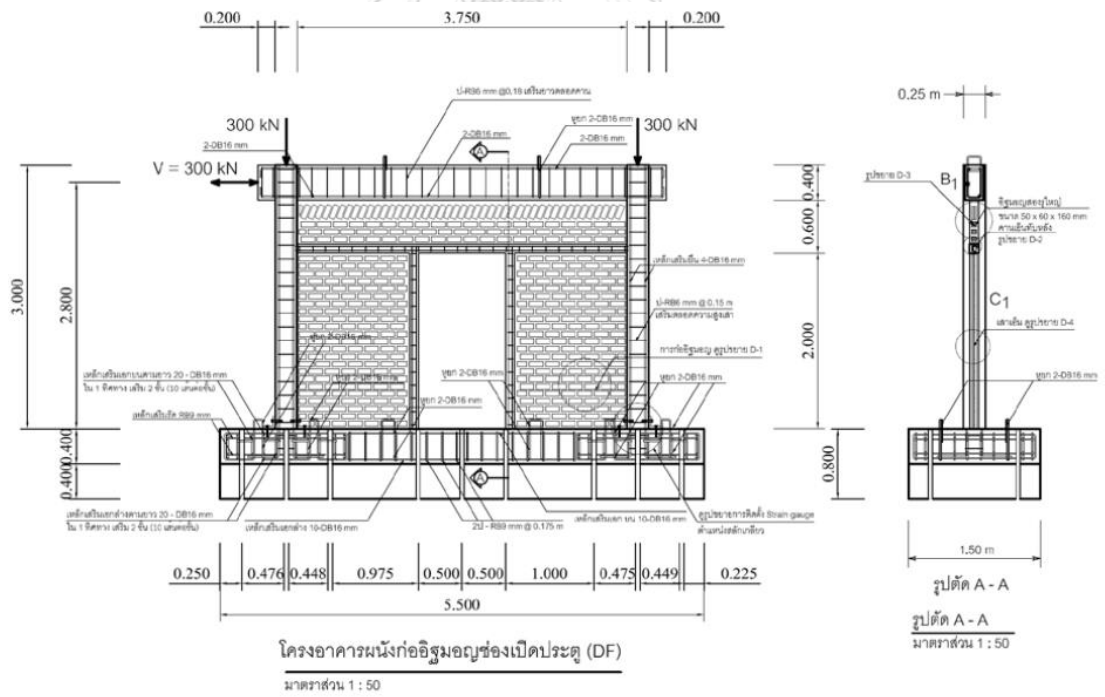


Figure 2.43 Infilled frame with door opening (DW) NRCT (2023)

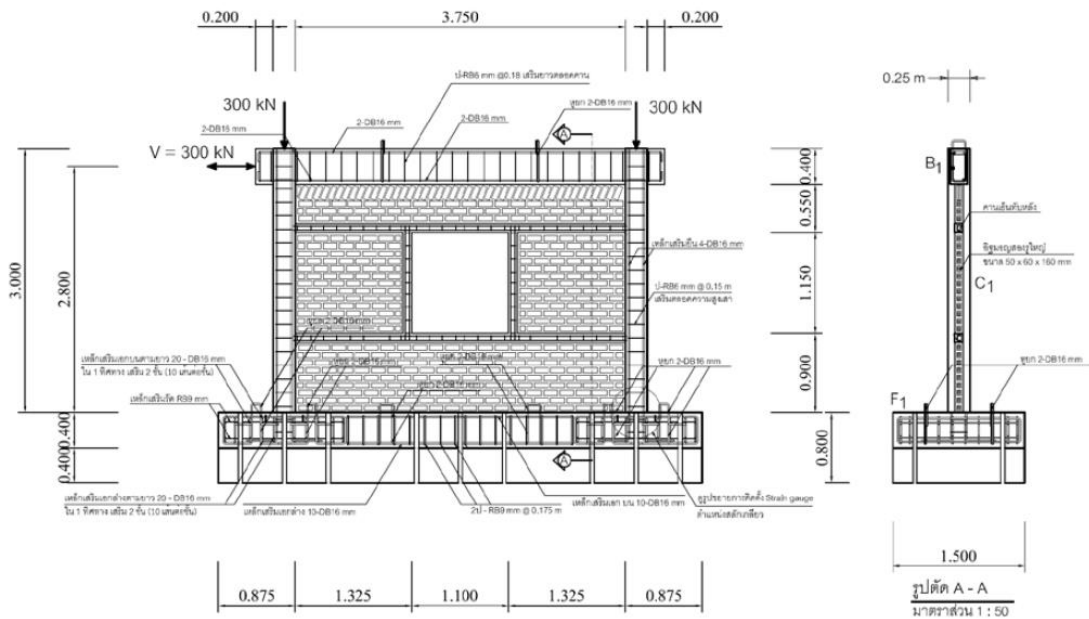


Figure 2.44 Infilled frame with window opening (WF) NRCT (2023)

2.4.1 BARE FRAME (BF)

The bare frame failed due to flexural failure at the base of the column and near the top, close to the beam-column joint, resulting in concrete crushing caused by the yielding of the reinforcement rebar. Meanwhile, the beam components generally exhibited no signs of damage. Through the observation of the damage behavior, it can be characterized that the frame exhibited weak column and strong beam behavior.

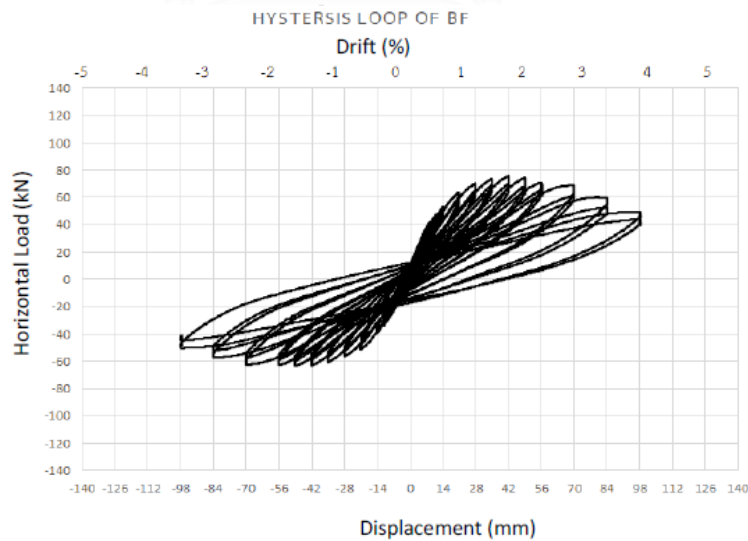


Figure 2.45 Hysteresis behavior of specimen BF NRCT (2023)

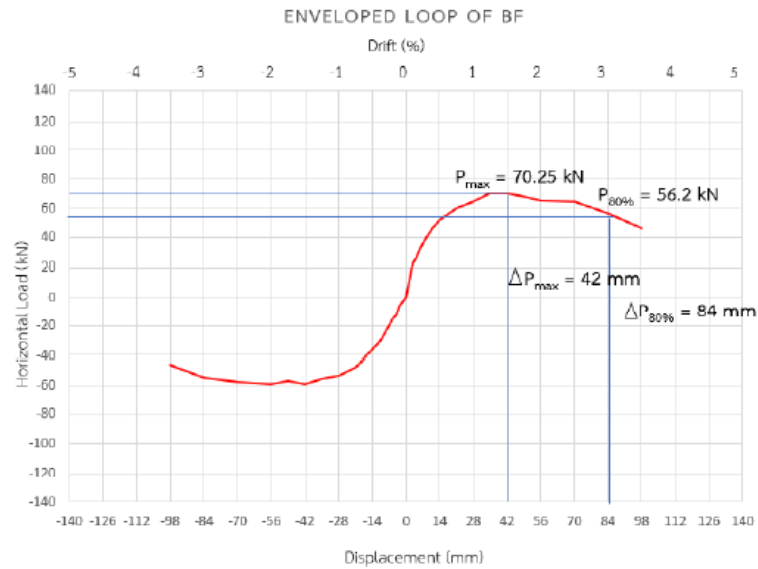


Figure 2.46 Force displacement of specimen BF NRCT (2023)

#### 2.4.2 INFILLED FRAME WITH CENTRAL DOOR (DF)

The infilled frame with a central door opening experiences initiation from sliding shear failure at the lintel beam above the door opening, extending along the entire wall panel. This failure is due to the diagonal compression forces on either side of the opening, causing the upper and lower wall panels to separate into two parts. On both sides of the door opening, failure occurs simultaneously due to diagonal compression.

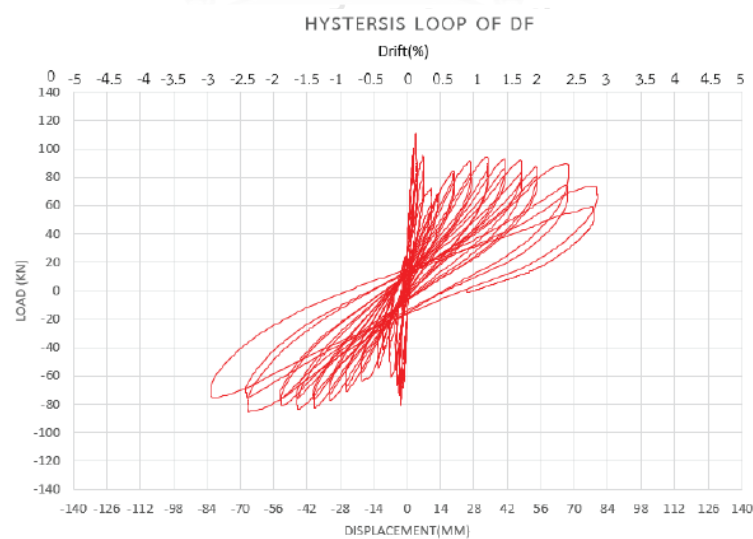


Figure 2.47 Hysteresis behavior of specimen DF NRCT (2023)

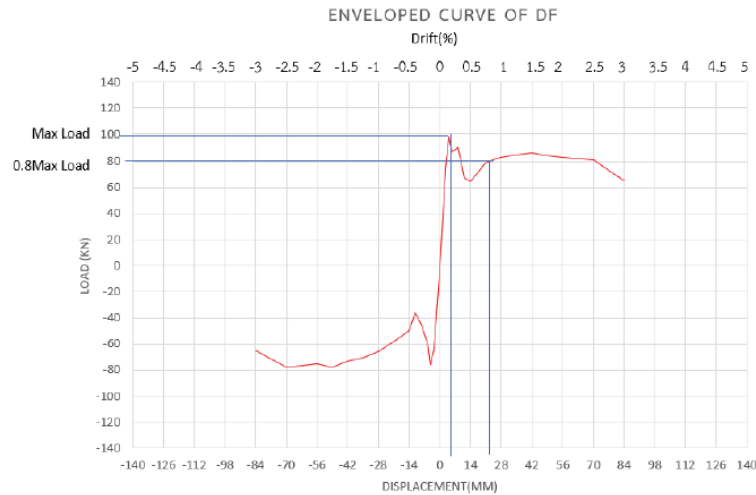


Figure 2.48 Force displacement of specimen DF NRCT (2023)

### 2.4.3 INFILLED FRAME WITH CENTRAL WINDOW OPENING (WF)

The test results for the infilled frame with a central window opening revealed the presence of diagonal cracks. These cracks originated from the bottom corners of the window and extended upwards on both sides towards the columns. These cracks were attributed to diagonal compression failure. Additionally, there was a separation between the upper and lower parts of the window opening, which occurred due to shear sliding.

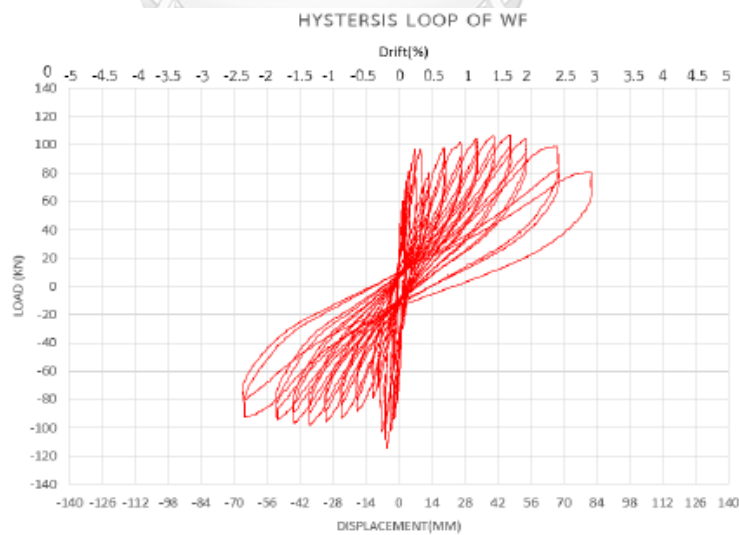


Figure 2.49 Hysteresis behavior of specimen WF NRCT (2023)



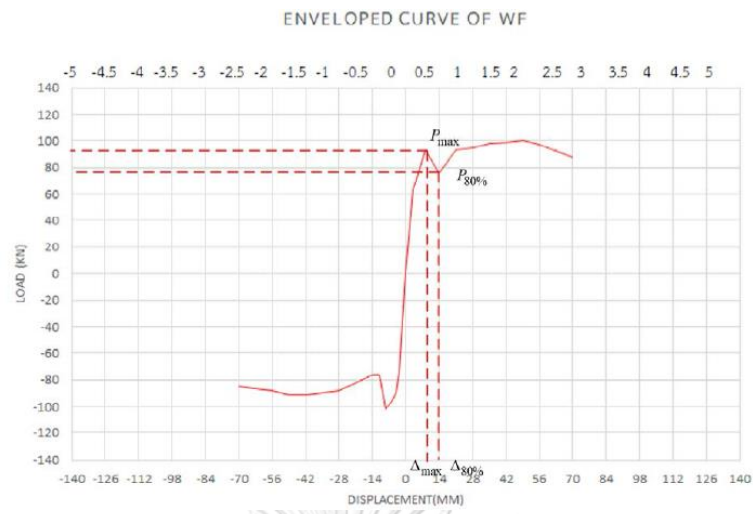


Figure 2.50 Force displacement of specimen BF NRCT (2023)



## CHAPTER 3

### METHODOLOGY

The section describes the assessment study of three macro models to simulate the structure response of masonry-infilled RC frame presence of window and door opening under later loading. This study will focus exclusively on in-plane loading and will not involve the strengthening of either the frame or its members. It will specifically investigate a single-story, single-bay infilled RC frame, as illustrated in Figure 3.1. The analysis will concentrate on the specimens listed in Table 3.1 for comparison with the experimental results of the existing frame NRCT (2023).

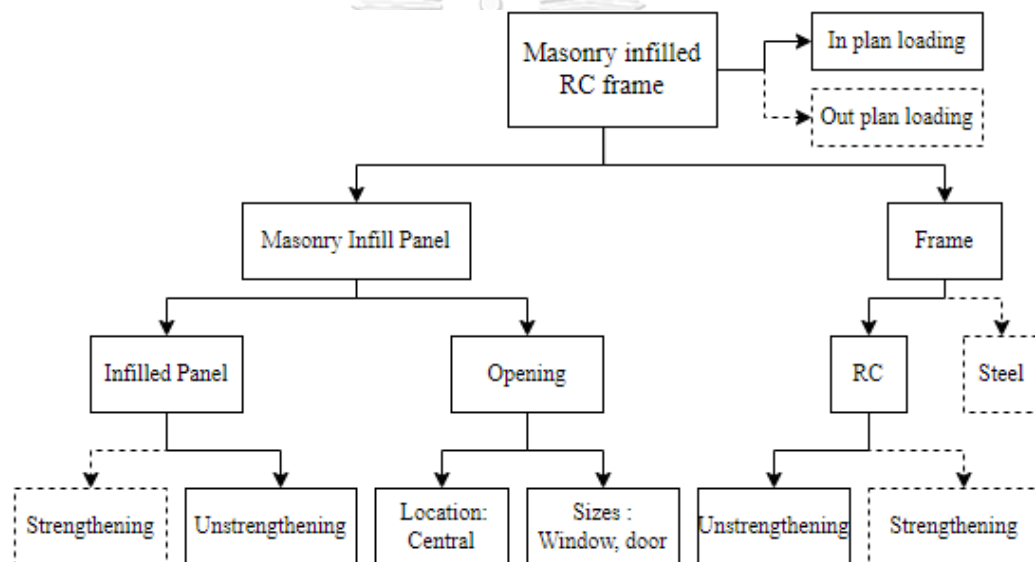


Figure 3.1 Scope of research study

Table 3.1 The studied specimens

Specimen	Description
BF	RC bare frame
DF	Masonry infilled RC frame with central door opening
WF	Masonry infilled RC frame with central window opening

The aim is to evaluate the most precise model and give recommendations for practical use. The three model includes:

- Multiple equivalent strut Method Yekrangnia & Asteris (2020)
- Discretized macro element Method Calio & Pantò (2014)
- Reduction factor of stiffness and strength

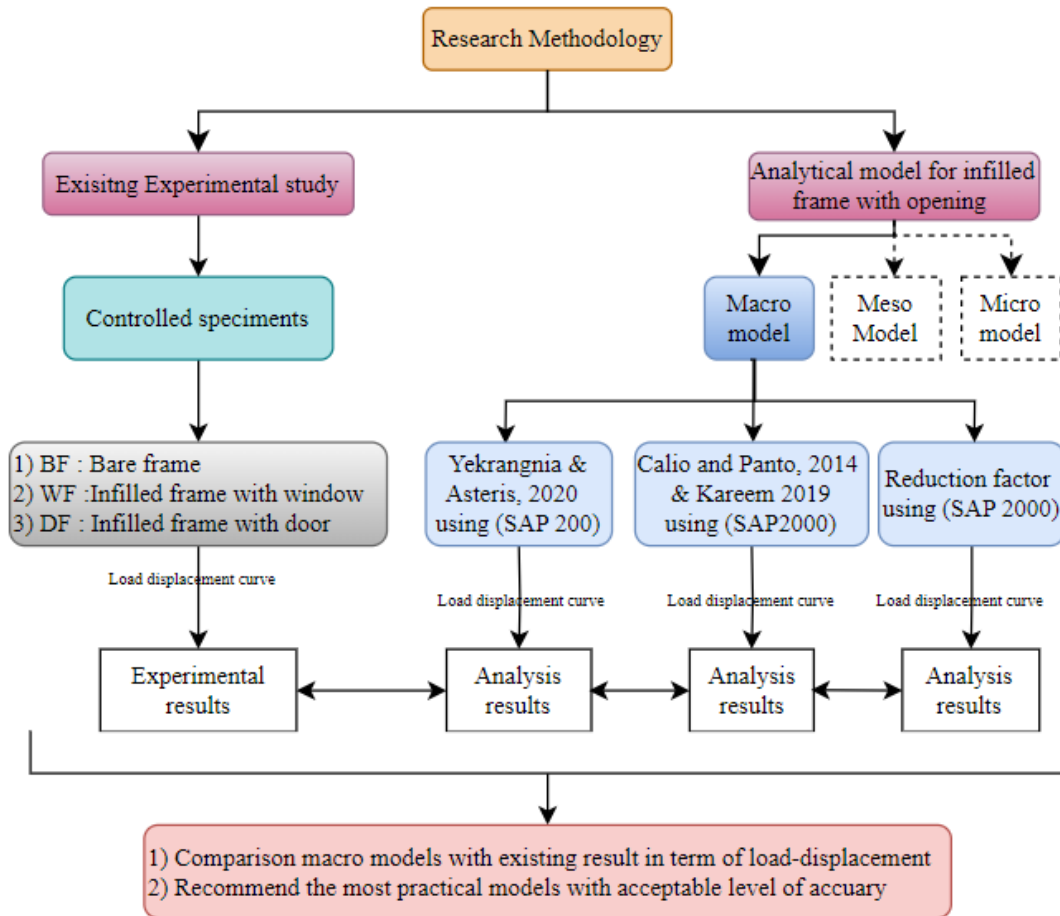


Figure 3.2 Framework of research Methodology

### 3.1 MULTIPLE EQUIVALENT STRUT METHOD

To address the significant computational demands, particularly for entire structures, a shift was made from the micro approach to the macro approach to capture the overall interactive behavior of infilled frames. Various formulas for geometric and mechanical properties of struts were developed through analysis of experimental studies. The complicated behavior of an infilled frame, particularly when considering local effects, cannot be adequately captured through the use of a single equivalent strut. Consequently, various models utilizing multiple equivalent struts with different arrangement layouts were suggested to imitate the performance of such frames. The diagonal and off-diagonal struts in this model are considered to possess solely compressive characteristics. This macro model relies exclusively on the diagonal compressive failure mode. The diagonal and off-diagonal struts in this model are considered to possess solely compressive characteristics. This macro model relies exclusively on the diagonal compressive failure mode.

#### 3.1.1 NONLINEAR PROPERTIES OF RC FRAME

When it comes to seismic modeling, the nonlinear structural model outperforms the linear elastic model in terms of identifying structural damage and performance. This numerical model employs a nonlinear distributed plasticity approach or fiber modeling to model the beam and column of RC frame members as illustrated in Figure 3.3 below. In this approach, section members will divide into several uniaxial fibers with stress-strain relationships to represent the nonlinear material of fiber. The Mander stress-strain model and the Park model which is available in SAP 2000 will be used for confined concrete RC material and reinforcement rebar material respectively.

The equivalent of plastic hinge length,  $L_p$  will follow the empirical formula proposed by Paulay & Priestley (1992) in Eq(3.1)). P-M2-M3 fiber hinges can account only for axial-flexural interaction and hence for axial deformation caused by bending in the element. Thus, shear behavior in frame members, Sezen & Patwardhan (2012) shear-deformation model will be modeled separately to capture flexural-shear and shear behavior.

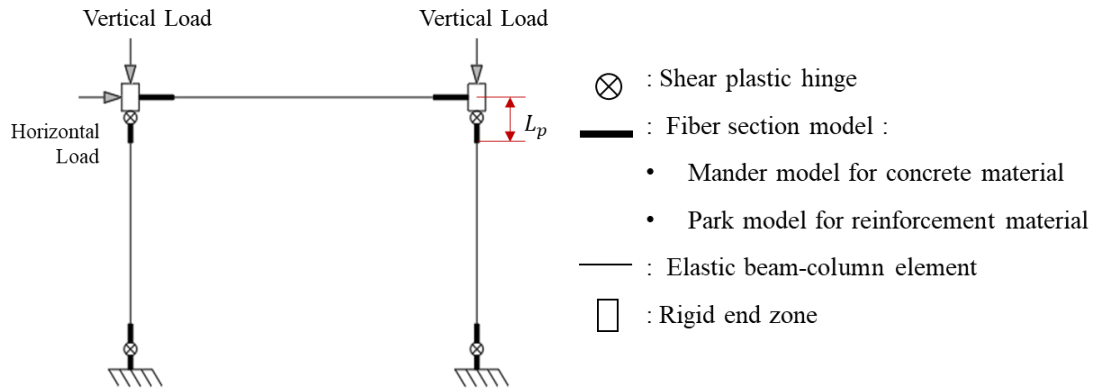


Figure 3.3 Analytical model of RC bare frame

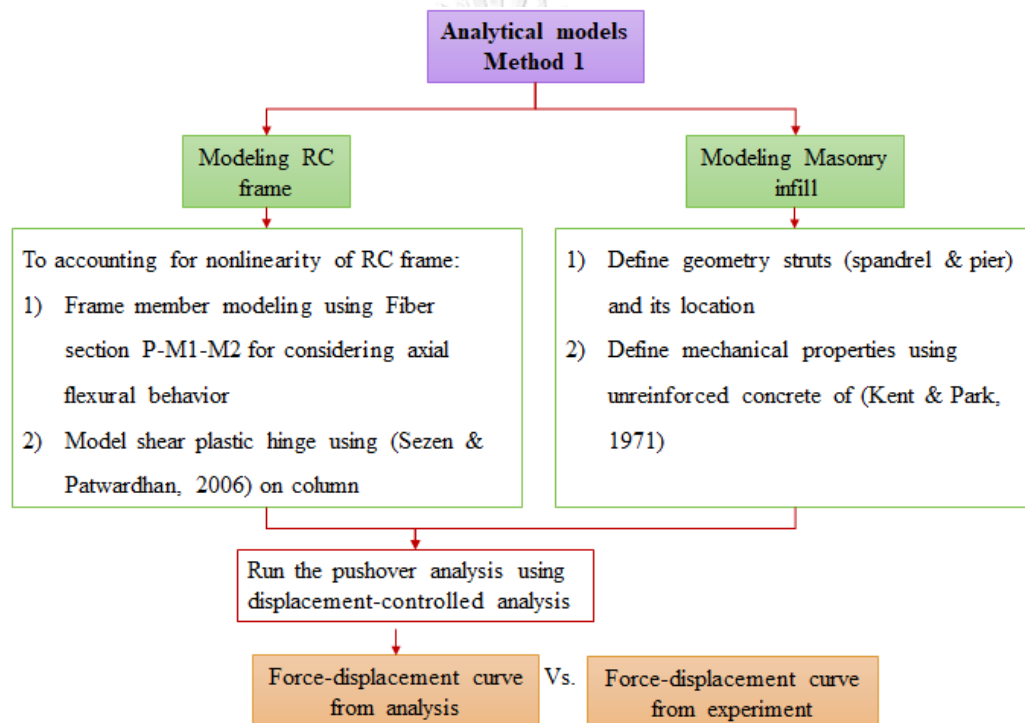


Figure 3.4 Solution procedure of Method 1

$$L_p = 0.08L + 0.022d_b f_y \geq 0.044f_y d_b \quad (3.1)$$

where,  $L_p$  is the plastic hinge length,  $L$  is the distance from the critical section of plastic hinge to the point of contra flexure,  $d_b$  is the diameter of longitudinal reinforcement,  $f_y$  is the expected yield strength of longitudinal reinforcement in MPa.

Shear-deformation model by Sezen & Patwardhan (2012)

The cracking shear displacement  $\Delta_{v,cr}$  (mm)

$$\Delta_{v,cr} = \frac{P}{8898} + 0.155 \quad (3.2)$$

where P is axial force (kN)

The cracking shear strength  $V_{cr}$  (kN)

$$V_{cr} = \Delta_{v,cr} \frac{GA_g}{1000L} \quad (3.3)$$

where G is concrete shear modulus (MPa),  $A_g$  is gross cross section of column ( $\text{mm}^2$ ), L is the length of column (mm).

The maximum shear strength,  $\Delta_{v,n}$  (kN)

$$\Delta_{v,n} = \gamma_n L \quad (3.4)$$

For flexural-shear failure mode, average shear strain at maximum shear strength  $\gamma_n$

$$\gamma_n = \frac{1}{227370} \times \frac{f_y \sqrt{\rho}}{\left(\frac{a}{d}\right) \sqrt{\frac{P}{A_g f'_c}}} \quad (3.5)$$

For shear failure mode, the average shear strain at maximum shear strength  $\gamma_n$

$$\gamma_n = \frac{1}{172250} \times \frac{\left(\frac{a}{d}\right) f_{yt} \rho_{sh}}{\sqrt{\frac{P}{A_g f'_c}}} - 0.0011 \quad (3.6)$$

where a and d are shear span length and effective depth of column,  $f_y$  and  $f_{yt}$  are the tensile yield of longitudinal and transverse rebar respectively (MPa),  $\rho$  and  $\rho_{sh}$  are the longitudinal and transverse rebar ratio in (%).

The maximum shear capacity of the column ACI 318-08,  $V_n$  (kN)

$$V_n = 0.17 \left( 1 + \frac{P}{14A_g} \right) \lambda \sqrt{f'_c} b d + A_{sh} f_{yt} \frac{d}{s} \quad (3.7)$$

where  $\lambda$  is the correction factor of concrete unit weight ( $\lambda = 1$ , for normal weight),

$s$  is the transverse reinforcement spacing.

The Shear displacement of the column at the onset of shear strength degradation (mm)

$$\Delta_{v,u} = \left( 4 - 12 \frac{(V_n/bd)}{f'_c} \right) \gamma_n L \quad (3.8)$$

The shear displacement at axial load failure by Elwood and Moehle (2005) (mm)

$$\Delta_{v,f} = \frac{4}{100} \left( \frac{1 + \tan^2 \phi}{\tan \phi + P \frac{s}{A_{sh} f_{yt} d_c}} \right) \gamma_n L \quad (3.9)$$

where, expected shear crack angle  $\phi = 65^\circ$ , recommended Elwood and Moehle (2005),  $d_c$  is core concrete depth.

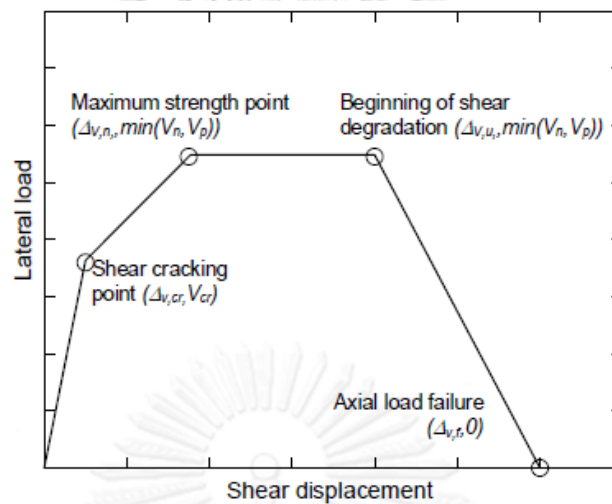


Figure 3.5 Shear plastic hinge Sezen & Patwardhan (2012) force-displacement

### 3.1.2 MASONRY INFILLED FRAME WITH OPENING

Yekrangnia & Mohammadi (2017) proposed a multiple equivalent strut model in based on the calibration of FEM and a comparison with existing models, to simulate masonry infilled frames. Yekrangnia & Asteris (2020) extended their macro modeling research to simulate the seismic behavior of infilled frames by introducing a novel approach for infilled frames with openings. This Method involves incorporating pier struts ( $S_p$ ) on both sides of the opening, along with spandrel struts ( $S_s$ ) positioned above and below the aperture. The diagonal struts are angled along the openings, and

it's important to consider the path and actual dimensions of the struts, as shown in Figure 3.5.

- For a window within infilled frames: the masonry panel is replaced by four struts surrounding the opening.
- For a door within infilled frames: the masonry panel is replaced by three struts surrounding the opening.

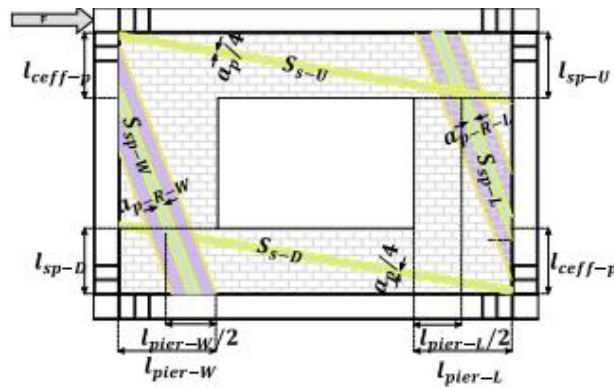


Figure 3.6 Proposed strut model for IF with an opening Yekrangnia & Asteris (2020)

### Geometry of strut

Diagonal strut width by Mainstone (1972),  $w_m$

$$w_m = 0.174\lambda_l^{-0.4}d \quad (3.10)$$

The Smith & Carter (1969) relative stiffness  $\lambda_l$

$$\lambda_l = h \left( \frac{E_m t \sin(2\theta)}{4E_c I_c h_w} \right)^{\frac{1}{4}} \quad (3.11)$$

Off diagonal strut width,  $w_p$

$$w_p = 0.001w_m(6\theta + 7.5\theta_p) \quad (3.12)$$

Effective contact length of off-diagonal struts,  $l_{ceff-p}$

$$l_{ceff-p} = 0.006h(\theta + \theta_p - 10\lambda_l h) \quad (3.13)$$

where,  $h$  is the frame's height.

$d, t$  are panel's diagonal length and thickness respectively.



$\theta, \theta_p$  are the angle of the diagonal strut and angle of the off-diagonal strut respectively.

Table 3.2 Parameters to model infilled frame with opening

	Width	Angle	End-location
$S_{p-L}$	$w_p$	$\theta_{p-L}$ $= \max \begin{cases} \theta_p = \tan^{-1} \frac{1}{\mu} - \lambda_1 h \\ \theta_{p-L} = \tan^{-1} \left( \frac{L - L_{ceff-p} - L_{sp-U}}{\frac{L_{pier-L}}{2}} \right) \end{cases}$	$l_{ceff-p}$
$S_{p-w}$	$w_p$	$equal \theta_{p-L}$ $= \max \begin{cases} \theta_p = \tan^{-1} \frac{1}{\mu} - \lambda_1 h \\ \theta_{p-L} = \tan^{-1} \left( \frac{L - L_{ceff-p} - L_{sp-D}}{\frac{L_{pier-w}}{2}} \right) \end{cases}$	$l_{ceff-p}$
$S_{s-U}$	$w_p/4$	From the IF corner to the above the opening level $\tan^{-1}(l_{sp-U}/l_w)$	NA
$S_{s-D}$	$w_p/4$	From the IF corner to the below the opening level $\tan^{-1}(l_{sp-D}/l_w)$	NA

Note: All angles are in degree

#### Mechanical properties of masonry infill

The compressive-only truss elements are employed for the struts, utilizing stress-strain characteristics Kent & Park (1971) models stress-strain model for unconfined concrete to represent the masonry infill characteristics as shown in Figure 3.6.

The ascending branch used Hognestad parabolic as shown in Eq. (3.46) replacing  $0.85f'_c$  by  $f'_c$  and  $\epsilon_{c0} = 0.002$ .

$$f_c = f'_c \left[ \frac{2\varepsilon_c}{\varepsilon_{c0}} - \left( \frac{2\varepsilon_c}{\varepsilon_{c0}} \right)^2 \right] \quad (3.14)$$

The post-peak branch was assumed to be a straight line with slope as shown in Eq.(3.47) below:

$$f_c = f'_c [1 - Z(\varepsilon_c - \varepsilon_{c0})] \quad (3.15)$$

where

$$Z = \frac{0.5}{\varepsilon_{50u} - \varepsilon_{c0}} \quad (3.16)$$

The strains corresponding to the stress equal to 50% of the maximum concrete strength for unconfined concrete,  $\varepsilon_{50u}$

$$\varepsilon_{50u} = \frac{3 + 0.29f'_c}{145f'_c - 1000} \quad (3.17)$$

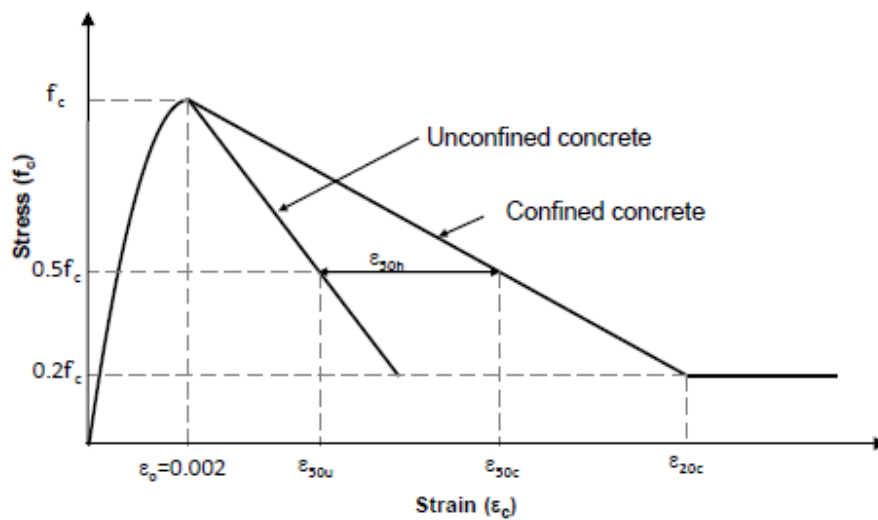


Figure 3.7 Stress-strain model for confined and unconfined concrete Kent & Park (1971)

### 3.2 DISCRETIZED MACRO ELEMENT METHOD

Caliò et al. (2012) introduced an innovative Method using discretized macro elements for evaluating the seismic behavior of unreinforced masonry buildings and accurately reproducing the in-plane failure mechanism behavior of masonry walls subjected to earthquake loading. Caliò & Pantò (2014) integrated the previous Method to simulate the interaction between the frame and infill using lumped plasticity beam-column elements for the frame members and plane macro-elements for the infills which are suitable for practical engineering purposes. Kareem & Pantò (2019) implemented the mentioned approach to perform in the structural software SAP 2000.

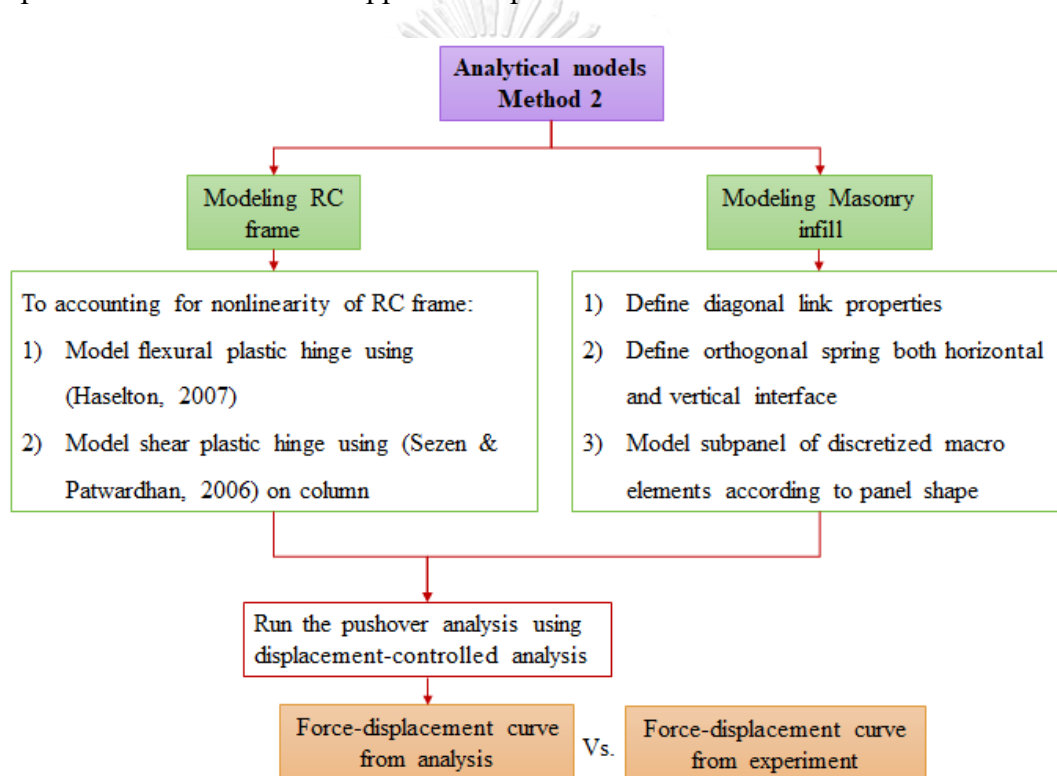


Figure 3.8 Solution procedure of Method 2

#### 3.2.1 NONLINEAR PROPERTIES OF RC FRAME

The RC frame elements are modeled using non-linear beam-column elements with concentrated plasticity or lump plasticity, which is described using a lumped plasticity approach proposed by Haselton & Deierlein (2007), where plastic hinges are introduced at both ends of each element. The plastic moment-rotation relationship is defined for these hinges, considering the plastic moment of the section and the axial load on the columns.

### Flexural capacity

The plastic rotation capacity

$$\theta_{\text{cap\_pl}} = 0.12 \left( \frac{\max\left(0.01, \frac{\rho_2 f_y}{f'_c}\right)}{\max\left(0.01, \frac{\rho_1 f_y}{f'_c}\right)} \right)^{0.225} (1) + 0.55a_{sl}(0.16)^v(0.02 + 40\rho_{sh})^{0.43} (0.54)^{0.01C_{\text{unit}}f'_c} (0.66)^{0.15n} (2.27)^{10\rho} \quad (3.18)$$

The total rotation capacity

$$\theta_{\text{cap\_tot}} = 0.12 \left( \frac{\max\left(0.01, \frac{\rho_2 f_y}{f'_c}\right)}{\max\left(0.01, \frac{\rho_1 f_y}{f'_c}\right)} \right)^{0.175} (1) + 0.4a_{sl}(0.20)^v(0.02 + 40\rho_{sh})^{0.52} (0.56)^{0.01C_{\text{unit}}f'_c} (2.27)^{10\rho} \quad (3.19)$$

The post-capping rotation capacity

$$\theta_{\text{pc}} = 0.76(0.031)^v(0.02 + 40\rho_{sh})^{1.02} \leq 0.10 \quad (3.20)$$

The yielding moment capacities ratio

$$\frac{M_c}{M_y} = (1.25)(0.89)^v(0.91)^{0.01C_{\text{unit}}f'_c} \quad (3.21)$$

The yielding moment of the column

$$\frac{M_c}{bd^3} = \varphi_y \left\{ E_c \frac{\xi_y^2}{2} \left[ 0.5(1 + \delta_1) - \frac{\xi_y}{3} \right] + \frac{E_s}{2} \left[ (1 - \xi_y)\rho_1 + (\xi_y - \delta_1)\rho_2 + \frac{\rho_v}{6}(1 - \delta_1) \right] (1 - \delta_1) \right\} \quad (3.22)$$

The ratio of neutral axis depth at yielding and effective depth can be determined as follows:

$$\xi_y = (n^2 A^2 + 2nB)^{\frac{1}{2}} - nA \quad (3.23)$$

$$n = \frac{E_s}{E_c} \quad (3.24)$$

- If the section yielding is controlled by tension reinforcement yielding:

$$\varphi_y = \frac{f_y}{E_s(1 - \xi_y)d} \quad (3.25)$$

$$A = \rho_1 + \rho_2 + \rho_v + \frac{P}{bdf_y} \quad (3.26)$$

$$B = \rho_1 + \rho_2 \delta_1 + 0.5\rho_v(1 + \delta_1) + \frac{P}{bdf_y} \quad (3.27)$$

- If the section yielding is controlled by compression zone, yielding curvature and ratio of neutral axis depth at yielding and effective depth can be determined as follows:

$$\phi_y = \frac{\varepsilon_c}{\xi_y d} \approx \frac{1.8f'_c}{E_s \xi_y d} \quad (3.28)$$

$$A = \rho_1 + \rho_2 + \rho_v - \frac{P}{\varepsilon_c E_s b d} \approx \rho_1 + \rho_2 + \rho_v - \frac{P}{1.8nbdf'_c} \quad (3.29)$$

$$B = \rho_1 + \rho_2 \delta_1 + 0.5\rho_v(1 + \delta_1) \quad (3.30)$$

$$\delta_1 = \frac{d_1}{d} \quad (3.31)$$

### Shear capacity

To capture the flexural shear and shear failure, the plastic shear hinge needs to be adapted in column member only due to the beam member being less likely to fail by shear failure. For more details on calculation of plastic hinge See reference (3.1.1)

### 3.2.2 MASONRY INFILLED FRAME

The discrete macro element considers the infill panel as a discrete macro element, consisting of diagonal links and interface links including many orthogonal 1D links and a single longitudinal link. The 2D discrete macro-model uses rigid elements hinged at the vertexes of the panel to simulate the edges of the quadrilateral infill. The interface of each panel consists of multiple 1D links that simulate various failure modes such as flexural, sliding, shear diagonal, and mixed failure modes as shown in Figure 3.9 for the solid infill frame and Figure 3.10 for the infilled frame with opening.

### For diagonal springs

The diagonal springs are used to model the shear behavior of the infill walls in infilled frames. The diagonal connections within the infill panel exhibit a symmetric, linear-softening elastic constitutive law, as illustrated in Figure 3.7. This modeling approach is used to replicate the brittle shear behavior typically observed in infill walls.

By assuming equivalence between the panel and the masonry wall, we can estimate the elastic stiffness of the diagonal link, denoted as  $k_d$ . The yielding force,  $F_y$  of the links is determined by a specific criterion, as described in equation (3.6). In this analysis, we treat the masonry wall as a pure shear deformable homogeneous plate.

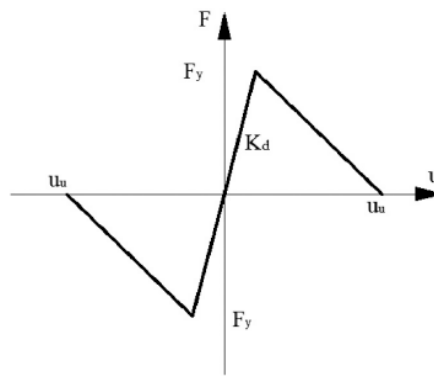


Figure 3.9 Constitutive law for diagonal shear springs

The elastic stiffness of the diagonal Link results  $k_d$ :

$$k_d = \frac{G_m A}{2H \cos^2 \alpha} \quad (3.32)$$

$G_m$  shear modulus of masonry

$A$  cross section of the panel

$H$  the height of the panel

$\alpha$  the angle between the diagonal and the horizontal side of the panel

The ultimate shear force  $F_y$ :

$$F_y = \frac{V_d}{2 \cos \alpha} \quad (3.33)$$

The ultimate displacement  $u_u$ :

$$u_u = \gamma_u \frac{H}{\cos \alpha} \quad (3.34)$$

$\gamma_u$  the ultimate in-plane drift of the panel

The ultimate shear strength  $V_d$  in infilled frames can be determined by two Methods:

- The Turnsek and Cacovic criteria, which presume that diagonal shear failure corresponds to the principal tensile stresses in the central region of the infill panel, is the first approach. The ultimate shear strength  $V_d$ :

$$V_d = \frac{f_{v0}Lt}{b} \sqrt{1 + \frac{\sigma_n}{f_{v0}}} \quad (3.35)$$

$f_{v0}$  is the ultimate shear stress without the axial load.

$\sigma_n$  is the average vertical compressive stress transferred to the masonry panel due to the gravity loads.

$b$  is the influence of the aspect ratio  $H/L$  of the wall, where  $0 \leq b \leq 1.5$

- The second Method is the Mohr-Coulomb law, involving parameters like the friction coefficient and average compressive stress, which require experimental determination. This criterion is also applied to explain sliding-shear failure, albeit with distinct parameter values.

$$V_d = f_{v0} + \mu_c \sigma_n \quad (3.36)$$

#### For longitudinal link

Longitudinal links of interface to simulate the bed mortar joint sliding and typically characterized by the Mohr-Coulomb criteria, which accounts for the sliding behavior of the bed mortar joints. In numerical simulations, the sliding mechanisms of longitudinal interface links are often neglected, and internal rigid constraints are used instead.

#### For orthogonal springs

The behavior of masonry can be understood by considering its flexural and shearing characteristics as a finite portion of an orthotropic inelastic continuum. By calibrating the horizontal and vertical interfaces independently, the flexural behavior approximated by interface orthogonal springs and the orthotropic character of the masonry were considered as shown in Figure 3.8.

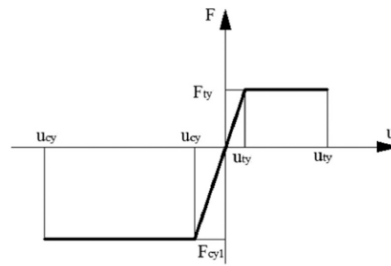


Figure 3.10 Constitutive law for orthogonal Links

Table 3.3 Calibration of the orthogonal link interface Kareem &amp; Pantò (2019)

Parameters for orthogonal links	Vertical interface	Horizontal interface
Initial elastic stiffness, $K_p$	$K_{hp} = 2 \frac{E_h \lambda_h S}{L'}$	$K_{vp} = 2 \frac{E_v \lambda_v S}{H}$
Compression yielding force, $F_{cy}$	$F_{hcy} = s \lambda_h \sigma_{hc}$	$F_{vcy} = s \lambda_v \sigma_{vc}$
Tensile yielding force, $F_{ty}$	$F_{hty} = s \lambda_h \sigma_{ht}$	$F_{hty} = s \lambda_h \sigma_{ht}$
Compression ultimate displacement, $u_{cu}$	$u_{hcu} = \frac{1}{2} \varepsilon_{hcu}$	$u_{vcu} = \frac{1}{2} \varepsilon_{vcu}$
Tensile ultimate displacement, $u_{tu}$	$u_{htu} = \frac{1}{2} \varepsilon_{htu}$	$u_{vtu} = \frac{1}{2} \varepsilon_{vtu}$

For solid infilled frame

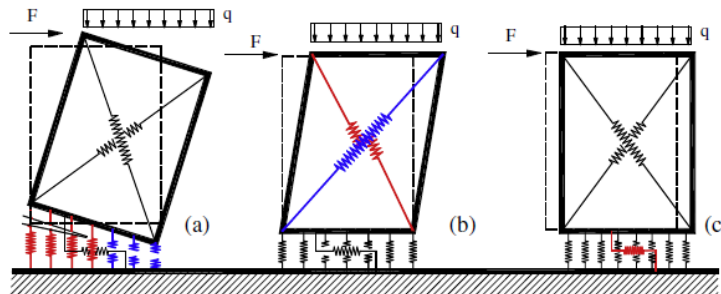


Figure 3.11 model for simulation infilled frame model by Caliò & Pantò (2014)  
 (a) flexural failure; (b) shear-diagonal failure and (c) shear sliding failure.

For an infilled frame with an opening

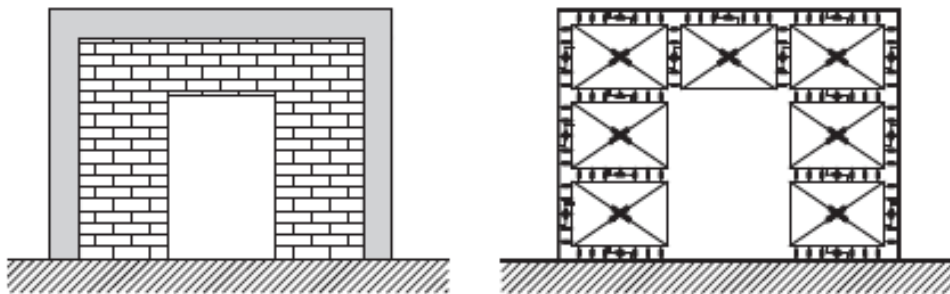


Figure 3.12 Model of the infilled frame with central door opening Caliò & Pantò (2014)



### 3.3 REDUCTION FACTOR METHOD

#### 3.3.1 NONLINEAR PROPERTIES OF RC FRAME

The reinforced concrete (RC) frame components are simulated using nonlinear beam-column elements featuring a lumped plasticity approach.

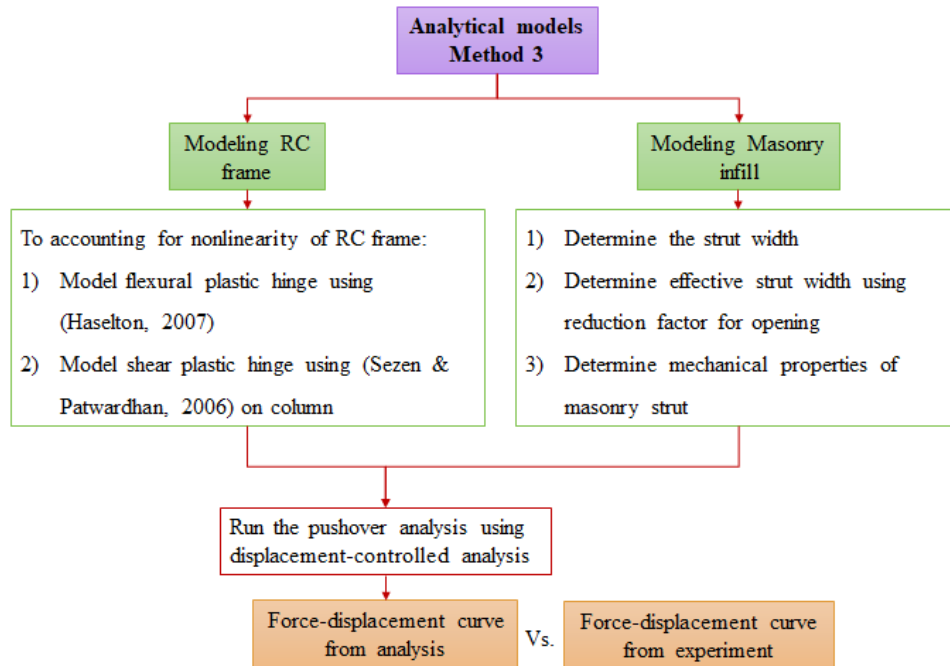


Figure 3.13 Solution procedure of Method 3

#### 3.3.2 MODELING INFILLED FRAME

##### Strut width formula

The diagonal equivalent width serves as an analytical representation of the contribution of the infilled wall to both the lateral stiffness and strength of the frame. This is the simplified approach utilized for representing the behavior of a masonry-infilled frame subjected to cyclic lateral loads. Based on both experimental observations and theoretical considerations, the analytical formulas for the width of diagonal equivalent strut were developed by various researchers. Here are three diagonal equivalent strut width formulas that are commonly used in the field of structural engineering for masonry infilled frames:

Table 3.4 Selection formula width of the equivalent strut

Holmes (1961)	$w = \frac{d_m}{3}$	(3.37)
Mainstone (1972)	$w = 0.175d_m\lambda_h^{-0.4}$	(3.38)
Liauw & Kwan (1984)	$w = 0.95h\frac{\cos \theta}{\lambda_h}$	(3.39)

where  $\lambda_h$  is the Smith & Carter (1969) relative stiffness,  $d_m$  is the diagonal length of the infilled panel.

#### Reduction factor formula

A recent study has demonstrated that the presence of openings has substantially affected the seismic behavior of masonry-infilled frames, notably leading to a decrease in the infilled frame's stiffness, strength, and ability to dissipate energy. Many researchers have suggested empirical formulas that incorporate this concern, employing reduction factors to accurately model with presence of openings, either windows or doors, within the infilled frame. The objective of this research is to examine the three most frequently employed reduction factor expressions to account for the presence of a central opening. This comparison will be made against the results obtained from analyzing using multiple equivalent struts and macro element Methods. Kurmi & Haldar (2022) examined the impact of openings in infilled frames on seismic response using five different reduction factor models. The research determined that the reduction factor suggested by Decanini et al. (2014) offers the most precise assessment of peak strength, surpassing the simplicity of models proposed by G. Al-Chaar et al. (2003; Mohammadi & Nikfar (2013), while still providing reasonably accurate predictions.

Table 3.5 Selected reduction factor formula for central opening.

Researchers	Reduction factor for central opening	(Eq.)
G. Al-Chaar et al. (2003)	$R_k, R_s = 0.6 \left( \frac{A_o}{A_p} \right)^2 - 1.6 \left( \frac{A_o}{A_p} \right) + 1$	(3.40)
Mohammadi & Nikfar (2013)	$R_k = 1.1859 \left( \frac{A_o}{A_p} \right)^2 - 1.6781 \left( \frac{A_o}{A_p} \right) + 1, \left( \frac{A_o}{A_p} \right) < 0.4$	(3.41)
	$R_s = -1.085 \left( \frac{A_o}{A_p} \right) + 1, \left( \frac{A_o}{A_p} \right) < 0.4$	(3.42)
Decanini et al. (2014)	Unreinforced and partially reinforced opening: $R_k, R_s = 0.55e^{-0.035 \frac{A_o}{A_p}} + 0.44e^{-0.025 \frac{l_o}{l_p}}$	(3.43)
	Reinforced opening $R_k, R_s = 0.63e^{-0.020 \frac{A_o}{A_p}} + 0.40e^{-0.010 \frac{l_o}{l_p}}$	(3.44)

#### Selection backbone curves

The shear strength of the infilled frame was determined based on experimental findings, allowing for the prediction of the maximum shear strength by considering the observed failure mechanism during testing. The primary objective is to establish the hysteresis characteristics of the equivalent strut. Typically, the backbone curves obtained from a literature review adopt trilinear or quadrilinear representations to effectively depict the stepwise progression of damage observed during horizontal loading tests. This includes phenomena such as the separation of the infill from the frame, the development of cracks in the panel, maximum lateral strength, and residual capacity.

Panagiotakos & Fardis (1996): A quadrilinear backbone curve, as depicted in Figure 3.11, was derived from ten experiments carried out on reinforced concrete frames infilled with horizontally hollow masonry bricks:

- Maximum strength,  $F_{\max} = 1.3F_{cr}$
- $F_{cr}$  cracking strength

- Residual strength,  $F_{res} = \beta F_{max}$
- Elastic stiffness,  $K_{fc} = 4K_{sec}$
- $K_{sec}$  cracking strength secant stiffness according to Mainstone (1972)
- Softening-to-peak stiffness,  $K_{deg} = -\alpha K_{sec}$

where,  $0.5\% \leq \alpha \leq 10\%$  and  $1\% \leq \beta \leq 2\%$

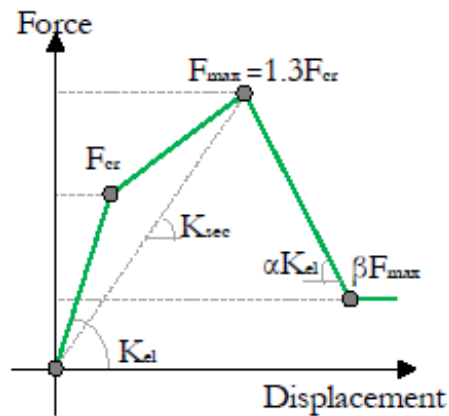


Figure 3.14 Force-displacement relation for infilled adopted by Mucedero et al. (2020)

Leeanansaksiri et al. (2018)

The bilinear backbone curve was used to represent the equivalent strut of masonry infills, as illustrated in Figure 3.16. The parameter for modeling the force-displacement relationship will be shown below:

For diagonal compressive failure

Yield strength by diagonal compressive strength,  $V_y$  Saneinejad & Hobbs (1995)

$$V_y = R_t = 2\sqrt{2}th'f_t \cos \theta \quad (3.45)$$

where  $f_t = 0.25\phi\sqrt{f'_m}$

$$\phi = 0.65$$

$\theta$  is the inclination angle of the diagonal strut.

$f_t$  is the tensile strength of the masonry prism.

$f'_m$  is the compressive strength of the masonry prism Figure 65

Maximum strength,  $V_m$  can be determined based on the diagonal compressive strength:

$$V_m = R_{DC} = \frac{0.5h'tf_a}{\cos \theta} \quad (3.46)$$

$f_a$  is the tensile strength of the masonry prism.

$$\text{where } f_a = 0.6\phi f'_m$$

$$\phi = 0.65$$

For corner-crushing failure

Maximum strength,  $V_m$  can be determined based on corner crushing:

$$V_m = R_{CC} = \frac{(1 - \alpha_c)\alpha_c t h \sigma_c + \alpha_b t l \tau_b}{\cos \theta} \quad (3.47)$$

$$\text{where, } \alpha_c = \frac{1}{h} \sqrt{\frac{2M_{pj} + 2\beta_c M_{pc}}{\sigma_c t}}$$

$$\alpha_b = \frac{1}{l} \sqrt{\frac{2M_{pj} + 2\beta_b M_{pb}}{\sigma_b t}}$$

$$\sigma_c = \frac{f'_m}{\sqrt{1 + 3\mu^2 r^4}}$$

$$\sigma_b = \frac{f'_m}{\sqrt{1 + 3\mu^2}}$$

$$\tau_b = \mu \sigma_b$$

$M_{pc}, M_{pb}$  the plastic moments of column and beam, respectively

$$M_{pj} = \min (M_{pc}, M_{pb})$$

$\mu$  is the coefficient of friction of the frame and the infill interface

$r = h/l$  is the aspect ratio of the frame

$\beta_c, \beta_b$  are the reduction factors for the column and beam which can be taken as 0.2

$h, l$  are the center-to-center dimensions of the height and the length of the frame

The lateral yield strength by corner crushing can be approximated by considering as below:

$$V_y = R_{yCC} = \frac{(1 - \alpha_C)\alpha_C t h \sigma_{yc} + \alpha_b t l \tau_{yb}}{\cos \theta} \quad (3.48)$$

where,  $\sigma_{yc} = \frac{f_{ym}}{\sqrt{1 + 3\mu^2 r^4}}$

$$\tau_{yb} = \mu \sigma_{yb}$$

$$\sigma_{yb} = \frac{f_{ym}}{\sqrt{1 + 3\mu^2}}$$

$\sigma_{yc}$  is the contact normal yield stress at the loaded corner of the column

$\sigma_{yb}$  is the contact normal yield stress.

$\tau_{yb}$  is the contact yield shear stress at the beam infill interface.

$f_{ym}$  is the yield strength of the masonry prism

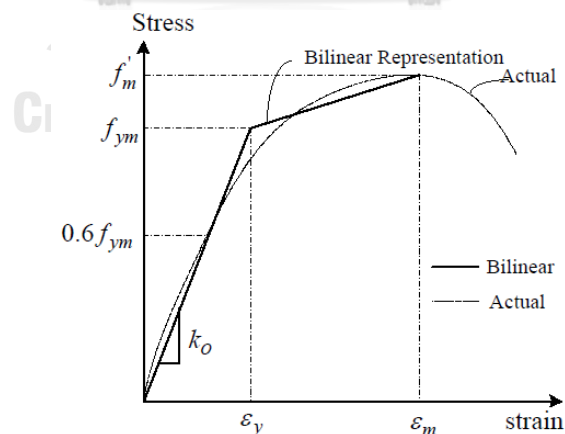


Figure 3.15 Stress-strain relationship of masonry prism Leeanansaksiri et al. (2018)

Yield displacement,  $\Delta_y = \frac{\epsilon_y L_d}{\cos \theta} \quad (3.49)$

Maximum displacement,  $\Delta_m = \frac{\epsilon_m L_d}{\cos \theta} \quad (3.50)$

Length of the equivalent diagonal strut,  $L_d = \sqrt{(1 - \alpha_c)^2 h'^2 + l'^2}$  (3.51)

Initial stiffness,  $k_0 = \frac{V_y}{\Delta_y}$  (3.52)

Secant stiffness,  $k_{sec} = \frac{V_m}{\Delta_m}$  (3.53)

post-yield stiffness,  $\alpha k_0 = \frac{V_m - V_y}{\Delta_m - \Delta_y}$  (3.54)

Bilinear factor,  $\alpha = \frac{V_m - V_y}{\Delta_m - \Delta_y} \times \frac{V_y}{\Delta_y}$  (3.55)

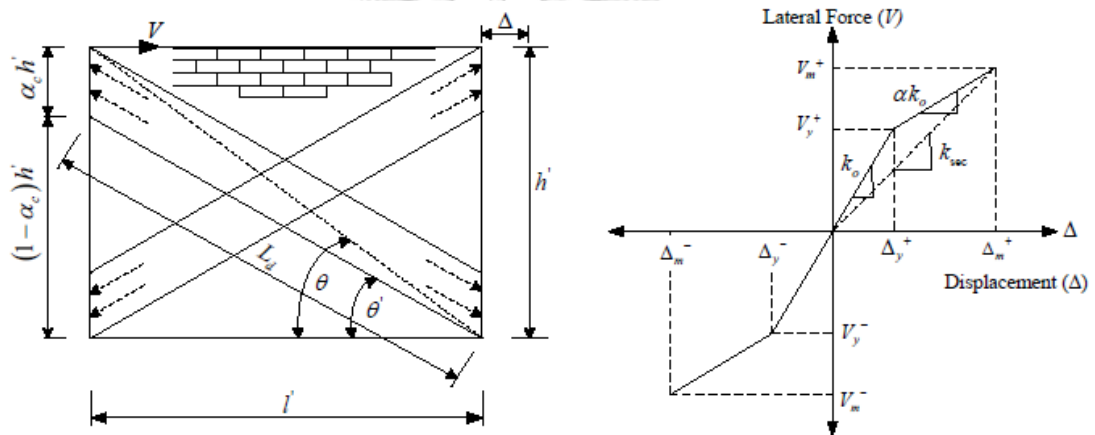


Figure 3.16 Force displacement of the equivalent strut of masonry infills  
Leeanansaksiri et al. (2018)

### 3.4 SELECTED SOFTWARE AND EXPECTED RESULT

In this study, SAP2000 will be employed to simulate the behavior of infilled RC frames using the three macro Methods mentioned above. SAP2000 simplifies the modeling and analysis of complex structures, providing options for both linear and nonlinear analyses. With its dynamic analysis capabilities, it is well-suited to evaluate structural responses to dynamic forces, such as earthquakes and wind loads. In essence, SAP2000 empowers engineers to address a wide range of structural challenges efficiently and effectively. The force-displacement curve results of each analytical model will be compared to the existing experimental results from NRCT (2023) to evaluate how well each analytical model captures the behavior of an infilled

RC frame with the presence of openings, including central door and window configurations. Through this comparative study, we aim to identify the most accurate and precise model and provide recommendations for practical engineering applications.





## CHAPTER 4

### ANALYTICAL MODELS

#### 4.1 MULTIPLE EQUIVALENT STRUT PROCEDURE (METHOD 1)

To verify the analytical model, a calibration study should be conducted. Ahani et al. (2019) experimental study was used to calibrate in Kareem et al. (2022) study by using multiple equivalent struts Method implemented in ABAQUS FEM software.

Similarly, this study will use bare frame result from Ahani et al. (2019) to verify the result for the bare frame (BF), and masonry infilled frame with 19% opening from previous experimental study and analytical model using ABAQUS FEM software to compare with the analytical model using SAP 2000 while using fiber element for consider axial-flexural behavior and shear plastic hinge to consider shear and flexural shear behavior.

##### 4.1.1 CALIBRATION OF THE ANALYTICAL MODEL METHOD 1

The geometrical and mechanical properties of the Ahani et al. (2019) test are shown in Table 4.1 and Table 4.2 below respectively.

###### a) Calibration of the bare frame (BF)

Follow the Methodology in section 3.1.1, the comparison of the static pushover analysis curve of experimental and analytical illustration as the Figure 4.1. The comparison between analytical results implemented in SAP2000 and experimental results of the bare frame shows a good agreement. This means that the analytical model could be used to estimate the nonlinear response of the bare frame.

Table 4.1 Reinforcement detail of frame member of verification study

RC Members	Size (b x h) mm	Longitudinal rebar	Transverse rebar
Column	(250x250)	8DB14	RB6.5@50
Beam	(250x300)	5DB14	RB6.5@100
Footing	(300x407)	6DB16	RB6.5@150

Table 4.2. Material properties of concrete, reinforcement

Concrete			Longitudinal rebar			Transversal rebar	
$E_c$ (MPa)	$f'_c$ (MPa)	$\epsilon_{cu}$ (%)	$E_s$ (MPa)	$f_s$ (MPa)	$f_u$ (MPa)	$f_s$ (MPa)	$f_u$ (MPa)
22661	31.59	0.53	196200	392.4	588.6	294.3	490.5

Table 4.3 Modeling parameter of the shear plastic hinge of the verification study

$\Delta_{v,n}$ (mm)	23.69
$V_n$ (kN)	133.45
$\Delta_{v,u}$ (mm)	72.05
$\Delta_{v,f}$ (mm)	190.11

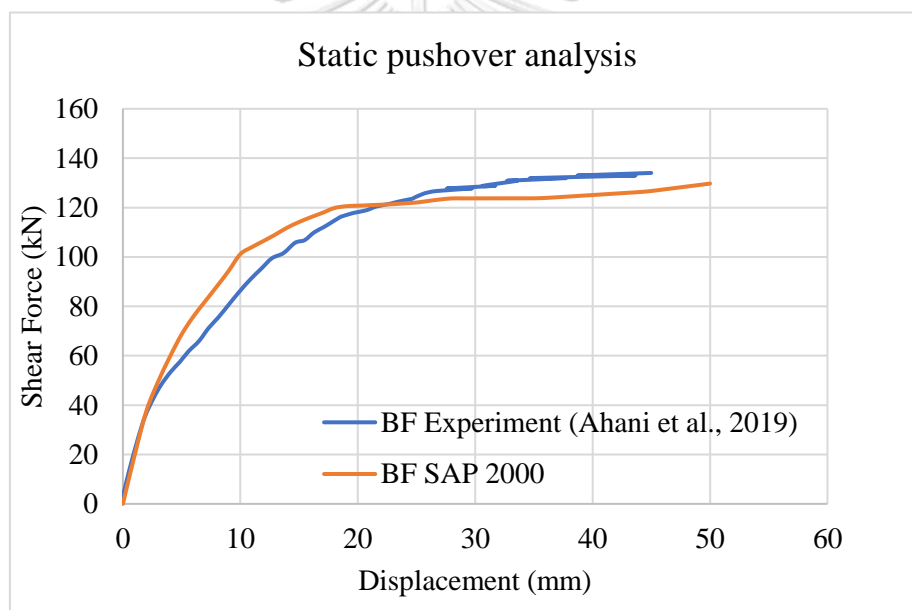


Figure 4.1 Comparison of experimental and analytical results of bare frames by using Method 1

## b) Calibration of the infilled frame with 19% of window opening (IF-19)

Using the multiple equivalent strut Method by Yekrangnia & Asteris (2020) as described Section 3.1, and from the dimension of opening and mechanical properties of masonry as shown in Table 4.4, the width dimension of equivalent struts could be determined as illustrated in Table 4.5. Nonlinear pushover analysis was performed using displacement controlled in SAP 2000. The comparison result between the experimental result of Ahani et al. (2019), the analytical study of Kareem et al. (2022)

implemented in ABAQUS FEM software, and using SAP 2000 is illustrated in Figure 4.2, shows that the analytical model could predict the response of masonry infilled RC frame with 19% of opening with compromise estimation.

Table 4.4 Material properties of masonry

$w_m$ (kN/m <sup>3</sup> )	$E_m$ (MPa)	$f_m$ (MPa)	$f_{tm}$ (MPa)	$\lambda$ (cm)	$G_m$ (MPa)	$f_{v0}$ (MPa)
18	5088	7.42	0.06	10	598	0.135

Table 4.5 Geometrical properties of the strut with door opening (IF-19)

Struts	Width(mm)	Angle(degree)	End-location(mm)
$w_{p-l}$	215	54	571.4
$w_{p-w}$	215	54	571.4
$w_{sp-u}$	54	9	428.5
$w_{sp-d}$	54	9	428.5

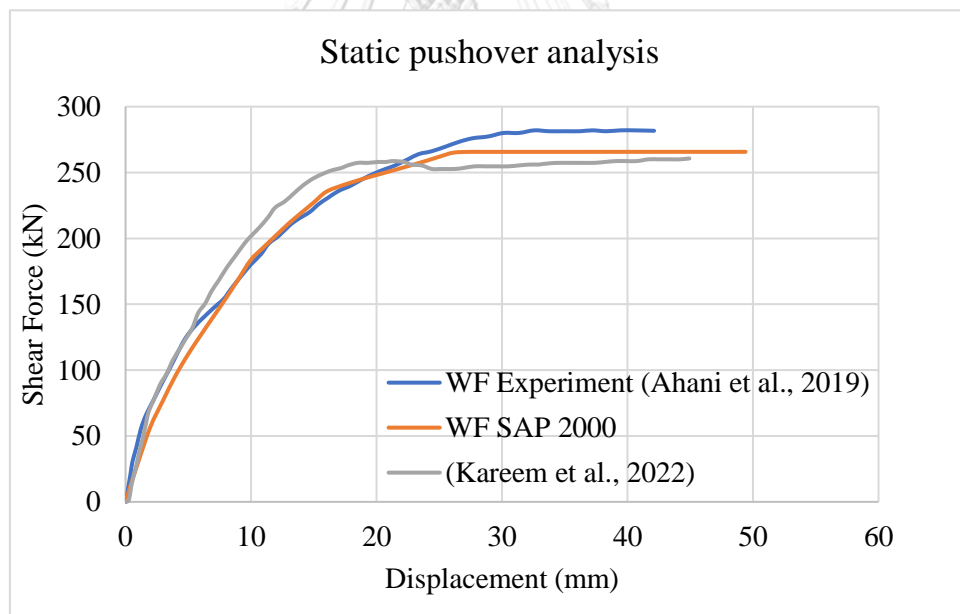


Figure 4.2 Comparison of experimental and analytical results of WF using multiple equivalent struts.

#### 4.1.2 ANALYTICAL STUDY OF RC BARE FRAME

Follow the same way of Methodology in section 3.1.1 and the verification study in section 4.1.1, are used to model the nonlinearity properties of the bare frame. In this approach, section members will divide into several uniaxial fibers with stress-strain relationships to represent the nonlinear material of fiber. The Mander stress-strain model which is available in SAP 2000 will be used for confined concrete RC members. The equivalent of plastic hinge length,  $L_p$  will follow the empirical formula proposed by Paulay & Priestley (1992). P-M2-M3 fiber hinges can account only for axial-flexural. Thus, shear behavior in frame member, Sezen & Patwardhan (2012) shear-deformation model will be modeled separately to capture flexural-shear and shear behavior. The modeling parameters for the shear plastic hinge are illustrated in Table 4.6.

Table 4.6 Modeling parameter of the shear plastic hinge of column

$\Delta_{v,n}$	(mm)	1.602
$V_n$	(kN)	68.62
$\Delta_{v,u}$	(mm)	5.126
$\Delta_{v,f}$	(mm)	50.651

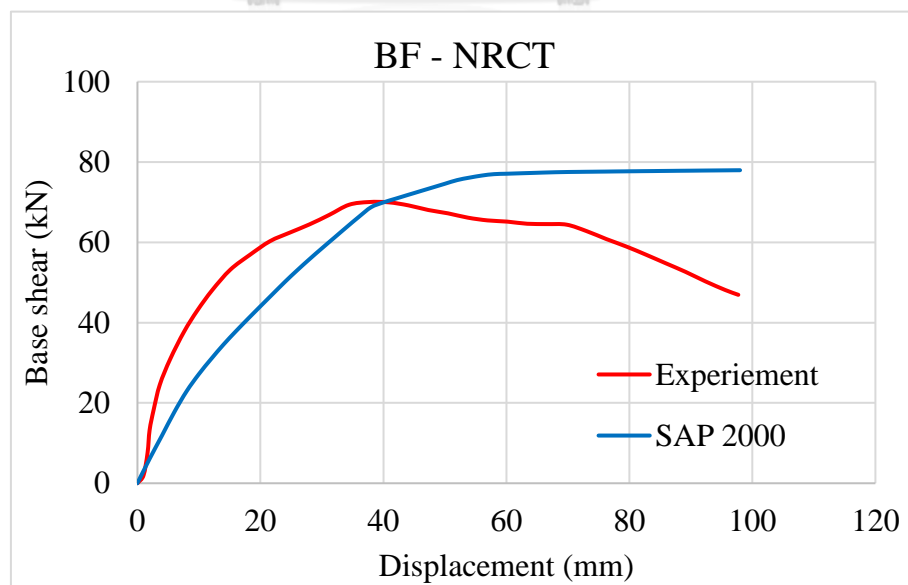


Figure 4.3 Compare the result of BF between analytical and experimental results

#### 4.1.3 ANALYTICAL STUDY OF MASONRY INFILLED RC FRAME WITH WINDOW OPENING (WF)

From the Methodology in section 3.1.2 and Table 3.2, the geometry and location of struts could be determined as the result in table Table 4.7.

##### Geometry and placement of strut

Table 4.7 Geometrical properties of the strut with door opening (WF)

	Width(mm)	Angle(degree)	End-location(mm)
$w_{p-l}$	257.9	56	914.2
$w_{p-w}$	257.9	56	914.2
$w_{sp-u}$	64.5	11	725
$w_{sp-d}$	64.5	11	725

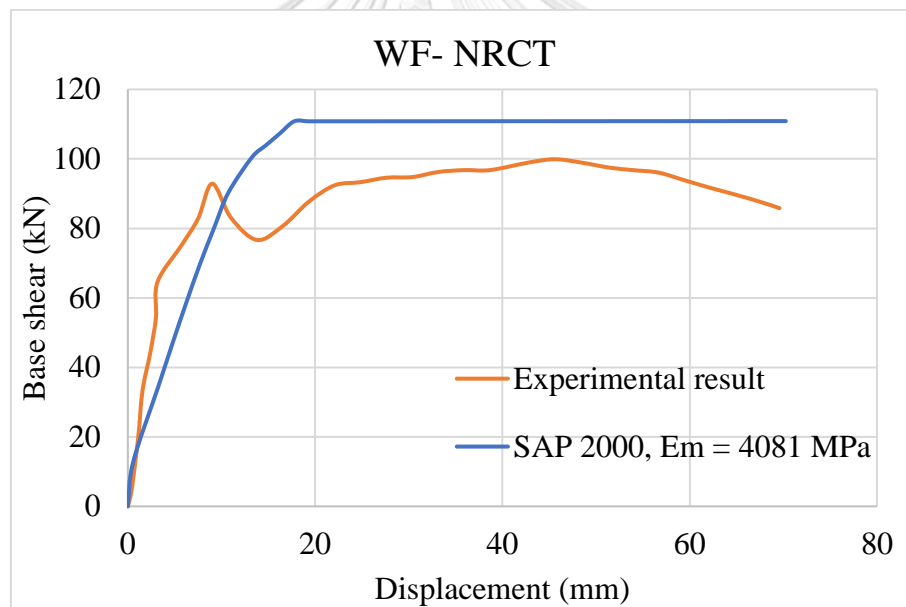


Figure 4.4 Compare result of WF between analytical and experimental results using Method 1

#### 4.1.4 ANALYTICAL STUDY OF MASONRY INFILLED RC FRAME WITH DOOR OPENING (DF)

From the Methodology in section 3.1.2 and Table 3.2, the geometry and location of struts could be determined as the result in table Table 4.8.

Table 4.8 Geometrical properties of the strut with door opening (DF)

Strut	Width(mm)	Angle(degree)	End-location(mm)
$w_{p-l}$	257.9	58	914.2
$w_{p-w}$	257.9	68	914.2
$w_{sp-u}$	64.5	9	600

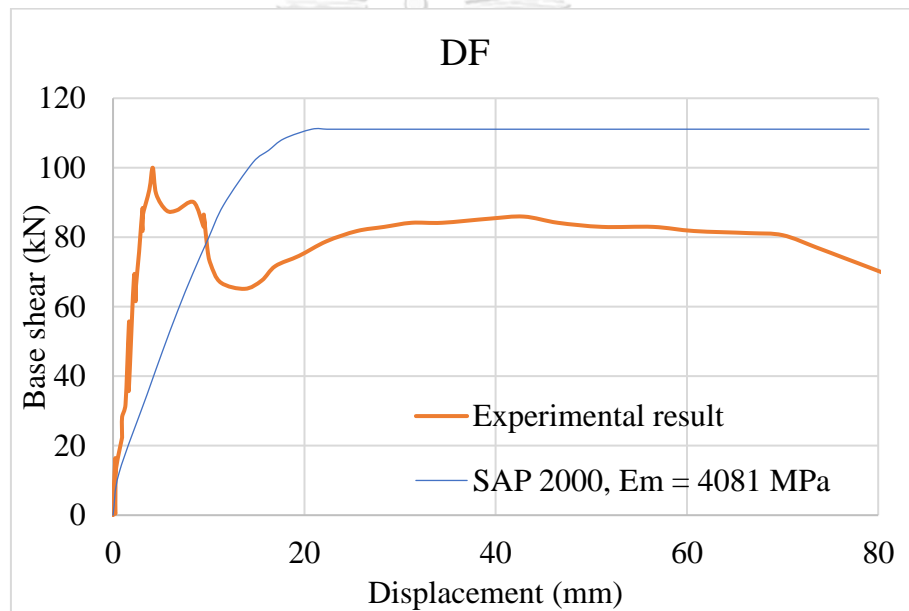


Figure 4.5 Compare result of DF between analytical and experimental results

#### 4.1.5 PARAMETER STUDY

The sensitivity study reveals that increasing the modulus of elasticity of the masonry wall increases the initial stiffness of the infilled frame at small displacements, as shown in Table 4.9. Specifically, increasing the modulus by 2, 3, and 4 times leads to a respective increase in initial stiffness of 42%, 64%, and 88%.

Table 4.9 Displacement, force, and stiffness at yield of the WF and DF

Modulus elasticity of masonry, $E_m$	WF			DF		
	$\Delta_y$ (mm)	$P_y$ (kN)	$K_i$ (kN/mm)	$\Delta_y$ (mm)	$P_y$ (kN)	$K_i$ (kN/mm)
$E_m = 4081$ MPa	14.76	103.95	7.04	16.26	104.97	6.46
$E_m = 3000$ MPa	17.28	105.30	6.09	18.88	106.17	5.62
$E_m = 2000$ MPa	21.53	107.21	4.98	21.59	104.78	4.85
$E_m = 1000$ MPa	30.40	108.49	3.57	31.37	107.48	3.43

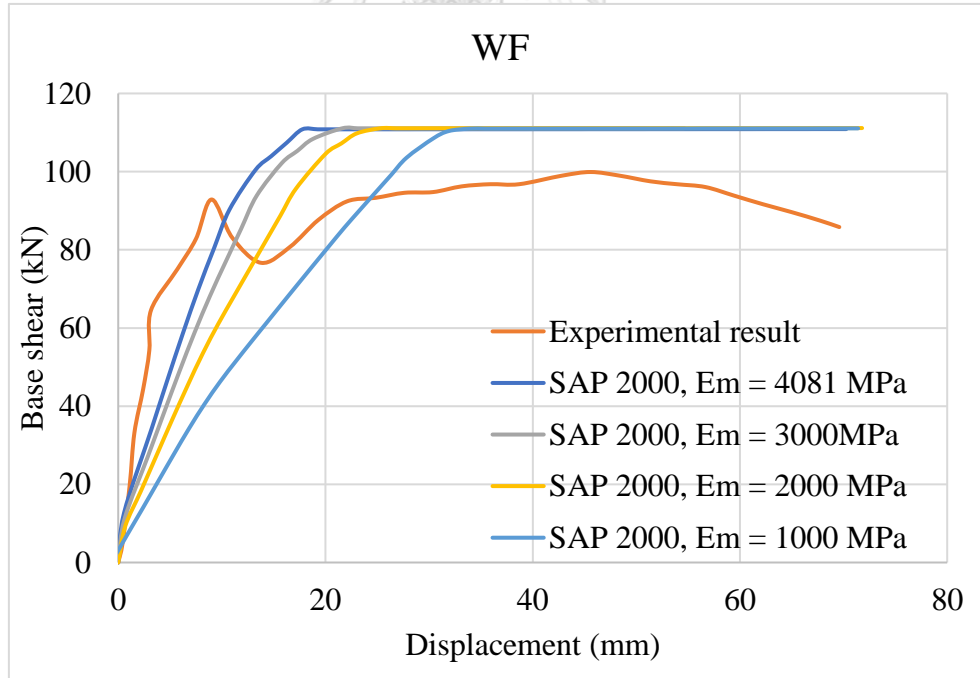


Figure 4.6 Parameter study of modulus elasticity of infill for WF

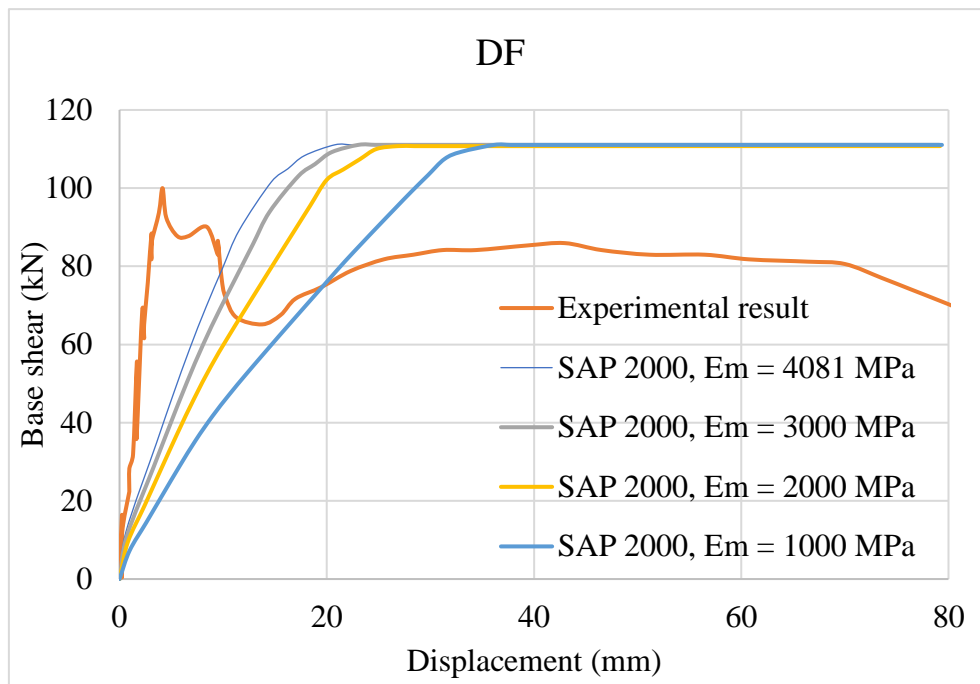


Figure 4.7 Parameter study of modulus elasticity of infill for DF According to Yekrangnia & Asteris (2020), the numerical model for WF includes a nonlinear RC frame with four compressive-only struts, while the DF frame consists of three struts (with the removal of a 65mm-wide lower spandrel strut). The analysis reveals that both frames are controlled by shear failure in the windward column, matching the failure mode observed in the experiments. This justifies the similarity in the results for WF and DF from the analytical model.



## 4.2 DISCRETIZED MACRO ELEMENT PROCEDURE (METHOD 2)

### 4.2.1 CALIBRATION OF THE ANALYTICAL MODEL METHOD 2

A calibration study has been carried out to authenticate the accuracy of the analytical model (Method 2) by using discretized macro element. Same experimental study from Ahani et al. (2019) and was conducted the analysis study by Kareem et al. (2022) is used to calibrate in the discretized macro element (Method 2).

#### a) Calibration the bare frame

##### Flexural Plastic Hinge

Follow the analytical solution procedure illustrated in Figure 3.8, and model the flexural plastic hinge with the equivalent length distance from the column joint. The moment-curvature analytical model by Haselton & Deierlein (2007) will be used in the lumped plastic hinge.

The details of the reinforcement and material properties of verification study frame have been presented in Table 4.1 and Table 4.2 respectively. By following the calculation procedure in the section 3.2.1 for flexural moment-curvature relation, the modeling parameter of flexural plastic hinge can be determined. Please refer to the Table 4.10 for the relevant value.

Table 4.10 Modeling parameter of the flexure plastic hinge of the verification study

Properties		RC column	RC beam
$M_y$	(kN-m)	62.15	58.68
$M_c$	(kN-m)	75.41	71.19
$\theta_y$	(rad)	0.0093	0.0121
$\theta_{cap\_pl}$	(rad)	0.0423	0.0223
$\theta_{cap\_tot}$	(rad)	0.0516	0.0344
$\theta_{pc}$	(rad)	0.1715	0.092

##### Shear Plastic Hinge

Table 4.3 contains the modeling parameter for the shear plastic hinge in the verification study. The frame is subjected to monotonic loading in the windward direction, and displacement controls the analysis. Figure 4.9 displays the comparison analysis and experimental results of the verification frame.

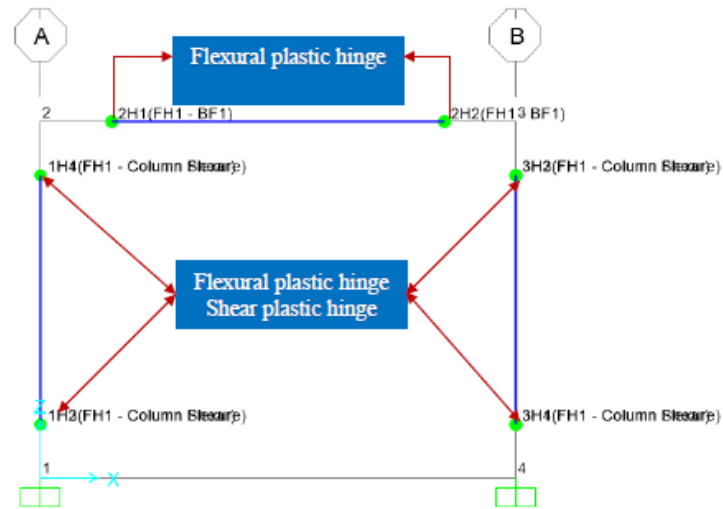


Figure 4.8 Modeling nonlinear bare frame in SAP 2000 using Method 2

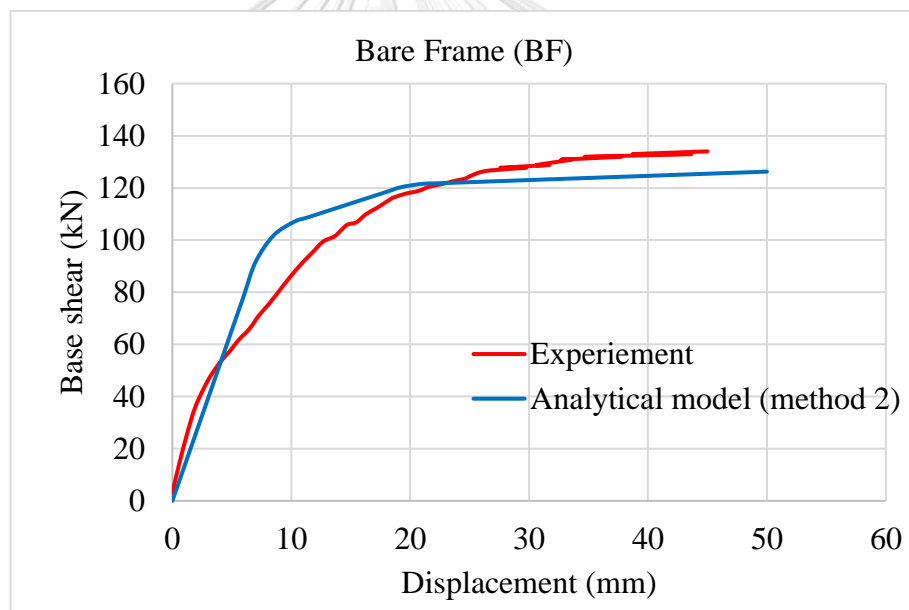


Figure 4.9 Comparison of experimental and analytical result of bare frame by using Method 2

The initial stiffness of the bare frame, as determined through both experimental study and analytical analysis in Method 2, displays satisfactory concordance. However, as the analysis progresses, a pronounced divergence emerges, with analytical results exhibiting increased severity in comparison to experimental findings. Subsequently, there is a modest but discernible augmentation in analytical outcomes relative to experimental results. These observations suggest a degree of compromise in the

analytical model for the bare frame, albeit one that demonstrates adaptability in capturing the nonlinearity inherent in the reinforced concrete (RC) bare frame.

b) Calibration of fully infilled frame

In accordance with the procedural framework delineated in Section 3.3.2, explicating the Methodology for computing the properties of orthogonal links pertaining to both vertical and horizontal interfaces, as well as diagonal links, the pertinent values encompassing both geometrical and mechanical parameters are delineated in Table 4.11 below.

Table 4.11 Geometrical and mechanical parameters to model link

Element	$\lambda$	k	$F_y^+$	$F_y^-$	$U_y^+$	$U_u^-$
	mm	kN/mm	kN	kN	mm	mm
Horizontal interface link	150	21.92	8.55	54.15	1.17	7.41
Vertical interface	150	20.36	8.55	54.15	6.30	39.9
Diagonal link	-	113.93	50	50	0.44	0.44

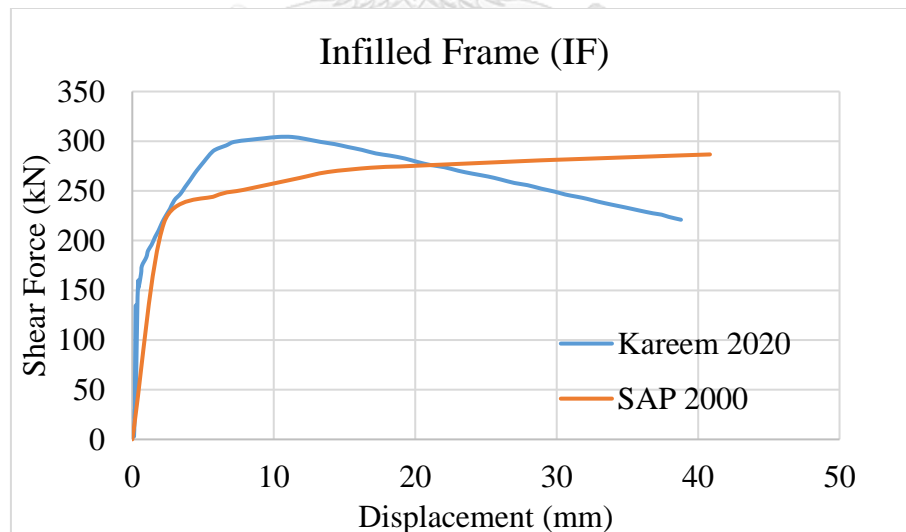


Figure 4.10 Compare fully infilled frame between analytical and experimental results using Method 2

The findings extrapolated from the experimental results outlined in the work of Kareem et al. (2022), when compare to the analytical model generated through the utilization of discretized macro elements in Method 2, reveal a compatible initial

stiffness at small displacements. Nevertheless, as the analysis progresses, there is a discernible incremental enhancement in the lateral strength of the analytical model. While the experimental results show a descent after the peak load, there's a minor difference in the later part. Despite this, the initial stiffness between the two graphs remains quite consistent. Therefore, the analytical model in Method 2 seems worth exploring in our specific study case.

#### 4.2.2 NONLINEAR PROPERTIES OF RC FRAME

The procedure to calculate the moment plastic hinge for lump plasticity of nonlinearity of frame member, can be found in section 3.2.1.

Table 4.12 Modeling parameters of the flexural plastic hinge of the frame member

Properties		RC column	RC beam
$M_y$	(kN-m)	54.46	97.34
$M_c$	(kN-m)	64.98	117.32
$\theta_y$	(rad)	0.0102	0.0118
$\theta_{cap\_pl}$	(rad)	0.0124	0.0111
$\theta_{cap\_tot}$	(rad)	0.0227	0.0229
$\theta_{pc}$	(rad)	0.0262	0.0308

To account for the nonlinearity of RC frame members, besides the flexural plastic hinge, the shear plastic hinge is also necessary to cooperate to simulate the flexural shear behavior on frame members. To calculate the parameter for modeling the shear plastic hinge, it is illustrated in section 3.1.1. The result of the modeling parameter can be found in Table 4.6.

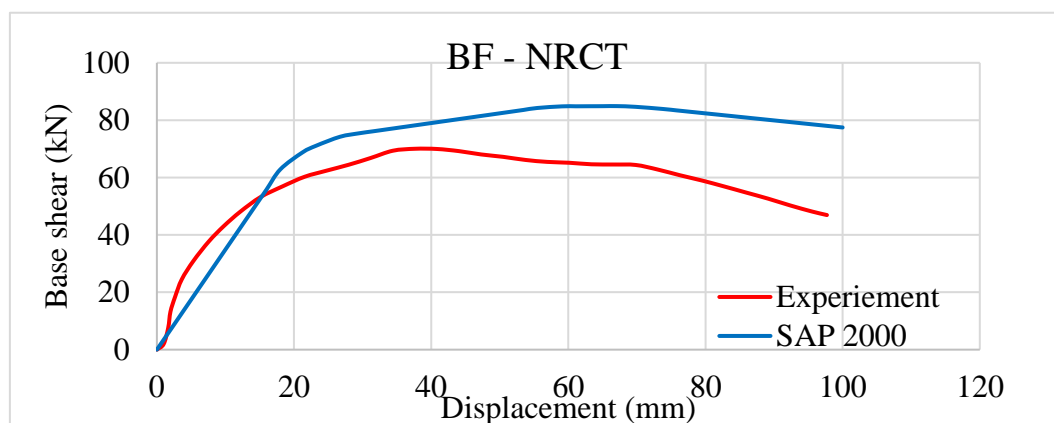


Figure 4.11 Comparison of analytical analysis with experimental result of BF

### 4.2.3 MODELING INFILLED FRAME WITH WINDOW OPENING (WF)

In the discretized macro element Method, the masonry panel could be replaced by a subpanel that consists of four rigid edges with constraint joints at the vertex, a series of orthogonal links to capture the flexural failure, two diagonal shear links to capture the behavior of diagonal shear failure and longitudinal link for shear sliding failure. To cooperate with the opening, the infill panels are divided into subpanels according to the exact geometry of the masonry infill panel.

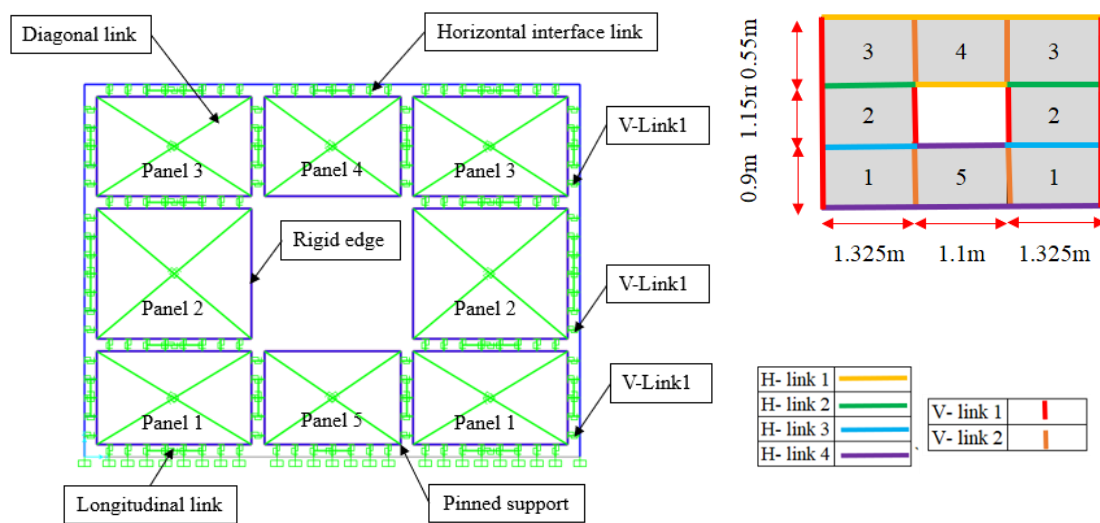


Figure 4.12 Modeling of masonry infilled frame with window opening Method 2  
 Calculate the geometrical and mechanical parameters of each link, which can be found in Table 4.12 and section 3.2.2. The parameters of modeling horizontal and vertical interface links are shown in Table 4.11 for infilled frame with window opening (WF) and Table 4.12 for infilled frame with door opening (DF).

Table 4.13 Geometrical and mechanical parameters of the links of WF

Element	$\lambda$	k	$F_y^+$	$U_y^+$	$U_u^+$	$F_y^-$	$U_y^-$	$U_u^-$
	mm	kN/mm	kN	mm	mm	kN	mm	mm
Horizontal interface link								
H-Link 1	150	136.03	42.12	0.31	0.93	-108	-0.79	-2.38
H-Link 2	150	222.6	42.12	0.19	0.57	-108	-0.49	-1.46
H-Link 3	150	72.02	42.12	0.58	1.75	-108	-1.5	-4.5
H-Link 4	150	59.72	42.12	0.71	2.12	-108	-1.81	-5.43
Vertical interface link								
V-Link 1	150	92.4	42.12	0.46	6.84	-108	-1.17	-17.53
V-Link 2	150	50.487	42.12	0.83	12.51	-108	-2.14	-32.09
Diagonal Link								
Panel 1	-	170.6	154.86	0.91	1.92	-154.9	-0.91	-1.92
Panel 2	-	163.93	133.9	0.82	2.36	-133.9	-0.82	-2.36
Panel 3	-	229.18	228.94	1	0.92	-228.9	-1	-0.92
Panel 4	-	202.88	162.93	0.8	0.95	-162.9	-0.8	-0.95
Panel 5	-	165.58	115.07	0.69	1.8	-115.1	-0.69	-1.8

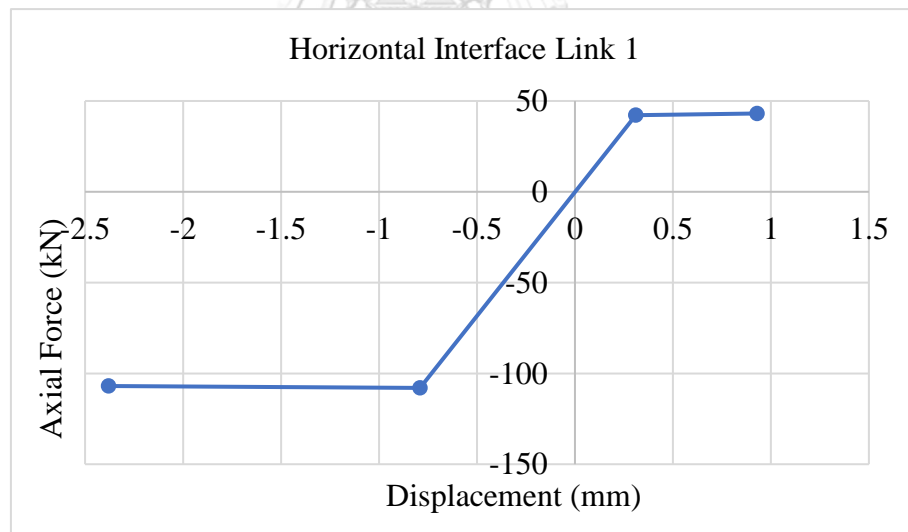


Figure 4.13 Horizontal interface link 1 of WF

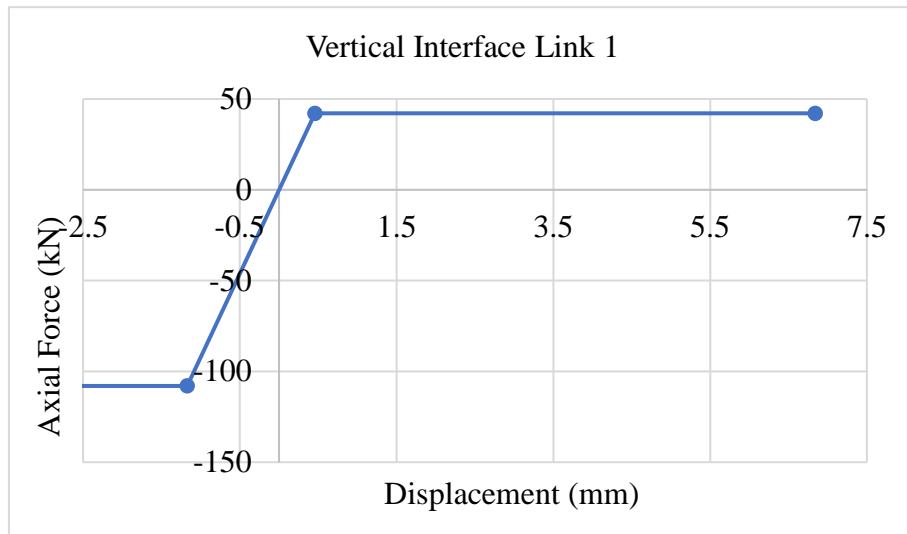


Figure 4.14 Vertical interface link 1 of WF

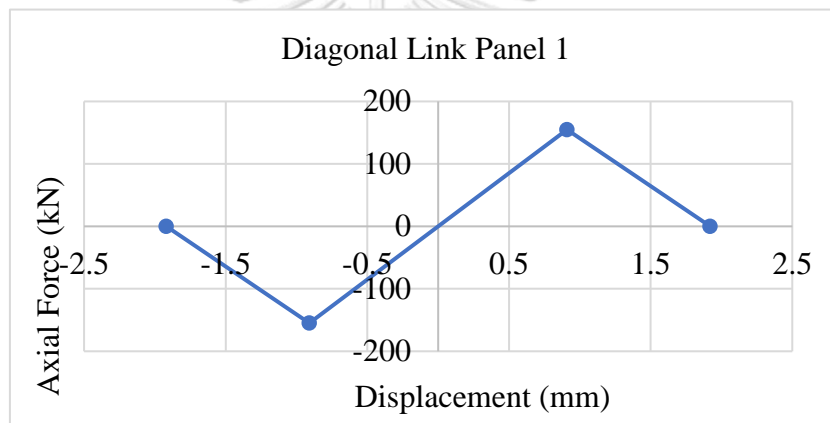


Figure 4.15 Diagonal link panel 1 of WF

After subjecting the modeling frame to monotonic lateral loading in the windward direction using SAP 2000, the analysis is conducted with the displacement control.

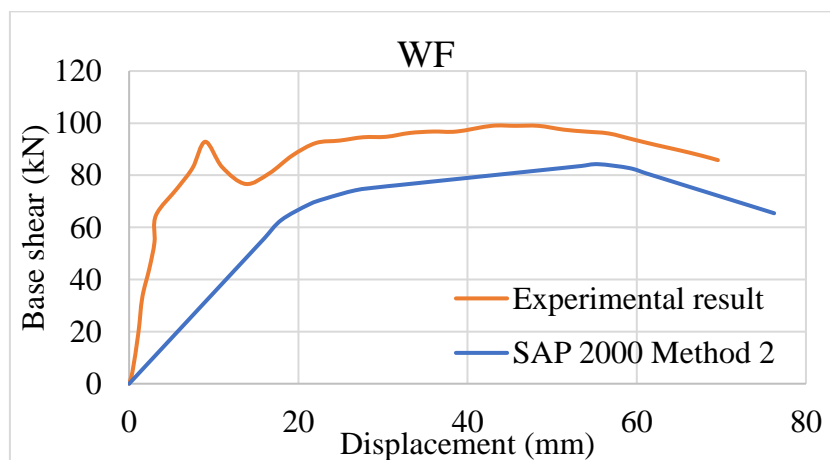


Figure 4.16 Comparison results of the analytical model using the discretized macro element with the experimental result.

The comparative analysis between the analytical and experimental outcomes for a masonry-infilled RC structure with a window opening reveals an initial stiffness from the analytical model that is approximately four times lower than the corresponding experimental value. As the analysis progresses, the discrepancy diminishes, with the analytical results trailing slightly, being less than 20% smaller than the experimental counterparts. Although exhibiting a similar trend, this suggests that the analytical model, particularly in Method 2, demonstrates enhanced performance in terms of strength. However, further calibration is warranted to refine the model for increased accuracy, particularly in capturing stiffness, especially during the initial stages.





#### 4.2.4 MODELING INFILLED FRAME WITH DOOR OPENING (DF)

When using the discretized macro element Method, it's important to break down the infilled panel with an opening into smaller subpanels. The size of these subpanels depends on the dimensions of the opening area, ensuring an accurate representation of the infill's structural features as illustrated Figure 4.17. To model the infilled frame using a discretized macro element as below, the link parameter needs to be calculated in section 3.2.2. The calculated parameter for modeling in this study can be seen in Table 4.12 below.

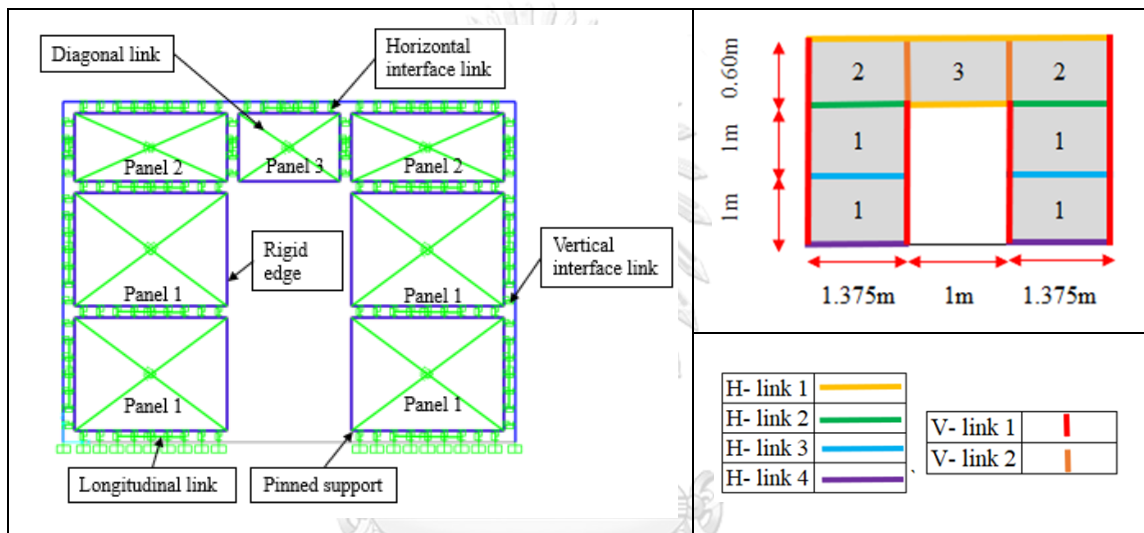


Figure 4.17 Modeling of masonry infilled frame with door opening Method 2

Table 4.14 Geometrical and mechanical parameters of the links of DF

Element	$\lambda$	$k$	$F_y^+$	$U_y^+$	$U_u^+$	$F_y^-$	$U_y^-$	$U_u^-$
	mm	kN/mm	kN	mm	mm	kN	mm	mm
<b>Horizontal interface link</b>								
H-Link 1	150	122.43	42.12	0.34	1.03	-108	-0.88	-2.65
H-Link 2	150	204.05	42.12	0.21	0.62	-108	-0.53	-1.59
H-Link 3	150	76.52	42.12	0.55	1.65	-108	-1.41	-4.23
H-Link 4	150	61.22	42.12	0.69	2.06	-108	-1.76	-5.29
<b>Vertical interface link</b>								
V-Link 1	150	89.04	42.12	0.47	7.1	-108	-1.21	-18.19
V-Link 2	150	51.55	42.12	0.82	12.26	-108	-2.1	-31.43
<b>Diagonal Link</b>								
Panel 1	-	170.6	154.86	0.91	1.92	-154.9	-0.91	-1.92
Panel 2	-	221.38	227.74	1.03	1.01	-227.7	-1.03	-1.01
Panel 3	-	183.94	128.75	0.7	1.08	-128.8	-0.7	-1.08

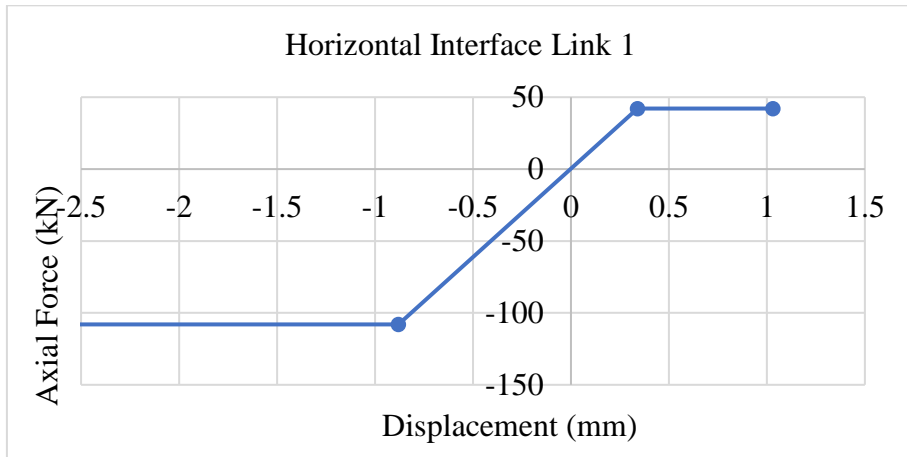


Figure 4.18 Horizontal interface link 1 of DF

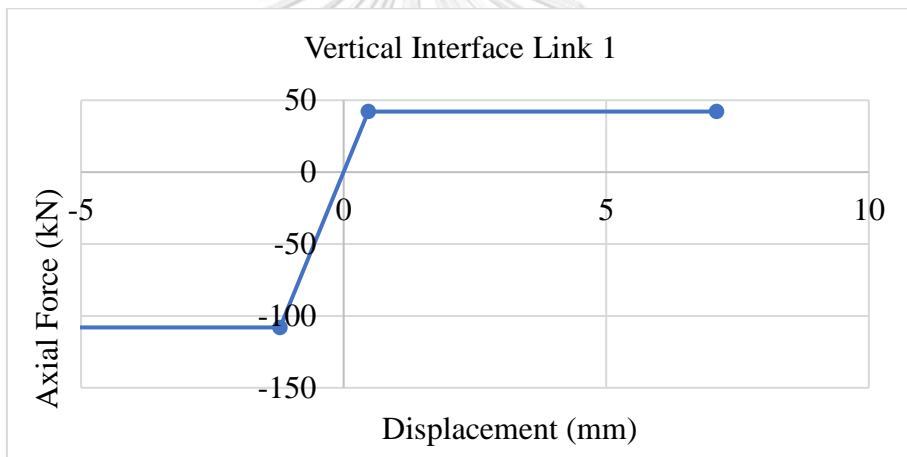


Figure 4.19 Vertical interface link 1 of DF

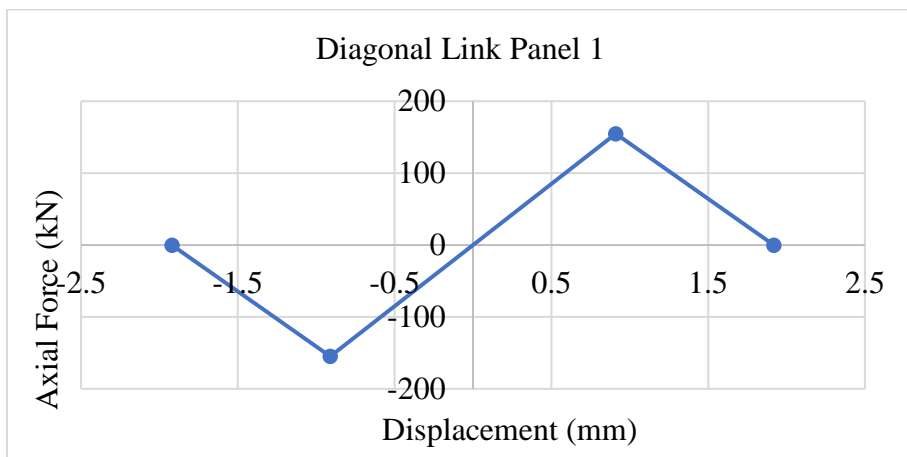
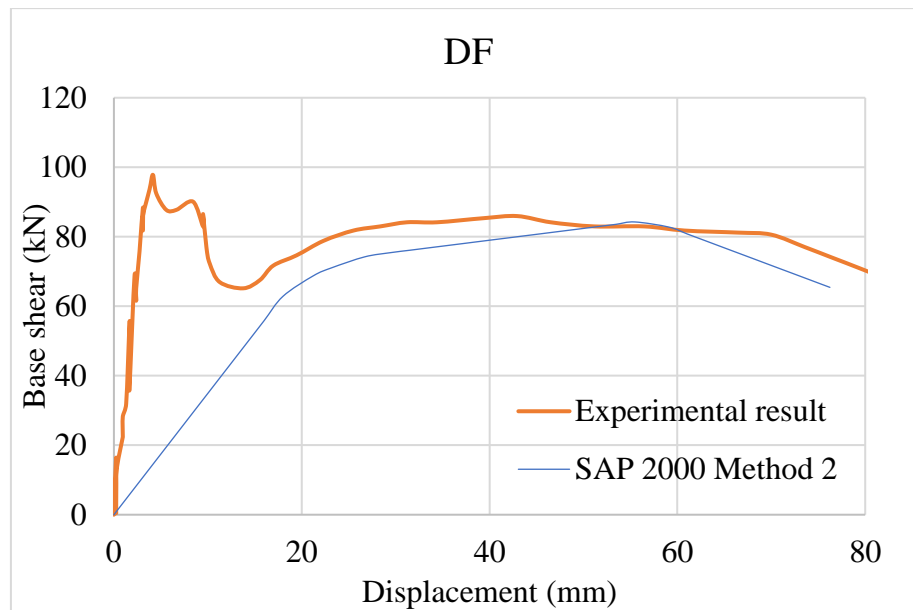


Figure 4.20 Diagonal link for panel 1 of DF



The masonry infilled panel is replaced by multiple discretized macro elements connected through orthogonal, longitudinal, and diagonal links. The frame is then subjected to monotonic loading, and an analysis with displacement control is performed in SAP 2000.

The comparison between the experimental results and the analytical model in Method 2 reveals an initial stiffness of the analytical model approximately four times lower than that of the experimental findings. As the analysis progresses, both the analytical model and experimental graph exhibit a convergence, displaying a similar trend at the peak load and post-peak load stages. This suggests that while the analytical model in Method 2 may exhibit a lower stiffness initially, it yields better results in terms of strength compared to stiffness as the analysis advances.

### 4.3 REDUCTION FACTOR PROCEDURE (METHOD 3)

Employing the reduction factor Method to integrate the masonry-infilled RC frame with an opening is considered the most simplified and resource-efficient approach. This Method involves the utilization of reduction factors to reduce the equivalent width of struts. For this study, the modeling approach will involve the use of a concentric equivalent strut layout, and push-over analysis will be executed using SAP 2000.

#### 4.3.1 NONLINEAR PROPERTIES OF RC FRAME

Similar to the discretized macro element Method, the lumped plasticity will be used to account for the flexural nonlinearity of the RC frame. The detailed calculation procedure and results can be found in section 3.2.1 and Table 4.10. And for the procedure for determining the shear plastic hinge modeling parameters can be found in 3.1.1 and the result in Table 4.6.

#### 4.3.2 MODELING OF EQUIVALENT STRUT

##### Effective strut width

Table 4.15 The effective strut width for window opening (WF)

Reduction factor account of opening	Width $w$ (mm)	Effective width $w_m$ (mm)			
		G. Al-Chaar et al. (2003)	Mohammadi & Nikfar (2013)		Decanini et al. (2014)
		$R_k, R_s$	$R_k$	$R_s$	$R_k, R_s$
		0.803	0.802	0.859	0.984
Holmes (1961)	1521.06	1220.66	1220.25	1306.93	1497.17
Mainstone (1972)	436.02	349.91	349.8	374.64	429.18
Liauw & Kwan (1984)	515.97	414.07	413.93	443.34	507.87

Table 4.16 The effective strut width for door opening (DF)

Reduction factor account of opening	Width w (mm)	Effective width $w_m$ (mm)			
		G. Al- Chaar et al. (2003)	Mohammadi & Nikfar (2013)		Decanini et al. (2014)
		$R_k, R_s$	$R_k$	$R_s$	$R_k, R_s$
		0.697	0.706	0.777	0.983
Holmes (1961)	1521.06	1060.24	1073.37	1182.52	1497.17
Mainstone (1972)	436.02	303.93	307.96	338.98	429.18
Liau & Kwan (1984)	515.97	359.65	364.11	401.14	507.87

#### 4.3.3 MECHANICAL PROPERTIES OF STRUTS

Following the calculation procedure in section 3.3.2, we can obtain the force-displacement relation as the graphs below.

##### Panagiotakos & Fardis (1996)

Due to the force-displacement relation of masonry strut Panagiotakos & Fardis (1996) based on the tensile strength of masonry force and required the equivalent struts. In order to consider the presence of the opening the reduction factor from three distinct empirical formula such as Decanini et al. (2014; G. Al-Chaar et al. (2003; Mohammadi & Nikfar (2013). The deduction will apply both strength and stiffness. Three types of struts empirical formula are considered, and three types of reduction factors are accounted for window and door opening. Therefore, six graphs were plotted to see the influence of strut width, and reduction factor in the Panagiotakos & Fardis (1996) model in the Figure 4.21 to Figure 4.26. From the plot graph, we could see that the reduction factor has strongly affected the strength and stiffness of the models.

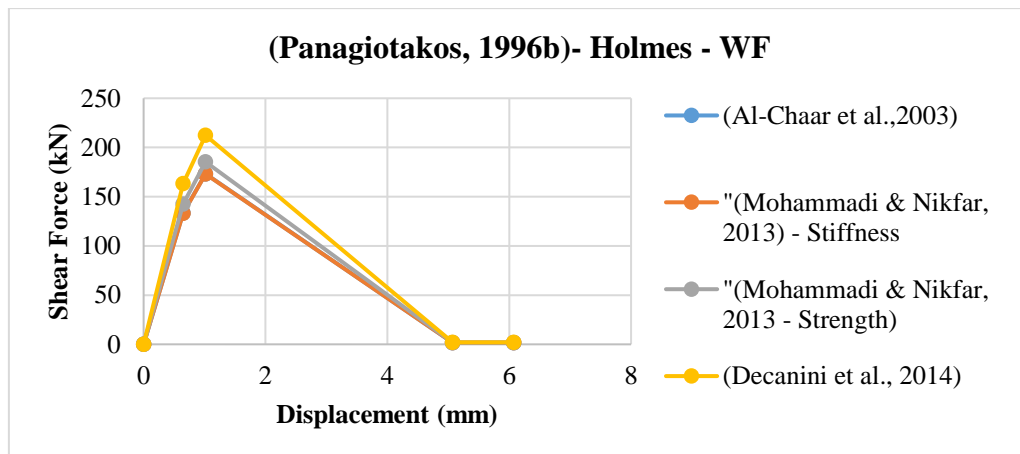


Figure 4.21 Force-displacement of masonry strut for WF Holmes (1961) for WF

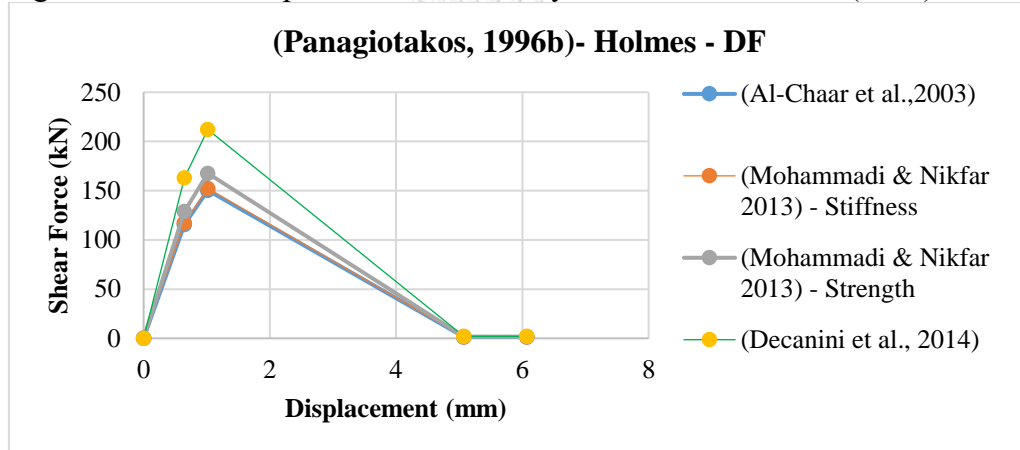


Figure 4.22 Force-displacement of masonry strut for WF Holmes (1961) for DF

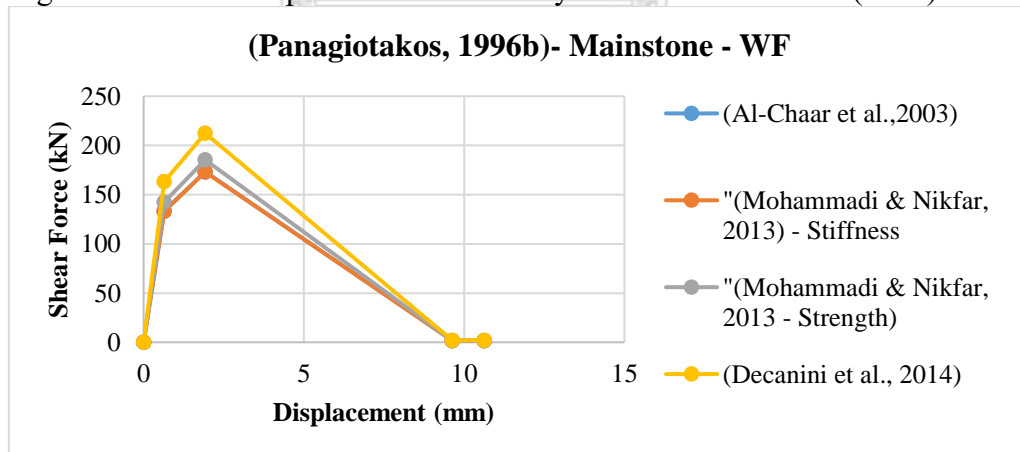


Figure 4.23 Force-displacement of masonry strut for WF Mainstone (1972) for DF

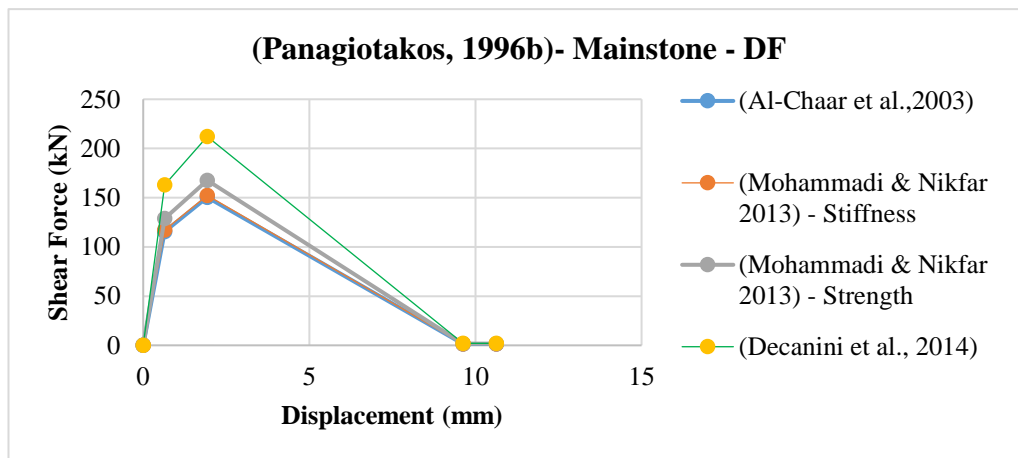


Figure 4.24 Force-displacement of masonry strut Mainstone (1972) for DF

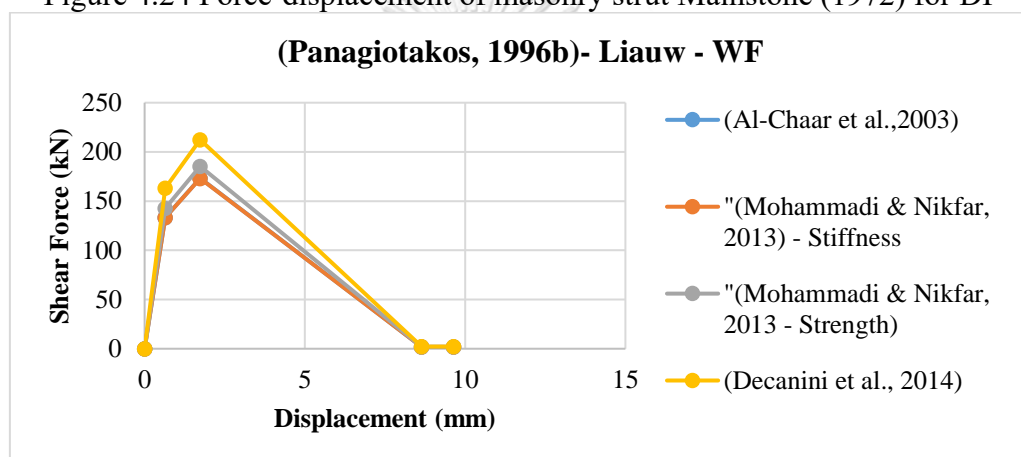


Figure 4.25 Force-displacement of masonry strut Liauw & Kwan (1984) for WF

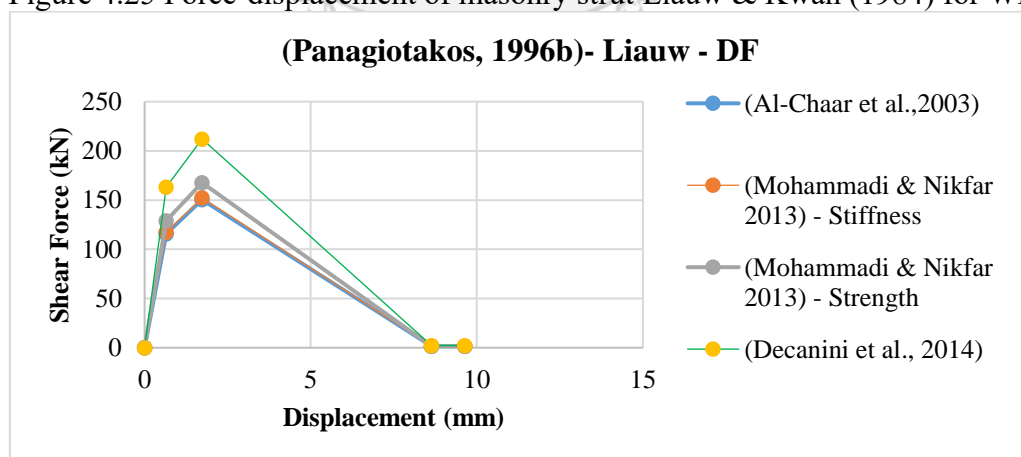


Figure 4.26 Force-displacement of masonry strut for WF Liauw & Kwan (1984) for DF

Based on the result of reduction factor for window and door opening obtained in Table 4.13 and Table 4.14 respectively, we could see the empirical formula for equivalent strut has and reduction factor for accounting the opening is less influence for the force-displacement above.

The study by Panagiotakos & Fardis (1996) is the most often used Method that offers a reasonable prediction. The model is made up of four branches: the first branch corresponds to yield strength, the second branch corresponds to maximum strength, the third branch to residual strength, and the horizontal segment at the fourth branch represents the end stage. The yield strength of the model depends on diagonal compression failure mode. The masonry infilled panel was replaced with a single equivalent strut in the structural analysis. A monotonic lateral force was applied to the frame from the windward direction. The analysis is governed by displacement control.

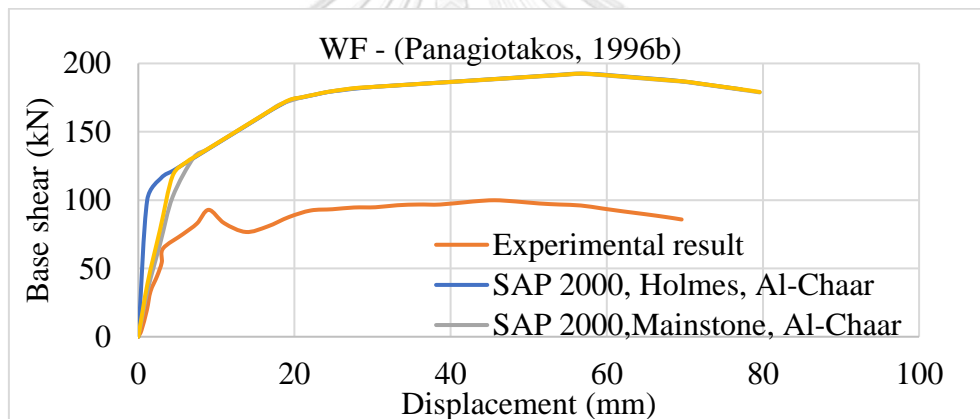


Figure 4.27 Comparison result of WF Panagiotakos & Fardis (1996) varying strut widths

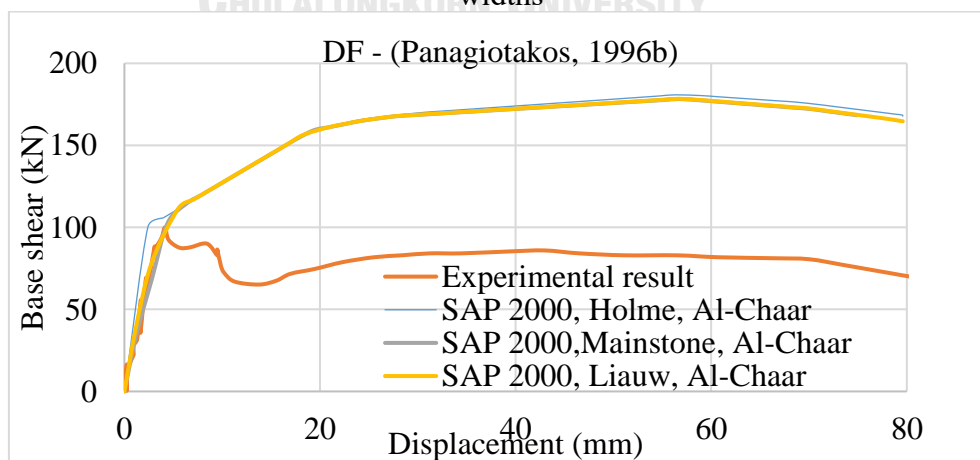


Figure 4.28 Comparison result of DF Panagiotakos & Fardis (1996) varying strut widths



Leeanansaksiri et al. (2018)

By following the calculated procedure in section 3.3.2, the modeling parameters can be found in Table 4.15 and the graph in Figure 4.29.

The lateral yield and maximum strength of the equivalent strut in a masonry infilled frame can be ascertained by considering two distinct failure modes: diagonal compression failure and corner-crushing failure. In accordance with the computational Methodology outlined in the model proposed by Leeanansaksiri et al. (2018), as detailed in section 3.3.2, the failure mode is predicated on diagonal compression failure, consistent with the failure mode observed in the experimental study.

Upon multiplication by the reduction factor by G. Al-Chaar et al. (2003) to account for the presence of openings, the modeling parameters for the force-displacement characteristics of the masonry infill are illustrated in Table 4.17.

Table 4.17 Modeling parameters for force-displacement of masonry infill  
Leeanansaksiri et al. (2018)

Yield strength	$F_y$	(kN)	186.45
Displacement at yield	$\Delta_y$	(mm)	3.81
Initial stiffness	$K_0$	(kN/mm)	48.94
Maximum strength	$F_{max}$	(kN)	319.07
Displacement at maximum strength	$\Delta_{max}$	(mm)	8.57
Post-yield stiffness	$\alpha K_0$	(kN/mm)	37.23

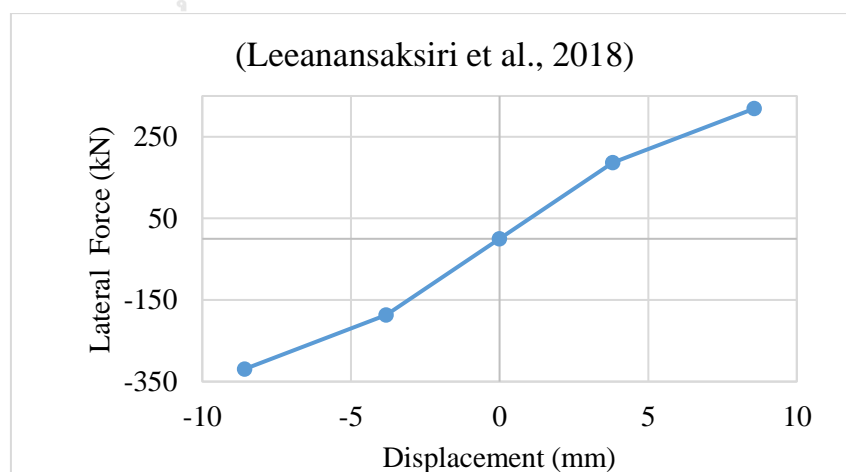


Figure 4.29 Force-displacement of masonry Leeanansaksiri et al. (2018)

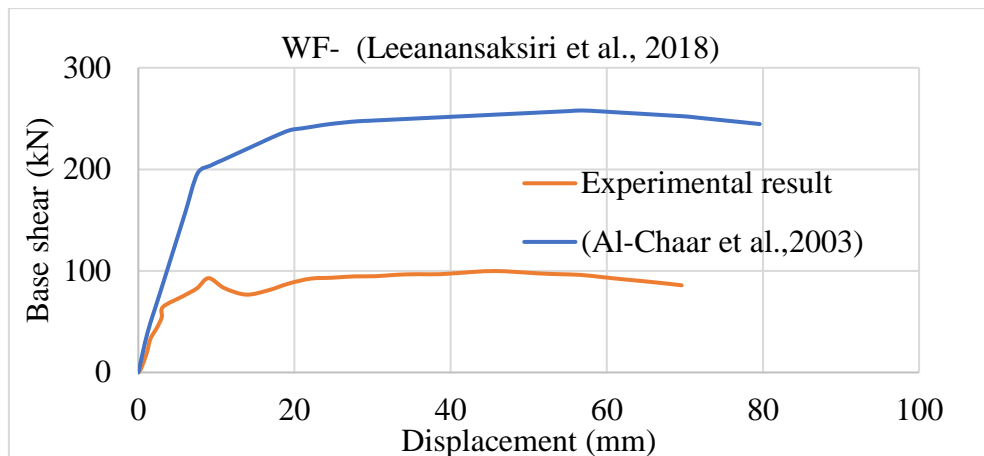


Figure 4.30 Comparison analytical and experimental result of WF Leeanansaksiri et al. (2018)

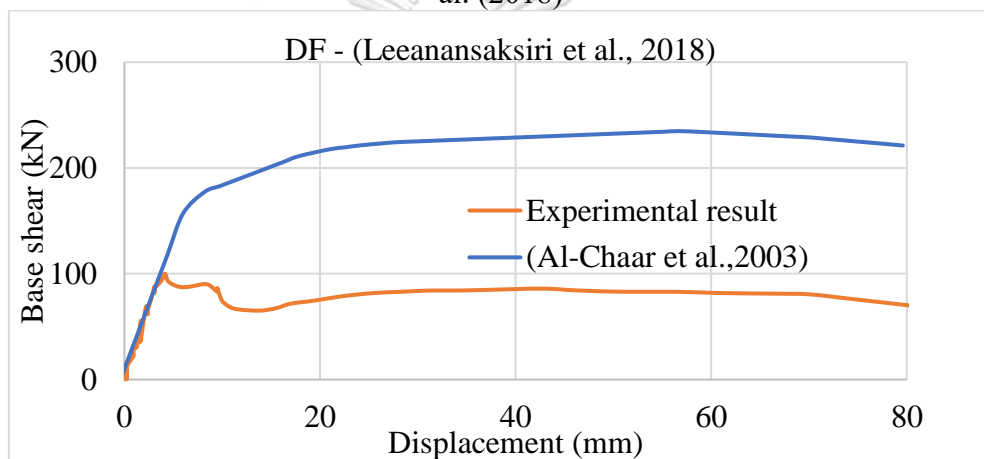


Figure 4.31 Comparison analytical and experimental result of DF Leeanansaksiri et al. (2018)

From the analytical model using a concentric single strut and accounting for the opening with the reduction factor Method, it could be seen that the response of the masonry infill frame is significantly dependent on the force-displacement relation for representing the masonry infill. Strut width contributed slightly to the initial stiffness of lateral resistance of the masonry infilled frame.

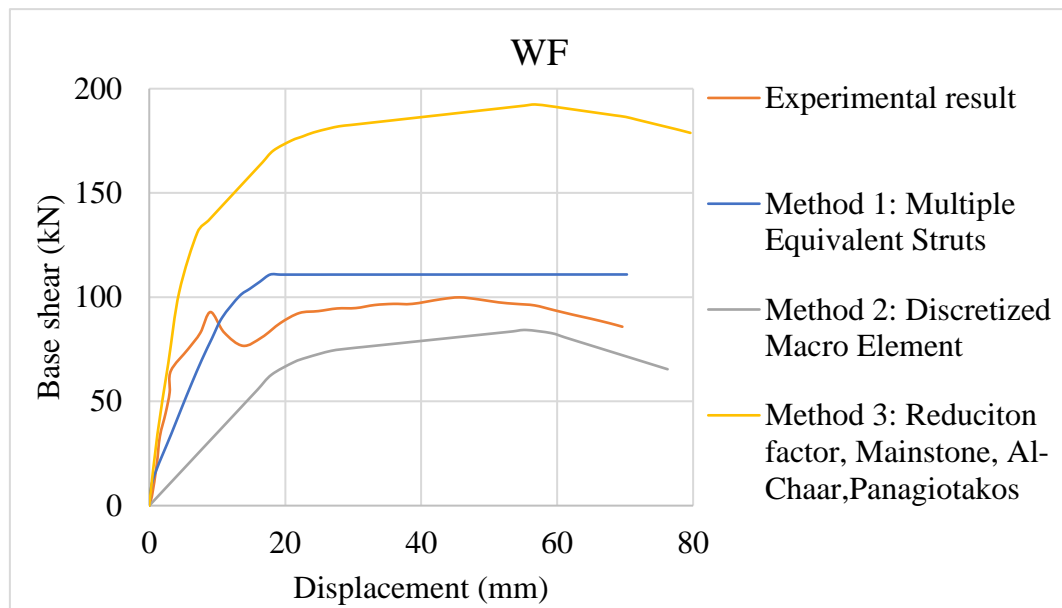


Figure 4.32 Compare analytical model with experimental results of WF

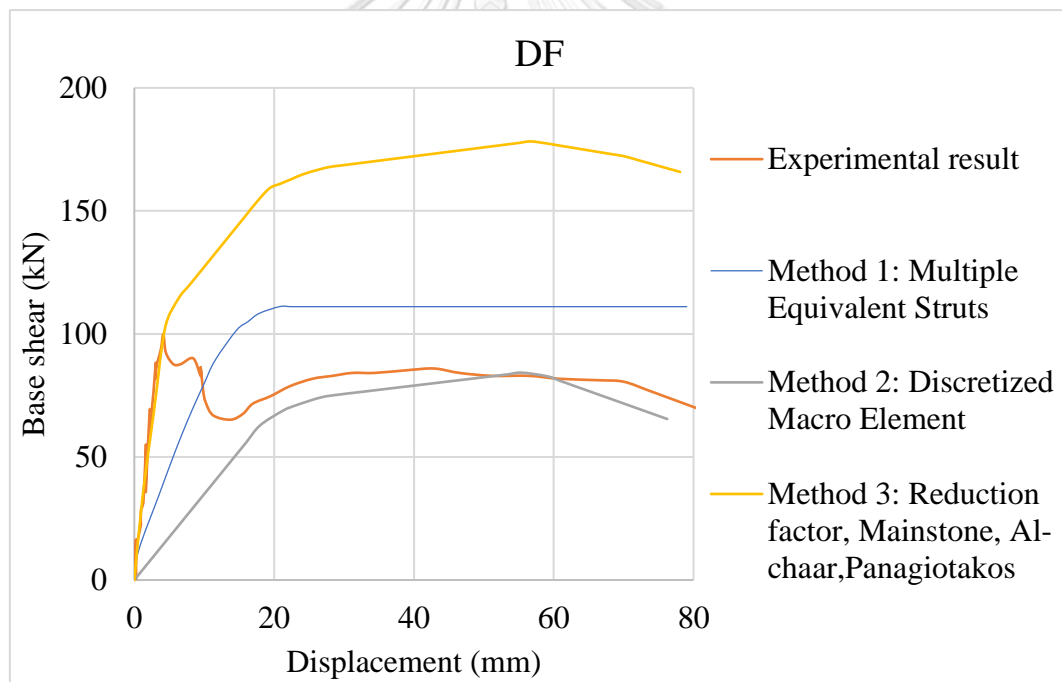


Figure 4.33 Compare the analytical model with the experimental results of DF

## CHAPTER 5

### CONCLUSIONS

Three macro models including multiple were employed to simulate the behavior of a masonry infilled reinforced concrete frame featuring central window and door openings. These macro models encompassed the Multiple Equivalent Strut approach (Method 1), a Discretized Macro Model (Method 2), and a Reduction Factor approach (Method 3). The outcomes derived from these three analytical Methods were compared with experimental results. It is essential to explore the concepts of stiffness and strength when studying pushover analysis for masonry infilled frames. For an overall seismic assessment of the masonry-infilled structural system, these parameters are essential in understanding the behavior and performance of the structure under lateral loads. The following findings were obtained:

- 1) For the initial stiffness, Method 3 fits well with the masonry-infilled RC frame with window (WF) and door opening (DF). Method 1 and Method 2 provide approximately 3 times and 6 times lower than initial stiffness from the experimental result, respectively.
- 2) The lateral strength of the masonry-infilled RC frame is in good agreement with Method 2 only for the infilled frame with door opening. Besides that, it could be seen that Method 3 provides the highest lateral strength, which is approximately twice as large as the experimental result.

**REFERENCES**

จุฬาลงกรณ์มหาวิทยาลัย  
**CHULALONGKORN UNIVERSITY**

- Ahani, E., Mousavi, M. N., Ahani, A., & Kheirollahi, M. (2019). The effects of amount and location of openings on lateral behavior of masonry infilled RC frames. *KSCE Journal of Civil Engineering*, 23(5), 2175-2187. <https://doi.org/10.1007/s12205-019-0714-x>
- Altin, S., Anil, Ö., Kara, M. E., & Kaya, M. (2008). An experimental study on strengthening of masonry infilled RC frames using diagonal CFRP strips. *Composites Part B: Engineering*, 39(4), 680-693. <https://doi.org/10.1016/j.compositesb.2007.06.001>
- Alwashali, H., Torihata, Y., Jin, K., & Maeda, M. (2017). Experimental observations on the in-plane behaviour of masonry wall infilled RC frames; focusing on deformation limits and backbone curve. *Bulletin of Earthquake Engineering*, 16(3), 1373-1397. <https://doi.org/10.1007/s10518-017-0248-x>
- ASCE. (2013). Seismic evaluation and retrofit of existing buildings (ASCE/SEI 41-13). *American Society of Civil Engineers*. [www.asce.org/pubs](http://www.asce.org/pubs)
- Asteris, P., Chrysostomou, C., Giannopoulos, I., & Smyrou, E. (2011). *Masonry infilled reinforced concrete frames with openings* COMPDYN 2011 - III ECCOMAS Thematic Conference on Computational Methods in Structural Dynamics and Earthquake Engineering,
- Asteris, P. G., Antoniou, S. T., Sophianopoulos, D. S., & Chrysostomou, C. Z. (2011). Mathematical macromodeling of infilled frames: state of the art. *Journal of Structural Engineering*, 137(12), 1508-1517. [https://doi.org/10.1061/\(asce\)st.1943-541x.0000384](https://doi.org/10.1061/(asce)st.1943-541x.0000384)
- Asteris, P. G., Cavaleri, L., Di Trapani, F., & Sarhosis, V. (2015). A macro-modelling approach for the analysis of infilled frame structures considering the effects of openings and vertical loads. *Structure and Infrastructure Engineering*, 12(5), 551-566. <https://doi.org/10.1080/15732479.2015.1030761>
- Basha, S. H., & Kaushik, H. B. (2016). Behavior and failure mechanisms of masonry-infilled RC frames (in low-rise buildings) subject to lateral loading. *Engineering Structures*, 111, 233-245. <https://doi.org/10.1016/j.engstruct.2015.12.034>
- Buonopane, S. G., & White, R. N. (1999). Pseudodynamic testing of masonry infilled reinforced concrete. *Journal of Structural Engineering*, 125(6), 578-589. [https://doi.org/https://doi.org/10.1061/\(ASCE\)0733-9445\(1999\)125:6\(578\)](https://doi.org/https://doi.org/10.1061/(ASCE)0733-9445(1999)125:6(578))
- Burton, H., & Deierlein, G. (2014). Simulation of seismic collapse in nonductile reinforced concrete frame buildings with masonry infills. *Journal of Structural Engineering*, 140(8), A4014016. [https://doi.org/10.1061/\(asce\)st.1943-541x.0000921](https://doi.org/10.1061/(asce)st.1943-541x.0000921)
- Cai, G., & Su, Q. (2017). Effect of Infills on Seismic Performance of Reinforced Concrete Frame structures—A Full-Scale Experimental Study. *Journal of Earthquake Engineering*, 23(9), 1531-1559. <https://doi.org/10.1080/13632469.2017.1387194>

- Caliò, I., Marletta, M., & Pantò, B. (2012). A new discrete element model for the evaluation of the seismic behaviour of unreinforced masonry buildings. *Engineering Structures*, 40, 327-338. <https://doi.org/10.1016/j.engstruct.2012.02.039>
- Caliò, I., & Pantò, B. (2014). A macro-element modelling approach of Infilled Frame Structures. *Computers & Structures*, 143, 91-107. <https://doi.org/10.1016/j.compstruc.2014.07.008>
- Cavaleri, L., & Di Trapani, F. (2014a). Cyclic response of masonry infilled RC frames: Experimental results and simplified modeling. *Soil Dynamics and Earthquake Engineering*, 65, 224-242. <https://doi.org/10.1016/j.soildyn.2014.06.016>
- Cavaleri, L., & Di Trapani, F. (2014b). Prediction of the additional shear action on frame members due to infills. *Bulletin of Earthquake Engineering*, 13(5), 1425-1454. <https://doi.org/10.1007/s10518-014-9668-z>
- Centeno, J., Ventura, C., Foo, S., & Lara, O. (2008). *Seismic performance of gravity load designed reinforced concrete frames with unreinforced masonry infill walls* Structures Congress 2008,
- Chen, X., & Liu, Y. (2015). Numerical study of in-plane behaviour and strength of concrete masonry infills with openings. *Engineering Structures*, 82, 226-235. <https://doi.org/10.1016/j.engstruct.2014.10.042>
- Chrysostomou, C. Z., Gergely, P., & Abel, J. F. (2002). A six-strut model for nonlinear dynamic analysis of steel infilled frames. *International Journal of Structural Stability and Dynamics*, 02(03), 335-353. <https://doi.org/10.1142/s0219455402000567>
- Crisafulli, F., & Carr, A. (2007). Proposed macro-model for the analysis of infilled frame structures. *Bulletin of the New Zealand Society for Earthquake Engineering*, 40, 69-77. <https://doi.org/10.5459/bnzsee.40.2.69-77>
- D.V. Mallick, & R.P. Garg. (1971). Effect of openings on the lateral stiffness of infilled frames. Proceedings of the Institution of Civil Engineers,
- Decanini, L. D., Liberatore, L., & Mollaioli, F. (2014). Strength and stiffness reduction factors for infilled frames with openings. *Earthquake Engineering and Engineering Vibration*, 13(3), 437-454. <https://doi.org/10.1007/s11803-014-0254-9>
- Di Trapani, F., Shing, P. B., & Cavaleri, L. (2017). Macroelement model for in-plane and out-of-plane responses of masonry infills in frame structures. *Journal of Structural Engineering*, 144(2), 04017198. [https://doi.org/10.1061/\(asce\)st.1943-541x.0001926](https://doi.org/10.1061/(asce)st.1943-541x.0001926)
- Dias-Oliveira, J., Rodrigues, H., Asteris, P., & Varum, H. (2022). On the seismic behavior of masonry infilled frame structures. *Buildings*, 12(8), 1146. <https://doi.org/10.3390/buildings12081146>

- El-Dakhkhni Wael, W., Elgaaly, M., & Hamid Ahmad, A. (2003). Three-strut model for concrete masonry-infilled steel frames. *Journal of Structural Engineering*, 129(2), 177-185. [https://doi.org/10.1061/\(ASCE\)0733-9445\(2003\)129:2\(177\)](https://doi.org/10.1061/(ASCE)0733-9445(2003)129:2(177))
- Erdem, I., Akyuz, U., Ersoy, U., & Ozcebe, G. (2006). An experimental study on two different strengthening techniques for RC frames. *Engineering Structures*, 28(13), 1843-1851. <https://doi.org/10.1016/j.engstruct.2006.03.010>
- Erol, G., & Karadogan, H. F. (2016). Seismic strengthening of infilled reinforced concrete frames by CFRP. *Composites Part B: Engineering*, 91, 473-491. <https://doi.org/https://doi.org/10.1016/j.compositesb.2016.01.025>
- Fiore, A., Netti, A., & Monaco, P. (2012). The influence of masonry infill on the seismic behaviour of RC frame buildings. *Engineering Structures*, 44, 133-145. <https://doi.org/10.1016/j.engstruct.2012.05.023>
- Fiore, A., Spagnoletti, G., & Greco, R. (2016). On the prediction of shear brittle collapse mechanisms due to the infill-frame interaction in RC buildings under pushover analysis. *Engineering Structures*, 121, 147-159. <https://doi.org/10.1016/j.engstruct.2016.04.044>
- Furtado, A., Rodrigues, H., & Arêde, A. (2015). Modelling of masonry infill walls participation in the seismic behaviour of RC buildings using OpenSees. *International Journal of Advanced Structural Engineering*, 7(2), 117-127. <https://doi.org/10.1007/s40091-015-0086-5>
- G. Al-Chaar, G. E. Lamb, & M. A. Issa. (2003). Effect of openings on structural performance of unreinforced masonry infilled frames. *ACI Symposium Publication*, 211, 247-262. <https://doi.org/10.14359/12593>
- Ghassan Al-Chaar, Mohsen Issa, & Steve Sweeney. (2002). Behavior of masonry-infilled nonductile reinforced concrete frames. *Journal of Structural Engineering*, 128(8), 1055-1063. [https://doi.org/https://doi.org/10.1061/\(ASCE\)0733-9445\(2002\)128:8\(1055\)](https://doi.org/https://doi.org/10.1061/(ASCE)0733-9445(2002)128:8(1055))
- Gokce Kurt, E., Kurc, O., Binici, B., Canbay, E., & Ozcebe, G. (2012). Performance examination of two seismic strengthening procedures by pseudodynamic testing. *Journal of Structural Engineering*, 138(1), 31-41. [https://doi.org/10.1061/\(asce\)st.1943-541x.0000434](https://doi.org/10.1061/(asce)st.1943-541x.0000434)
- Haselton, C., & Deierlein, G. (2007). *Assessing seismic collapse safety of modern reinforced concrete moment frame building* (John A. Blume Earthquake Engineering Center Technical Report 156., Issue. <http://purl.stanford.edu/ny266sf1883>
- Holmes, M. (1961). Steel Frames With Brickwork And Concrete Infilling. *Proceedings of the Institution of Civil Engineers*, 19(4), 473-478. <https://doi.org/10.1680/iicep.1961.11305>
- Huang, H., & Burton, H. V. (2020). A database of test results from steel and reinforced concrete infilled frame experiments. *Earthquake Spectra*, 36(3), 1525-1548. <https://doi.org/10.1177/8755293019899950>



- Huang, Q., Guo, Z., & Kuang, J. S. (2016). Designing infilled reinforced concrete frames with the 'strong frame-weak infill' principle. *Engineering Structures*, 123, 341-353. <https://doi.org/10.1016/j.engstruct.2016.05.024>
- Humayun Basha, S., Surendran, S., & Kaushik, H. B. (2020). Empirical models for lateral stiffness and strength of masonry-infilled RC frames considering the influence of openings. *Journal of Structural Engineering*, 146(4), 04020021. [https://doi.org/10.1061/\(asce\)st.1943-541x.0002562](https://doi.org/10.1061/(asce)st.1943-541x.0002562)
- Jia, M., Kong, J., & Wu, J. (2023). A macro-modelling approach for the analysis of masonry-infilled RC frames with different opening dimensions and locations. <https://doi.org/https://doi.org/10.21203/rs.3.rs-2961395/v1>
- Kakaletsis, D., & Karayannis, C. (2007). Experimental investigation of infilled r/c frames with eccentric openings. *Structural Engineering and Mechanics*, 26(3), 231-250. <https://doi.org/10.12989/sem.2007.26.3.231>
- Kakaletsis, D. J., & Karayannis, C. G. (2008). Influence of Masonry Strength and Openings on Infilled R/C Frames Under Cycling Loading. *Journal of Earthquake Engineering*, 12(2), 197-221. <https://doi.org/10.1080/13632460701299138>
- Kakaletsis, D. J., & Karayannis, C. G. (2009). Experimental investigation of infilled reinforced concrete frames with openings. *Structural Journal*, 106(2), 132-141. <https://doi.org/10.14359/56351>
- Kareem, K. M., Ahani, E., & Panto, B. (2022). Evaluating simplified macromodeling approaches of simulating infilled reinforced concrete frames with openings. *Structural Concrete*, 24(1), 721-737. <https://doi.org/10.1002/suco.202200051>
- Kareem, K. M., & Pantò, B. (2019). Simplified macro-modelling strategies for the seismic assessment of non-ductile infilled frames: a critical appraisal. *Journal of Building Engineering*, 22, 397-414. <https://doi.org/10.1016/j.jobe.2018.12.010>
- Kent, D. C., & Park, R. (1971). Flexural members with confined concrete. *Journal of the Structural Division*, 97(7), 1969-1990. <https://doi.org/https://doi.org/10.1061/JSDEAG.0002957>
- Khan, N. A., Zhou, L., Di Trapani, F., Demartino, C., & Monti, G. (2023). Experimental study of RC frames with window and door openings under cyclic loading. In *Energy-Based Seismic Engineering* (pp. 293-303). [https://doi.org/10.1007/978-3-031-36562-1\\_23](https://doi.org/10.1007/978-3-031-36562-1_23)
- Kim, M., & Yu, E. (2021). Experimental study on material-load-resisting capacity of masonry-infilled reinforced concrete frames. *Applied Sciences*, 11(21), 9950. <https://doi.org/10.3390/app11219950>
- Kurmi, P. L., & Haldar, P. (2022). Modeling of opening for realistic assessment of infilled RC frame buildings. *Structures*, 41, 1700-1709. <https://doi.org/10.1016/j.istruc.2022.05.110>
- Leeanansaksiri, A., Panyakapo, P., & Ruangrassamee, A. (2018). Seismic capacity of masonry infilled RC frame strengthening with expanded metal ferrocement.

- Engineering Structures*, 159, 110-127.  
<https://doi.org/10.1016/j.engstruct.2017.12.034>
- Liau, T. C., & Kwan, K.-H. (1984). Nonlinear behavior of non-integral infilled frames. *Computers & Structures*, 18(3), 551-560.  
[https://doi.org/https://doi.org/10.1016/0045-7949\(84\)90070-1](https://doi.org/https://doi.org/10.1016/0045-7949(84)90070-1)
- Longthong, S., Panyakapo, P., & Ruangrassamee, A. (2020). Seismic Strengthening of RC Frame and Brick Infill Panel using Ferrocement and Expanded Metal. *Engineering Journal*, 24(3), 45-59. <https://doi.org/10.4186/ej.2020.24.3.45>
- Lukkunaprasit, P., Ruangrassamee, A., Boonyatee, T., Chintanapakdee, C., Jankaew, K., Thanasisathit, N., & Chandrangu, T. (2015). Performance of Structures in the Mw6.1 Mae Lao Earthquake in Thailand on May 5, 2014 and Implications for Future Construction. *Journal of Earthquake Engineering*, 20(2), 219-242.  
<https://doi.org/10.1080/13632469.2015.1051636>
- Maidiawati, M. (2019). Experimental Investigation of Seismic Performance of Reinforced Brick Masonry Infilled Reinforced Concrete Frames with a Central Opening. *International Journal of GEOMATE*, 16(57).  
<https://doi.org/10.21660/2019.57.4592>
- Mainstone, R. J. (1972). *On the stiffnesses and strengths of infilled frames*. Building Research Station Garston, England. <https://search.worldcat.org/title/on-the-stiffnesses-and-strengths-of-infilled-frames/oclc/25248598>
- Mansouri, A., Marefat, M. S., & Khanmohammadi, M. (2014). Experimental evaluation of seismic performance of low-shear strength masonry infills with openings in reinforced concrete frames with deficient seismic details. *The Structural Design of Tall and Special Buildings*, 23(15), 1190-1210.  
<https://doi.org/10.1002/tal.1115>
- Mansouri, A., Marefat, M. S., & Khanmohammadi, M. (2018). Analytical estimation of lateral resistance of low-shear strength masonry infilled reinforced concrete frames with openings. *The Structural Design of Tall and Special Buildings*, 27(6). <https://doi.org/10.1002/tal.1452>
- Mehrabi Armin, B., Benson Shing, P., Schuller Michael, P., & Noland James, L. (1996). Experimental evaluation of masonry infilled RC frames. *Journal of Structural Engineering*, 122(3), 228-237.  
[https://doi.org/https://doi.org/10.1061/\(ASCE\)0733-9445\(1996\)122:3\(228\)](https://doi.org/https://doi.org/10.1061/(ASCE)0733-9445(1996)122:3(228))
- Misir, I. S., Ozcelik, O., Girgin, S. C., & Kahraman, S. (2012). Experimental work on seismic behavior of various types of masonry infilled RC frames. *Structural Engineering and Mechanics*, 44(6), 763-774.  
<https://doi.org/10.12989/sem.2012.44.6.763>
- Mohammadi, M., & Nikfar, F. (2013). Strength and Stiffness of Masonry-Infilled Frames with Central Openings Based on Experimental Results. *Journal of Structural Engineering*, 139(6), 974-984.  
[https://doi.org/10.1061/\(asce\)st.1943-541x.0000717](https://doi.org/10.1061/(asce)st.1943-541x.0000717)

- Mondal, G., & Jain, S. K. (2008). Lateral stiffness of masonry infilled reinforced concrete (RC) frames with central opening. *Earthquake Spectra*, 24(3), 701-723. <https://doi.org/https://doi.org/10.1193/1.2942376>
- Mostafaei, H., & Kabeyasawa, T. (2004). Effect of infill masonry walls on the seismic response of reinforced concrete buildings subjected to the 2003 Bam earthquake strong motion: a case study of Bam Telephone Center. *Bulletin of the Earthquake Research Institute*, 79(3/4), 133-156.
- Mucedero, G., Perrone, D., Brunesi, E., & Monteiro, R. (2020). Numerical Modelling and Validation of the Response of Masonry Infilled RC Frames Using Experimental Testing Results. *Buildings*, 10(10). <https://doi.org/10.3390/buildings10100182>
- Niyompanitpattana, S., & Warnitchai, P. (2017). Effects of masonry infill walls with openings on seismic behaviour of long-span GLD RC frames. *Magazine of Concrete Research*, 69(21), 1082-1102. <https://doi.org/10.1680/jmacr.17.00008>
- NRCT. (2023). *Final Report on seismic enhancement of low-rise buildings by strengthening of members and infilled walls*. National Research Council of Thailand Bangkok Thailand.
- P.G. Asteris, D.J. Kakaletsis, C.Z. Chrysostomou, & E.E. Smyrou. (2011). Failure mode in infill-frame. *Electronic Journal of Structural Engineering*, 11, 11-20. <https://doi.org/https://doi.org/10.56748/ejse.11139>
- Panagiotakos, T. B., & Fardis, M. N. (1996). Seismic response of infilled RC frames structures. 11th World Conference on Earthquake Engineering, Acapulco, Mexico.
- Paulay, T., & Priestley, M. N. (1992). *Seismic design of reinforced concrete and masonry buildings*. Wiley New York. <https://doi.org/10.1002/9780470172841>
- Rodrigues, H., Varum, H., & Costa, A. (2010). Simplified Macro-Model for Infill Masonry Panels. *Journal of Earthquake Engineering*, 14(3), 390-416. <https://doi.org/10.1080/13632460903086044>
- Roosta, S., & Liu, Y. (2022). Development of a macro-model for concrete masonry infilled frames. *Engineering Structures*, 257, 114075. <https://doi.org/10.1016/j.engstruct.2022.114075>
- Saneinejad, A., & Hobbs, B. (1995). Inelastic design of infilled frames. *Journal of Structural Engineering*, 121, 634-650. [https://doi.org/10.1061/\(ASCE\)0733-9445\(1995\)121:4\(634\)](https://doi.org/10.1061/(ASCE)0733-9445(1995)121:4(634))
- Schneider, S. P., Zagers, B. R., & Abrams, D. P. (1998 ). Lateral strength of steel frames with masonry infills having large openings. *Journal of Structural Engineering*, 124(8), 896-904. [https://doi.org/https://doi.org/10.1061/\(ASCE\)0733-9445\(1998\)124:8\(896\)](https://doi.org/https://doi.org/10.1061/(ASCE)0733-9445(1998)124:8(896))
- Sezen, H., & Patwardhan, C. (2012). Shear displacement model for reinforced concrete columns. In *Structures Congress 2006: Structural Engineering and Public Safety* (pp. 1-10). [https://doi.org/https://doi.org/10.1061/40889\(201\)41](https://doi.org/https://doi.org/10.1061/40889(201)41)

- Sigmund, V., & Penava, D. (2013). Influence of Openings, With and Without Confinement, on Cyclic Response of Infilled R-C Frames — An Experimental Study. *Journal of Earthquake Engineering*, 18(1), 113-146. <https://doi.org/10.1080/13632469.2013.817362>
- Smith, B. S., & Carter, C. (1969). A method of analysis for infilled frames. *Proceedings of the Institution of Civil Engineers*, 44(1), 31-48. <https://doi.org/10.1680/iicep.1969.7290>
- Su, Q., Cai, G., & Cai, H. (2016). Seismic behaviour of full-scale hollow bricks-infilled RC frames under cyclic loads. *Bulletin of Earthquake Engineering*, 15(7), 2981-3012. <https://doi.org/10.1007/s10518-016-0074-6>
- T.C. Liauw, & S.W. Lee. (1977). On the behaviour and the analysis of multi-storey infilled frames subject to lateral loading. *Proceedings of the Institution of Civil Engineers*, 63(3), 641-656. <https://doi.org/https://doi.org/10.1680/iicep.1977.32593>
- Tasnimi, A. A., & Mohebkah, A. (2011). Investigation on the behavior of brick-infilled steel frames with openings, experimental and analytical approaches. *Engineering Structures*, 33(3), 968-980. <https://doi.org/10.1016/j.engstruct.2010.12.018>
- Tawfik Essa, A. S. A., Kotp Badr, M. R., & El-Zanaty, A. H. (2014). Effect of infill wall on the ductility and behavior of high strength reinforced concrete frames. *HBRC Journal*, 10(3), 258-264. <https://doi.org/10.1016/j.hbrcj.2013.12.005>
- Thiruvengadam, V. (1985). On the natural frequencies of infilled frames. *Earthquake Engineering & Structural Dynamics*, 13(3), 401-419. <https://doi.org/https://doi.org/10.1002/eqe.4290130310>
- Wael W. El-Dakhkhni, S. M. A., Mohamed Elgaaly, F. ASCE, and Ahmad A. Hamid. (2003). Three-Strut Model for Concrete Masonry-Infilled Steel Frames. *Journal of Structural Engineering*, 129(2), 177-185. [https://doi.org/https://doi.org/10.1061/\(ASCE\)0733-9445\(2003\)129:2\(177](https://doi.org/https://doi.org/10.1061/(ASCE)0733-9445(2003)129:2(177)
- Wararuksajja, W., Srechai, J., & Leelataviwat, S. (2020). Seismic design of RC moment-resisting frames with concrete block infill walls considering local infill-frame interactions. *Bulletin of Earthquake Engineering*, 18(14), 6445-6474. <https://doi.org/10.1007/s10518-020-00942-9>
- Wararuksajja, W., Srechai, J., Leelataviwat, S., Sungkamongkol, T., & Limkatanyu, S. (2021). Seismic design method for preventing column shear failure in reinforced concrete frames with infill walls. *Journal of Building Engineering*, 44, 102963. <https://doi.org/10.1016/j.jobe.2021.102963>
- Yáñez, F., Astroza, M., Holmberg, A., & Ogaz, O. (2004, 01/01). Behavior of confined masonry shear walls with large openings. 13th World Conference on Earthquake Engineering, Vancouver, B.C., Canada.
- Yekrangnia, M., & Asteris, P. G. (2020). Multi-strut macro-model for masonry infilled frames with openings. *Journal of Building Engineering*, 32, 101683. <https://doi.org/10.1016/j.jobe.2020.101683>

- Yekrangnia, M., & Mohammadi, M. (2017). A new strut model for solid masonry infills in steel frames. *Engineering Structures*, 135, 222-235. <https://doi.org/10.1016/j.engstruct.2016.10.048>
- Yuksel, E., Ozkaynak, H., Buyukozturk, O., Yalcin, C., Dindar, A. A., Surmeli, M., & Tastan, D. (2010). Performance of alternative CFRP retrofitting schemes used in infilled RC frames. *Construction and Building Materials*, 24(4), 596-609. <https://doi.org/10.1016/j.conbuildmat.2009.09.005>
- Zhai, C., Kong, J., Wang, X., & Chen, Z. (2016). Experimental and Finite Element Analytical Investigation of Seismic Behavior of Full-Scale Masonry Infilled RC Frames. *Journal of Earthquake Engineering*, 20(7), 1171-1198. <https://doi.org/10.1080/13632469.2016.1138171>
- Zovkic, J., Sigmund, V., & Guljas, I. (2013). Cyclic testing of a single bay reinforced concrete frames with various types of masonry infill. *Earthquake Engineering & Structural Dynamics*, 42(8), 1131-1149. <https://doi.org/10.1002/eqe.2263>



## VITA

**NAME** Sreyneth Lath

**DATE OF BIRTH** 02 January 1994

**PLACE OF BIRTH** Cambodia

**INSTITUTIONS ATTENDED** The author, Sreyneth Lath, completed her Bachelor's degree in Civil Engineering from the Institute of Technology of Cambodia in 2018. Beginning of 2022 she continued her Master's degree in Civil Engineering at Chulalongkorn University under the supervision of Professor Dr. Anat Ruangrasamee, achieving the CU ASEAN and NON-ASEAN Scholarship

